2012

Assessment of optic neuropathy as a result of direct and indirect injury using non- invasive functional and structural analytical tools

Kabhilan Mohan
Iowa State University

Assessment of optic neuropathy as a result of direct and indirect injury using non-invasive functional and structural analytical tools

by

Kabhilan Mohan

A dissertation submitted to the graduate faculty

in partial fulfillment of the requirements for the degree of

DOCTOR OF PHILOSOPHY

Major: Biomedical Sciences (Cell Biology)

Program of Study Committee:

Donald Sakaguchi (Major Professor)

Sinisa Grozdanic

Matthew Harper

Mark Ackermann

Anumantha Kanthasamy

Iowa State University

Ames, Iowa

2012

TABLE OF CONTENTS

ABSTRACT

Optic neuropathy, as a result of various factors, is a leading cause of blindness in the world. The early diagnosis of optic nerve damage can aid therapeutic intervention, and experimental studies characterizing relevant diagnostic tools in different optic neuropathy models are currently lacking. In order to address this gap in current scientific literature, we aim to validate the following overarching hypothesis in this dissertation.

The progression of optic neuropathy as a result of direct and indirect injury to the optic nerve can be reliably assessed using non-invasive functional and structural analytical tools.

In order to verify this hypothesis, we have conceived and implemented the following specific aims.

Specific Aim I: To characterize optic nerve structure and function using non-invasive tools in healthy C57/bl6 mice.

Specific Aim II: To evaluate optic nerve status in C57/bl6 mice with experimentally induced Parkinson's disease, as a model of indirect injury to the optic nerve.

Specific Aim III: To evaluate optic nerve status in C57/bl6 mice following blast injury, as a model of direct injury to the optic nerve.

CHAPTER I. GENERAL INTRODUCTION

Dissertation Organization

An alternative format has been adopted for this dissertation; it includes modified versions of manuscripts either accepted or to be submitted for publication. The dissertation contains a general introduction (Chapter I), 3 research papers (Chapters II-IV), and a general conclusion (Chapter V). References from all sections are combined together at the end of the conclusion. Prior to the introduction, the central hypothesis governing the study is elucidated. The general introduction consists of 3 sections. The first section reviews the current non-invasive imaging routines for the retina and optic nerve and their utility in monitoring disease progression. The second section reviews Parkinson's disease, the prevalent visual symptoms, and current non-invasive imaging techniques. The third section reviews traumatic brain injury resulting from blast exposure, the prevalent visual symptoms, and the current non-invasive imaging techniques. Chapter II titled "Characterization of structure and function of the mouse retina using pattern electroretinography, pupil light reflex and optical coherence tomography" is a manuscript accepted for publication at the journal Veterinary Ophthalmology. Chapter III titled "Protein kinase C delta mediates retinal ganglion cell function loss following MPTP treatment in mice" is a manuscript prepared for submission to the journal Investigative Ophthalmology and Visual Sciences. Chapter IV titled "Retina and optic nerve damage in an experimental rodent model of blast-mediated traumatic brain injury" is a manuscript prepared for submission to the journal Investigative Ophthalmology and Visual Sciences.

Visual information is transmitted from the photoreceptors to the final output cells of the retina, the retinal ganglion cells (RGC). The axons of the RGC bundle together to form the optic nerve that projects to the primary visual cortex via the lateral geniculate nucleus. The optic nerve is susceptible to damage by various factors, such as ischemia, compression, inflammation, trauma, toxins, and nutrient deficiency, which can cause visual dysfunction and, eventually, blindness. The optic nerve is also vulnerable to degeneration as a result of central nervous system (CNS) diseases, whose primary pathology is observed elsewhere. Currently, there are no means to clinically reverse optic nerve degeneration. Early diagnosis

can aid therapeutic interventions aimed at slowing RGC degeneration and maintaining their function. Further, the optic nerve is the most accessible region of the CNS and could provide an avenue to study disease processes affecting other regions of the CNS. The experimental study of CNS diseases and their impact on the retina and optic nerve could eventually provide means to monitor disease progression. With these goals in mind, it is crucial to define optic nerve degeneration in different disease models and standardize imaging techniques that can non-invasively monitor the structure and function of the retina and optic nerve. In the following pages, we review current methods of imaging the optic nerve structure and function; this is followed by reviews of Parkinson's disease and traumatic brain injury as a result of blast exposure, two disease models that affect the anterior visual pathway.

Literature Review I: Non-invasive imaging of the optic nerve

Optic neuropathies are among the leading causes of blindness in the world and can manifest due to hereditary and acquired factors. Commonly observed pathological changes in optic neuropathy include optic nerve head (ONH) abnormalities and thinning of the retinal nerve fiber layer (RNFL) as a result of degeneration of RGCs or its axons[1]. However, structural changes are not always apparent, and optic nerve dysfunction might be the only indication of disease[2]. Currently, many techniques exist to monitor structure and function of the optic nerve non-invasively, and we review some of the most important here.

Structural imaging

Optical coherence tomography

Optical coherence tomography (OCT) is a non-invasive biological imaging technique, earliest versions of which utilized low-coherence interferometry to provide two-dimensional images of the imaged tissue[3]. The technique involves an optical beam that scans the retina and the magnitude and echo time delay of the backscattered light is measured. The low-coherence interferometer has two arms, one which directs light on the sample and collects the returning backscattered light, and another mechanically controlled reference arm with a reflecting mirror varies time delay and measures interference[4]. Low-coherence interference

occurs when the distance travelled by light in the biological sample and the reference arm match to within the coherence length[4]. This early iteration of OCT, called time-domain OCT (TD-OCT), has been improved upon to utilize interference spectrum from light of different wavelengths using a stationary reference mirror. Image data is then acquired by a spectrometer that acts as a detector, which is then Fourier-transformed to extract depth information. This technique called Fourier-domain or spectral domain OCT (SD-OCT) has greater resolution and acquisition speed[5]. SD-OCT enables rapid imaging of the different retinal layers to monitor progression of diseases and the effects of treatment. Further, modern versions of the OCT (e.g., Spectralis, Heidelberg Engineering) also incorporate confocal scanning laser ophthalmoscopy (cSLO) into the same platform, enabling improved fundus imaging. SD-OCT has been extensively used to diagnose and monitor diseases including glaucoma[6], retinitis pigmentosa[7], and macular degeneration[8]. In addition, OCT has been used extensively in studying MS-associated optic neuritis[4,9,10]. SD-OCT can also be modified with adaptive optics and 78D lens for use in rodents[11], enabling its use in experimental studies. Drawbacks of the system include problems with the automated segmentation of RNFL which might not exactly reflect actual retinal anatomy, especially in disease conditions. Further, media opacities, like cataracts, can affect the quality of the image obtained[12].

Diffusion tensor imaging

Diffusion tensor imaging (DTI), a modification of magnetic resonance imaging (MRI), enables the study of axon degeneration. This technique utilizes the direction of water diffusion through white matter tracts for imaging. Diffusion proceeds faster along the direction of the fiber tract, while it is much slower in the direction perpendicular to the main axis of the tract. This directional selectivity of diffusion (called anisotropy) is affected when pathological processes affect the integrity of the white matter tract, thereby increasing diffusivity through the tract[13]. This variation in anisotropy can be used to determine optic nerve integrity. DTI axial diffusivity has been recently observed to be predictive of visual outcome following optic neuritis[14]. DTI has also been found sensitive to optic nerve damage in patients with multiple sclerosis[15] and anterior ischemic optic neuropathy[16]. Further, recent experimental studies have characterized DTI use in mouse models of optic neuropathy[17,18].

Since DTI is highly sensitive to microscopic motion, macroscopic movement can affect imaging; this is especially a problem with the optic nerve. Further, the optic nerve is surrounded by fat and bone, which require modifications of the imaging protocol to enhance sensitivity[13].

Scanning laser polarimetry

Scanning laser polarimetry (SLP) is a technique that uses polarized light to detect RNFL thickness. The RNFL being birefringent, can retard polarized light; the degree of retardation is proportional to RNFL thickness, and is measured by SLP[13]. A recent study comparing OCT with SLP observed that OCT was better able to reflect RNFL thickening as a result of papilledema, while SLP was better at reflecting axon injury and associated swelling of the RNFL[19]. SLP has been used extensively in studying glaucoma progression[20-22]. Similar to the OCT, SLP can be affected by opacities in the ocular media, resulting in abnormal retardation. Further, birefringence can occur from other ocular components, thereby confounding the results[23].

Functional imaging

Pattern-evoked electroretinography

Pattern-evoked electroretinography (pERG) is an objective measure of RGC function and has been extensively used in the diagnosis of glaucoma[24-28]. The pERG stimulus consists of either bars or a checkerboard pattern, generally in black and white. Alternating reversal of the pattern at particular frequencies can elicit the pERG response, obtained either as a sinusoidal or transient waveform dependent on the frequency of reversal. This waveform consists of an initial negative component (N35), a prominent positive component (P50), and a delayed negative component (N95). The amplitude and latency of occurrence of the N95 component is indicative of RGC function[29]. The pERG response occurs as a result of RGC depolarization[30] and this response is abolished by optic nerve transection[31,32] or by pharmacologically eliminating action potentials using tetrodotoxin[30]. The technique has also been used in experimentally studying glaucoma and ocular hypertension in different animal models[33-36]. A disadvantage of this technique is that focal RGC loss or RNFL lesions may not

affect the full field pERG response; this can however be remedied by the use of multi-focal pERG techniques[37].

Chromatic pupil light reflex

The chromatic pupil light reflex (cPLR) is a modification of the PLR technique that can be used to assess the functional integrity of the optic nerve[38,39]. This technique utilizes the differences in spectral sensitivities of rods, cones, and melanopsin-containing RGC to localize function loss within the anterior visual pathway. Stimulation of the eye with red (630 nm) light activates a rod-cone mediated pupil light response, without activation of melanopsin mediated responses[39]. The degree of contribution of rods vs. cones depends on the state of retinal adaptation, the spectral sensitivity of the photoreceptors in the species being studied and the brightness of the light. The rod-cone mediated pupil response requires a functional and well-organized dendritic arborization of RGCs to allow for signal processing of rod-cone input to the RGCs mediating PLR responses. Stimulation of the eye with bright blue (480 nm) light can activate both a rod-cone mediated pupil response and a pupil response that is weighted towards an intrinsic melanopsin-mediated response and can provide information about the intracellular RGC status in PLR conducting RGCs[34,38,40].

Visual evoked potentials

Conventional visual evoked potentials (VEP) measure the cortical response to stimulation of the visual field, and it is obtained in response to the central 30 degrees of the visual field[13]. Abnormalities in the VEP waveform can be indicative of retina and optic dysfunction. Increased latency of the cortical signal has been observed using different VEP protocols in patients with multiple sclerosis[41,42]. Similar to other visual field techniques, VEP measures full field responses which might not reflect focal defects. Multi-focal VEP is a variation of conventional VEP by which specific sectors of the visual field are stimulated enabling better localization of dysfunction[43]; this paradigm has been extensively used in studying glaucoma[44-46].

Literature Review II: Parkinson's disease – more than just a motor disorder

Parkinson's disease (PD) is the second most common neurodegenerative disease, following Alzheimer's disease, with a high risk of incidence in the population above 60 years of age[47]. Diagnosis of PD is based on the expression of (a.) the cardinal motor symptoms—which include tremor, rigidity, postural instability and bradykinesia—of parkinsonism, originally expounded by James Parkinson in his description of the *shaking palsy*[48]; and (b.) the non-motor symptoms associated with the disease, which include olfactory dysfunction, visual abnormalities, sleep disturbances, constipation, and autonomic dysfunction[49]. Although a number of factors, both genetic and environmental, have been identified to contribute to disease progression, the etiology of PD is still unclear[50]. An early-onset familial form of PD accounts for 5%-10% of all reported cases; mutations in *α-synuclein*, *LRRK2*, *PINK1*, *parkin*, and *DJ1* have been reported in patients with this rare form of the disease[51]. However, the dominant manifestation accounting for majority of PD cases is the aging-related sporadic form of PD. Similar genetic mutations[52] —especially those of *α-synuclein*[53]—and environmental factors[50] have been implicated in the occurrence of late-onset PD. The primary pathology associated with PD is the progressive degeneration of mesencephalic dopaminergic neurons, present in the substantia nigra pars compacta (SNpc). Another defining characteristic is the occurrence of eosinophilic inclusions composed of α-synuclein, called Lewy bodies, in the neuronal cytoplasm[54]; these α-synuclein-positive Lewy bodies have been observed in the medullary, pontine, and mesencephalic nuclei of PD patients[55]. However, PD is a multisystem disorder, and these neuropathological correlates are also accompanied by degeneration in the peripheral and enteric nervous systems, and other regions of the central nervous system[56,57].

The mechanisms underlying PD pathology are still unclear. Currently, most therapeutic interventions aim to alleviate symptoms and do not treat underlying neurodegeneration. The primary line of treatment for PD involves oral administration of the dopamine precursor, levodopa (L-DOPA, L-3,4-dihydroxyphenylalanine) to increase the availability of dopamine. Many lines of evidence exist for the etiology of PD, with aging, environmental, and genetic factors contributing to pathology, although no single theory explains all characteristics of the disease [50,52,56,58,59]. However, a certain degree of consensus has been achieved regarding the final mechanisms mediating dopaminergic cell death. Oxidative stress- and inflammation-

mediated downstream cascades potentiate mitochondrial dysfunction and accumulation of mutant protein proteins, thereby mediating cell death via apoptosis or autophagy[60,61]. Much evidence in support of these cellular pathologies has been obtained from the study of various genetic and toxin-induced parkinsonian models[62]. Of particular relevance is the meperidine derivative, 1-methyl-4-phenyl-1,2,3,6-tetrahydropyridine (MPTP)-induced dopaminergic degeneration. It was discovered by Langston et al[63] that meperidine accidentally contaminated with MPTP, which was used by drug addicts, resulted in the development of PD symptoms. MPP+, the active oxidized form of MPTP, inhibits mitochondrial complex I activity leading to the uncoupling of oxidative phosphorylation[64]. The high specificity of MPTP for dopaminergic neurons further facilitates study of the molecular mechanisms underlying PD[62,65].

Dopaminergic basis of PD

The motor symptoms of PD are primarily attributed to hyperactivity of the subthalamic nucleus and internal globus pallidus as a result of dopaminergic neuron degeneration in the SNpc[66]. In particular, the ventrolateral tier of the SNpc is most susceptible to degeneration in PD[67], leading to a loss of dopamine in the putamen. These nuclei are part of the basal ganglia subcortical system, one of the major circuits mediating thalamo-cortical transmission[68].

Dopamine, a member of the catecholamine family, is a major neurotransmitter within the CNS. Dopamine is synthesized from the amino acid L-tyrosine within dopaminergic neurons, primarily at the SNpc and ventral tegmental area (VTA) of the midbrain[69]. L-Tyrosine is first converted to L-3, 4-dihydroxyphenylalanine (L-DOPA) by tyrosine hydroxylase (TH), the rate-limiting enzyme[70]; dopamine is then obtained by decarboxylation of L-DOPA in the presence of DOPA decarboxylase[71]. Dopamine turnover is dependent upon the presence of the dopamine transporter (DAT), which facilitates dopamine reuptake and metabolism[72].

Currently, functional imaging of dopamine uptake, dopamine receptor binding, or the presynaptic targets of dopamine are predominantly used in monitoring the progression of PD; these include variations in radionuclide-based positron emission tomography (PET) or single photon emission computed tomography (SPECT) methods and functional MRI (fMRI)

paradigms[73,74]. PET/SPECT studies of dopamine receptor binding have noted increased striatal D2 receptor binding and normal D1 receptor binding in early untreated PD patients[74,75]. Further, the supplementary motor area (SMA), in particular, the rostral pre-SMA, and the dorsolateral prefrontal cortex in PD patients have been consistently observed to be hypoactive using PET/SPECT and fMRI studies[76]. Similar results have been reported by electrophysiological studies. Reduced amplitudes or shifted latencies were recorded in the early Bereitschaftspotential, contingent negative variation, and the N30 component of somatosensory evoked potentials (SSEP), all of which originate at the SMA[76,77]. Dopamine generated in the midbrain is transmitted by means of 3 pathways: the nigrostriatal, mesolimbic, and mesocortical pathways[78]. PD pathology as a result of striatal dopamine depletion is attributed to degeneration of the nigrostriatal pathway. In addition to the midbrain dopaminergic pathways, there exist 6 other pathways in the CNS, namely, the tuberoinfundibular, diencephalospinal, and incerto-hypothalamic pathways from the hypothalamic nuclei; the periventricular pathway arising from the mesencephalic and diencephalic periaqueductal and periventricular gray; the olfactory bulb pathway from the periglomerular cells; and the retinal pathway from amacrine cells of the inner nuclear layer[79]. Degeneration of these dopaminergic pathways could potentially account for some non-motor symptoms associated with PD.

Non-motor symptoms of PD

Although the motor symptoms of PD frequently define the disease, they are not the only characteristic of PD. A number of non-motor symptoms—including olfactory dysfunction, visual disturbances, gastrointestinal disorders, cognitive decline, and autonomic dysfunction—manifest during both the early and late stages of PD[80,81]. The pathological basis for the occurrence of these symptoms is yet to be clearly established. Dopaminergic deficiency and treatment have been found to contribute to a number of non-motor symptoms[49,82]. In addition, evidence for dysfunction in cholinergic[83], noradrenergic[84] and serotoninergic[85,86] neurotransmitter systems are also present concurrently in PD and contribute to non-motor symptoms. Further, basal ganglia outputs are not exclusive to the motor cortex; extensive projections are made to various other regions of the cerebral cortex,

the hippocampus and the amygdala. In addition to the skeleto-motor circuit, frontal lobe targets of the basal ganglia include the oculomotor circuit, limbic circuit, and the prefrontal circuit[68]. Degeneration of these connections is also believed to contribute to the non-motor symptoms associated with PD[87-89]. It has been observed that some non-motor symptoms manifest much earlier clinically compared to the classic motor symptoms[90,91]. In an influential 2003 study, Braak et al[57] dissected the occurrence of Lewy body pathology and the progression of sporadic PD into 6 stages. Stages 1 and 2 predominantly affect the medulla oblongata and the pontine tegmentum, with lesions in the dorsal IX/X motor nuclei, caudal raphe nuclei, and the reticular nuclei. In a recent observational study, vagus nerve SSEP were observed to have longer latencies in PD patients when compared to controls[92]. Midbrain lesions begin to occur in stage 3, and these lesions become extensive by stage 4; cortical lesions, predominantly in the mesocortex and allocortex, also appear in this stage. Neocortical lesions occur in stages 5 and 6, with degeneration in sensory association areas. These morphological observations support the early occurrence of non-motor symptoms such as olfactory dysfunction[93,94], REM sleep behavior disorder[95,96], cognitive impairment/dementia[97-99], and autonomic dysfunction[100-102], which can arise long before motor symptoms manifest. Study of these non-motor symptoms and their progression could provide insight into development of the disease, and it could provide a means to predict disease occurrence later in life, thereby acting as valuable diagnostic tools. Treatment of these symptoms could prove crucial in the improvement of the quality of life in PD patients.

Visual dysfunction in PD

The retina has several neuronal populations that utilize dopamine for neurotransmission. In particular, dopamine has been observed to be present in the interplexiform and amacrine cells of the retina[103]. Dopaminergic transmission is involved in mediating the lateral pathways of amacrine cells and horizontal cells[104] and in modulating the center-surround functions of the retina that are crucial to receptive field organization[105]. Further, dopaminergic innervation could mediate adaptation to light and the concurrent transition from scotopic to photopic vision[106,107].

Figure 1: Dopaminergic transmission in the retina. Light-mediated dopamine release in the retina can modulate the interactions between horizontal cells, amacrine cells, and RGC. Source: Nature Reviews Neuroscience 10, 495-506 (July 2009)[108].

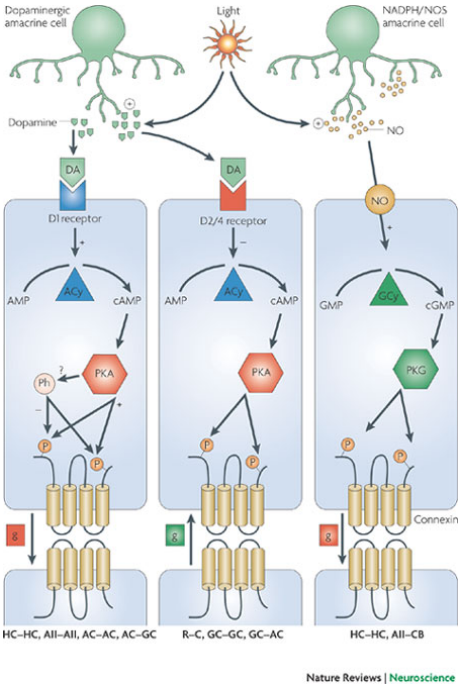

Visual dysfunction is frequently reported by PD patients, with impairment in primary and complex visual functions being commonly reported[109,110]. A correlation between disease severity and visual acuity loss was observed in a study on 39 PD patients[111]. A loss in visual contrast sensitivity[112] and spatiotemporal contrast sensitivity[113], [114] has been reported among PD patients. A clinical study of 30 PD patients[115] noted increased complaints of photophobia, dry eye, and hallucinations. Furthermore these patients exhibited reduced blink rates and decreased convergence amplitudes. Visual hallucinations[116-118], impaired color vision[119,120], and difficulties in eye movement[121-123] have been commonly reported among PD patients.

Many studies in PD patients have observed alterations in different electrophysiological parameters, such as the pERG, electro-oculogram (EOG), flash ERG (FERG), and pattern VEP[124-127]. Further, recent studies have reported reduction in RNFL thickness using OCT, primarily in the macular region[128,129]. Peppe et al[124,130] observed abnormal pERG amplitudes in their human PD patients, and these deficits were reversible by L-DOPA treatment. Another study using multifocal ERG reported a decrease in electrical activity in the foveal region of PD patients[129]. Similarly, experimental studies using MPTP and 6-OHDA injections in monkeys have found abnormalities in pattern VEP and pERG, which returned to normal with L-DOPA administration[131,132]. Further, morphological abnormalities of dopaminergic neurons have been observed in primates with experimentally induced PD[133]. In one study, post-mortem analysis of retinas revealed reduced dopamine content in PD patients

without L-DOPA treatment; however, among PD patients treated with L-DOPA, dopamine content was similar to those measured in controls[134]. These studies suggest a role for retinal dopamine in mediating visual dysfunction. However, it is unlikely that retinal dopaminergic deficiency alone is responsible for all observed symptoms; visual processing at the primary visual cortex and associated regions could also be affected[86,135].

Literature Review III – Blast exposure and traumatic brain injury

Traumatic brain injury (TBI) is a debilitating condition that can lead to the development of significant cognitive and neurological symptoms, years after the event of injury. Currently, it is estimated that more than 1.5 million people in the U.S alone sustain some form of TBI every year. TBI can be further classified into mild, moderate, and severe based on the degree of injury sustained and the expression of specific clinical symptoms. Mild TBI (mTBI), frequently referred to as concussion, accounts for up to 85% of medically treated TBI in the U.S[136]. It includes any injury to the brain that induces an alteration in mental status leading to physical, behavioral, and cognitive symptoms. Loss of consciousness does not necessarily have to occur for the development of these symptoms[137]. In addition, mTBI can cause chronic disorders, with 25% of patients reporting post-concussive symptoms (PCS) or cognitive defects that persist beyond one year despite the absence of morphological brain abnormalities[138]. A prospective study of 123 patients with mTBI at 1 week and 3 months after injury revealed severe PCS at 1 week and a higher likelihood for memory and concentration problems at 3 months compared to trauma-matched controls[139]. Further, Vanderploeg et al[140] reported the long-term prevalence of PCS with associated neurological and psychosocial disturbances in Vietnam-era veterans exposed to mTBI. Such mTBI has become of major concern, especially in light of the recent wars in Iraq and Afghanistan (Operation Iraqi Freedom [OIF] and Operation Enduring Freedom [OEF]). Due to advancements in armor and other protective gear, the incidence of severe penetrating injuries, which are usually fatal, has been greatly reduced. However, the frequent use of improvised explosive devices by insurgents in Afghanistan and Iraq has escalated the number of blast-mediated injuries in soldiers. In fact, exposure to high pressure blast waves is the leading cause of combat-related injuries in the recent wars, compelling it to be labeled the signature

injury of the recent wars[141]. In addition to the cognitive and neurobehavioral symptoms experienced by soldiers following TBI, a number of somatosensory abnormalities have been documented, with visual and auditory disturbances being predominantly observed[142-145]. A study on soldiers injured in OIF found the majority of eye injuries to be the result of blast exposure[146]. Lew et al[147] reported the occurrence of visual problems in 75% of the military patients at the Polytrauma Network Site, even though the majority of patients had near-normal corrected visual acuity and visual fields. Patients at the Polytrauma Rehabilitation Center, a population with multiple, life threatening injuries, sustained higher rates of visual impairment and visual dysfunction[148,149]. A recent study by Brahm et al[150] found 33% of all returning veterans to have some form of visual dysfunction primarily due to blast exposure; although visual acuity was near normal in most patients, visual field deficits and self-reported symptoms were increased among blast-injured soldiers. Commonly reported visual symptoms include diplopia, fixation instability, nystagmus, and blurred vision; in addition, abnormal vestibular ocular reflex, convergence insufficiencies, corneal injury, and oculomotor palsies have been observed clinically[149].

Blast wave physics

Blast injuries are caused by the interaction of an explosive blast wave with different tissues. The injuries resulting from blast trauma have different clinical presentations compared to TBI mediated by flying projectiles, or by TBI induced by the deformation of the brain against the rigid surface of the skull[151]. It is commonly believed that blast-related brain injury may be due to transient pressure changes (initial overpressure followed by a negative phase creating a temporary vacuum) as the blast wave passes the subject[151].

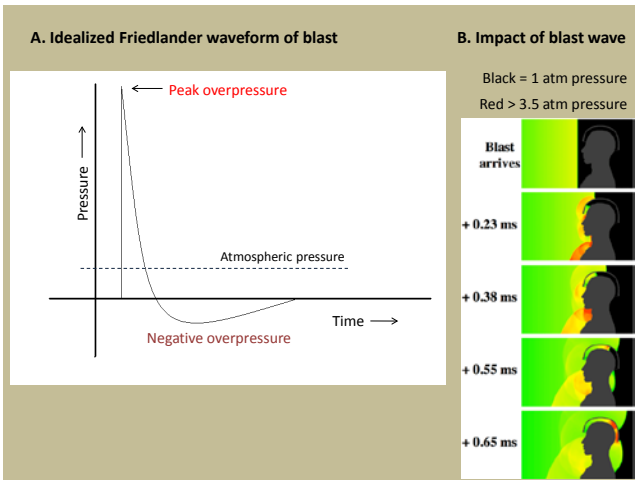

Figure 2: Blast wave dynamics. Figure 2A shows the idealized decay of a blast overpressure wave over time. Figure 2B (Source: David Mott, NRL Laboratory for Computational Physics and Fluid Dynamics[152]) shows the simulated effect of blast following the detonation of 1.5 kg C4

explosives from a distance of 3 meters. Rapid variation in pressure and the amplification of pressure in the space between the helmet and head can be observed.

Blast waves are created by the near instantaneous conversion of a solid/liquid explosive to a gas that occupies the same physical space. This gas promptly expands outwards, leading to an immediate increase in pressure, which rapidly dissipates over distance and time[153]. Following dissipation of the blast wave, a negative pressure phase develops as a result of the displaced air. This explanation however represents an idealized free-field blast wave; the non-linear dynamics of blast wave physics can be influenced by environmental conditions, and the blast wave can be amplified by interactions with blast-reflective surfaces[154]. Three major factors affect the likelihood of sustaining injuries as a result of blast exposure[155]. The medium in which the blast propagates determines the rapidity of expansion; for instance, due to the non-compressibility of water, an explosion in water generates a blast wave that propagates quicker than a blast wave in air, with minimal dissipation. The distance of the person from the blast epicenter also determines the peak overpressure exposure, since the blast wave dissipates over longer distances. The third factor is the location of the blast wave; an explosion within a closed space has greater potential for injury than one in an open space, due to reflection from walls and the containment of blast pressure within them. This also increases the risk for secondary and tertiary injuries, as a result, respectively, of penetrating projectiles and bodily impact against walls or other solid objects. Traditionally, blast wave has been predominantly thought to affect air-filled organs and viscera, such as the pulmonary system, gastrointestinal system, and auditory system[156]. However, this has been based on the premise that the blast peak overpressure is the only risk factor contributing to injury and does not explain brain injury[157]. Primary injury as result of blast wave can cause shear and stress forces that lead to edema, contusions, and diffuse axonal injury (DAI); ultimately, these shearing forces can damage cell bodies, axons, and vasculature in the brain and other organs[151,158]. A study of stress forces from explosions observed that the blast wave was capable of propagating directly to the brain; further, the equivalent of 0.324 kg TNT explosion at a distance of 0.6 m from epicenter was predicted capable of inducing brain injury comparable to those observed with sport concussions and mTBI[154]. These suggest a role for the blast wave itself contributing to CNS pathology.

Blast injury pathology

Since it is difficult to delineate the effect of blast wave from confounding factors, very few clinical studies explicitly describe the pathology associated with blast exposure[151]. A patient, exposed to blast overpressure as a result of steam boiler explosion, had normal vital signs and no signs of blunt or penetrating wounds to the head and neck at admission; CT head scans revealed mild cerebral edema and diffuse hemorrhage, and he succumbed to his injuries post-operatively[159]. A more recent event involved a soldier in Iraq, exposed to an explosive blast wave directly from her left side[160]. She was also in the vicinity of multiple blast events over the next 2 hours; it is notable that the patient remained conscious throughout. Three months after injury, MRI and DTI revealed abnormalities primarily in the auditory and cerebellar pathways; she also experienced persistent PCS. These case reports have been supported by recent experimental studies conducted with animal models of blast injury. Animals exposed to blast waves originating from a shock tube have been extensively studied[161-163]. The predominantly observed CNS pathology is diffuse axonal injury, and long axonal tracts appear to be the most susceptible to injury[164-166]. In particular, these studies reported degeneration localized to cerebellar, corticospinal, and optic tracts. Further evidence for neuronal injury, including expanded perineuronal spaces, cytoplasmic vacuoles, myelin deformation, and axoplasmic shrinkage, were observed in the hippocampus and brainstem reticular formation following blast injury[161,167]. Another factor that could influence DAI is increase in pressure within the cranial cavity. Increased intracranial pressure following exposure to blast wave has been reported experimentally and could potentiate the shearing effects of the shockwave itself[168,169]. Similar effects have been observed along the visual pathway. In one study, rats exposed to blast overpressure of 129-173 kPa had extensive degeneration of the primary visual pathway; axon degeneration was localized to the optic nerve, optic tracts, lateral geniculate body, and superior colliculus[170]. A recent study using the fluid percussion model of TBI has demonstrated the prechiasmatic region of the optic nerve is susceptible to traumatic axonal injury[171]. In this model, swollen optic nerve axons and disconnection of proximal and distal axonal segments were observed as early as 1-3 hours post injury; a resultant dieback of the segments, reminiscent of Wallerian degeneration, occurred within 48 hours of injury. The proximal segment in particular demonstrated

significant swelling early after injury and rapidly transitioned to a thinned and shrunken appendage. The effect of trauma due to shearing against the bony canal surrounding the optic nerve could be an important factor mediating such dieback. Axonal injury can be accompanied by mitochondrial degeneration, leading to the activation of apoptotic mechanisms, and eventually, to neuronal death[172]. It has also been observed that in addition to neurons, oligodendrocytes and astrocytes are also susceptible to apoptotic death following TBI, in a region-specific manner[173].

Imaging and diagnosis

Unlike the more severe forms of TBI with loss of consciousness, mTBI is difficult to diagnose due to subtle neurological symptoms and a lack of overt evidence of trauma. Currently, screening for mTBI in the theatre of war is predominantly by means of a self-reported questionnaire—the brief traumatic brain injury screen (BTBIS)[174]—which might be followed by a neurocognitive assessment such as the Military Acute Concussion Evaluation (MACE)[175]. Another such assessment is the Automated Neuropsychological Assessment Metric (ANAM), which is used to monitor cognitive function of soldiers before deployment and following injury. However, these tests are more predictive of moderate-severe TBI[176]. Since mTBI is largely characterized by DAI, the study of white matter tracts by DTI is currently the most effective method to study structural integrity[177]. DTI has been employed widely to study soldiers with blast injury[147,160,178], and it has been shown to be predictive of clinical outcome in patients with severe TBI[179]. However, in one study, no significant differences were observed using this technique in soldiers with milder injuries, although they revealed worse PCS and post-traumatic stress disorder (PTSD) scores compared to control subjects[180].

In addition to structural imaging, a number of functional changes have been documented using electrophysiological techniques. Evoked potentials (EP) and event-related potentials (ERP) have been widely utilized in the assessment of TBI and for the prediction of outcome[181]. Somatosensory EP (SEP), used to assess peripheral nerves, the spinal cord and somatosensory cortex pathways, has been reported to be the best overall predictor of outcome from severe TBI[182]. Median nerve SEP has been observed to predict negative outcome from

severe TBI or coma with high certainty[183,184]. However, SEP conducted in patients with milder injuries reveal no discernible difference compared to age-matched controls[185]. Pupil response to light has also been extensively used in TBI assessment. Pupillary responses have been reported to be the strongest predictor for awakening from coma[186] and to have highest sensitivity for the prediction of a favorable outcome[182]. Further, a recent meta-analysis of 8721 patients from the IMPACT database with moderate-severe TBI also found a strong correlation between unreactive pupils and negative outcome[187].

Of greater relevance to all severity levels of TBI are the long latency responses (LLR), a form of auditory ERP. This involves the presentation of auditory stimuli of constant frequency over the majority of the testing protocol; frequencies of different stimuli are interspersed with these tones at short intervals (an oddball paradigm)[181]. This elicits a P300 response, generated from the frontal cortex, reticulothalamus, and the medial septal area, in normal subjects and is useful in cognitive assessments. A recent study of the P300 amplitudes on athletes subject to multiple concussions revealed reduced amplitudes compared to controls[188]; although these athletes functioned normally, the persisting electrophysiological deficits could suggest susceptibility to further concussions. Further, a significant correlation between the P300 latency and fractional anisotropy from DTI has been reported in a study conducted on 11 patients with mild to moderate TBI[177]. Contingent negative variation (CNV), another ERP paradigm that tests attention, has been used to assess TBI patients; a study on 20 patients with mild TBI found abnormalities in the CNV when compared to control subjects[189].

Visual ERP (VERP) are valuable indicators of visual pathway integrity and cognitive function. In a VERP study on 17 patients with mild TBI[190], compared to control subjects, TBI patients presented with deficits in complex visual integrative tests and significantly delayed latencies in texture segregation paradigms. An interesting observation in the study was that TBI patients with electrophysiological abnormalities were at greater risk of a negative vocational outcome, when compared to TBI patients with normal electrophysiology. Several studies have also documented reduced amplitude and delayed latency of the visual P300 component in patients with mild-moderate TBI[189,191,192]. One study also found a positive correlation between higher concussive episodes and longer P300 latency[192]. Many

paradigms that test visual tracking abilities of patients have proven useful in assessment of mTBI. One study of visual tracking abilities in 17 mTBI patients found a significant correlation between errors in gaze positioning and fractional anisotropy from DTI[193]. Recently, the King-Devick test, another measure of visual tracking ability, has been applied toward the rapid assessment of sport-related concussion[194]. Combination of structural imaging and representative functional measures might prove more useful in diagnosis.

CHAPTER II. CHARACTERIZATION OF STRUCTURE AND FUNCTION OF THE MOUSE RETINA USING PATTERN ELECTRORETINOGRAPHY, PUPIL LIGHT REFLEX AND OPTICAL COHERENCE TOMOGRAPHY

A paper accepted for publication by Veterinary Ophthalmology, 2012

Kabhilan Mohan, Matthew M. Harper, Helga Kecova, Eun-Ah Ye, Tatjana Lazic, Donald S. Sakaguchi, Randy H. Kardon, Sinisa D. Grozdanic

Abstract

Objective: To perform *in vivo* analysis of retinal functional and structural parameters in healthy mouse eyes.

Animal Studied: Adult C57BL/6 male mice (n=37)

Procedures: Retinal function was evaluated using pattern electroretinography (pERG) and the chromatic pupil light reflex (cPLR). Structural properties of the retina and nerve fiber layer (NFL) were evaluated using spectral-domain optical coherence tomography (SD-OCT).

Results: The average pERG amplitudes were found to be 11.2 ± 0.7 µV (P50-N95, mean ± SEM), with an implicit time for P50-N95 interval of 90.4 ± 5.4 ms. Total retinal thickness was 229.5 ± 1.7 µm (mean ± SEM) in the *area centralis* region. The thickness of the retinal nerve fiber layer (mean ± SEM) using a circular peripapillary retinal scan centered on the optic nerve was 46.7 ± 0.9 µm (temporal), 46.1 ± 0.9 µm (superior), 45.8 ± 0.9 µm (nasal) and 48.4 ± 1 µm (inferior). The baseline pupil diameter was 2.1 ± 0.05 mm in darkness, and 1.1 ± 0.05 mm and 0.56 ± 0.03 mm after stimulation with red (630 nm, luminance 200 kcd/m^2) or blue (480 nm, luminance 200 kcd/m^2) light illumination, respectively.

Conclusions: Pattern electroretinography, cPLR and SD-OCT analysis are reproducible techniques, which can provide important information about retinal and optic nerve function and structure in mice.

Introduction

Non-invasive functional and structural assays such as electroretinography (ERG) and optical coherence tomography (OCT) can be utilized in animal models to obtain objective information regarding the status of the retina and optic nerve *in vivo* [195-197]. These techniques allow repeated analysis without the need to euthanize the animal, and can be effectively used for longitudinal evaluation of disease progression or treatment efficacy. The function of retinal ganglion cells (RGCs) in rodents can be measured by recording the amplitude and latency of the pattern evoked electroretinogram (pERG)[36,198-205]. The pERG response is a result of RGCs depolarization[30,206] with minimal glial cell contributions[207], which can be abolished by optic nerve transection[31,32] or pharmacological blockade targeting RGC action potential activity[30]. Considering that the electrical response originates from RGCs, pERG has been used to evaluate RGC damage associated with glaucoma and ocular hypertension in human patients[208-210] and in different animal models[33-35].

The chromatic pupil light response (cPLR) analysis is a relatively new diagnostic technique, which may provide information about the quality of rod-cone activity, rod-cone mediated electrical signal transmission to RGCs and characteristics of an intrinsically photosensitive subpopulation of RGCs (ipRGCs) containing the pigment melanopsin[38,211-216]. Recent reviews have excellently described the anatomy of ipRGCs and have summarized their role in mediating various functional properties[217-220]. Stimulation of the retina with red (630 nm) light activates strictly rod-cone mediated pupil light response, without activation of melanopsin mediated responses[211]. The degree of contribution of rods vs. cones depends on the state of retinal adaptation, the spectral sensitivity of the photoreceptors in the species being studied and the brightness of the light. The rod-cone mediated pupil response requires six components: 1. normal functioning rods and cones and their respective neurons in the inner nuclear layer; 2. functional and well-organized dendritic arborization of ipRGCs to allow for a rod-cone generated electrical response to be transmitted to the ipRGCs that results

in a generation of PLR responses; 3. functional axons of ipRGCs to transmit the electrical information to the pretectal brain regions mediating the PLR and photopic blink responses; 4. normal status of the pretectal olivary nucleus as a brain interneuron relay station for mediating the PLR to both Edinger-Westphal Nuclei; 5. intact pre and post ganglionic parasympathetic nerve pathway (oculomotor nerve) as an efferent pathway for mediation of PLR response; and 6. an intact iris sphincter as an effector organ. Stimulation of the retina with bright blue (480 nm) light can activate both a rod-cone mediated pupil response and a pupil response that is elicited by activation of the melanopsin in ipRGCs[38,40,197,221,222]. However, the melanopsin activated pupil response is typically more sustained after light termination.

Spectral-domain optical coherence tomography (SD-OCT) is a high-resolution imaging technique used for direct *in vivo* analysis of retina and optic nerve head structure[223-225]. Recent studies have demonstrated that OCT analysis of retinal thickness provides nearly identical values compared to analysis of the same retinal regions using position-matched histological analysis[226]. Different OCT segmentation protocols allow for the measurement of total retina thickness, photoreceptor layer thickness and thickness of the retinal nerve fiber layer (RNFL) in different retinal quadrants[227-231]. Recent utilization of OCT technology in rodent models of eye diseases has provided an objective measure of retinal structure, which can be used to monitor the structural effects of disease progression or treatment response[230-234].

The principal objective of this study was to perform a detailed characterization of RGC functional and structural parameters with the goal of establishing normative data for adult healthy C57BL/6 mice as a basis for further investigations by us and others on the experimental effects of retinal and optic nerve disorders and their treatment. In this study we used pERG and cPLR analyses to evaluate the retinal function, and particularly RGC function, while SD-OCT was used to provide structural information about the retina, photoreceptor layer and RNFL thickness.

Materials and Methods

Animals

All animal studies were conducted in accordance with the ARVO Statement for the Use of Animals in Ophthalmic and Vision Research and had the approval of the Iowa State University and VA Medical Center-Iowa City Institutional Animal Care and Use Committees. A total of 37 adult healthy male C57BL/6 mice (8-12 weeks of age, unless otherwise specified) were used for the purpose of this study.

Pattern electroretinography

Pattern evoked electroretinography (pERG) was used to objectively measure the function of the retinal ganglion cells by recording the amplitude and latency of the pERG waveform. Mice (n=37) were anesthetized with 0.8 l/min O_2, 0.4 l/min nitrous oxide and 3.5% halothane. After anesthesia induction the halothane concentration was decreased to 1.75% and mice were placed on a stainless steel recording table equipped with an internal circulating hot-water based warming system (maintained at 39 °C) to maintain body temperature. The mice were positioned 20 cm from the stimulus monitor with their body angle tilted at 45 degrees to provide direct exposure of the stimulus to the visual axis of the recorded eye. The pupil was then dilated using 1% tropicamide solution (Tropicamide; Falcon Pharmaceuticals, Fort Worth, TX, USA). Pattern ERG responses were evoked using alternating, reversing, black and white vertical stimuli delivered on a monitor (Fig. 1 A) with a Roland Consult ERG system (Roland Consult, Brandenburg, Germany). To record the pERG response, commercially available mouse corneal gold ring electrodes were used (S&V Technologies AG, Germany). A reference needle electrode was placed at the base of the head, and a ground electrode was placed at the base of the tail to complete the circuit. Each animal was placed at the same fixed position in front of the monitor to prevent recording variability due to animal placement. Stimuli (9° radius visual angle subtended on full field pattern, 1 Hz temporal frequency, 0.05 cycles/deg spatial frequency, 97% contrast, 80 cd/m^2 monitor luminance, 200 averaged signals with cut off filter frequencies of 1-30 Hz) were delivered under photopic conditions, since slower stimulation rates in mesopic and scotopic conditions can elicit rod-mediated full field ERG responses, which can completely conceal the pERG response. Retinal pERG responses were evaluated by measuring the amplitudes

(N35-P50 and P50-N95) and respective implicit times (Fig. 2). Implicit times were calculated for N35, P50 and N95 markers, in addition to the implicit time for N35-P50 and P50-N95 components. Seven mice were repeatedly recorded at 3, 11, and 15 months of age to determine whether aging has any effect on pERG amplitudes or implicit times.

Chromatic pupillography

Chromatic pupil light reflex (PLR) was characterized in mice (n = 8) using the A2000 computerized pupillometer (Neuroptics, San Clemente, CA). The pupillometer consists of a sensitive pupil tracking software, which can be programmed to include various PLR recording routines and can provide the required red/blue light illumination. Red light of 630 nm was used to elicit strictly rod-cone mediated PLR, since red light of 630 nm wavelength does not activate the intrinsic RGC photopigment melanopsin (Fig. 5). Blue light was used to elicit combined responses (rod-cone response + melanopsin intrinsic response). The wavelength of light emitted by the diodes was 622 ± 7 nm for red light and 463 ± 13 nm for blue light. Red and blue light stimuli were matched and had illuminance of 1 (0 log units), 4 (0.6 log units),16 (1.2 log units), 63 (1.8 log units), 251(2.4 log units) and 1000 (3 log units) lux. The maximum luminance measured at the position of the mouse eye using a photometer (J17LumaColor with luminance head model J1803; Tektronix, Wilsonville, OR) was 3700 cd/m2 for the illuminance of 1000 lux. The pupil was illuminated for a period of 500 milliseconds. All PLR testing routines were recorded in completely awake mouse without the use of general anesthetic or sedation. The mice were initially habituated to extensive handling with food rewards, in order for them to remain calm during recording. The experiments were then carried out under scotopic conditions with no background illumination from the pupillometer. Only the direct response of the pupil was observed following illumination with red/blue light stimulus. The pupil response was expressed as the percent contraction of the pupil from baseline.

To evaluate pupil responses with much higher light intensity, the PLR analysis was performed using a Melan-100 instrument (BioMed Vision Technologies, Ames, IA,). Similar as before, mice (n=11) were awake during the recording session and were held still using minimal manual restraint. Recording sessions in most animals lasted less than one minute.

The Melan-100 has two powerful diode based light sources with very narrow wavelength bands (630 ± 5 nm for red light, luminance 200 kcd/m^2; 475 ± 5 nm for the blue light, luminance 200 kcd/m^2). Baseline pupil diameter measurements in mice were taken in darkness prior to illumination using an infrared video camera (Sony Handycam, Sony Corporation). Red light stimuli with two second duration were used to illuminate one eye of the mouse at a distance of 4 cm from the ocular surface and direct pupil responses were recorded from the illuminated eye with the digital infrared camera. Prior to performing illumination with the blue light, pupils were allowed to completely dilate to the baseline diameter. Captured digital movies of pupil responses were analyzed using Adobe Photoshop (v. 10.0.1, Adobe Systems, Inc.). Calibrated dot grid with dot sizes of 0.5, 1,1.5, 2 and 3 mm in diameter were recorded with a camera from the 4 cm distance to calculate the regression equation so calculation of absolute pupil diameters from the recorded images could be performed.

Spectral domain optical coherence tomography

Spectral domain optical coherence tomography analysis (SD-OCT) was performed on anesthetized mice (n=22) using a Spectralis SD-OCT (Heidelberg Engineering, Vista, CA) imaging system (Fig. 1 B), coupled with a 25D lens for mouse ocular imaging (Heidelberg Engineering, Vista, CA). Mice were anesthetized using 2.5% halothane and 100% oxygen mixture on a heating pad to maintain body temperature. Pupils were dilated using a 1% tropicamide solution. The cornea was moisturized with a saline solution, which was applied every 20-30 seconds. Circular scans around the optic nerve region were performed to quantify NFL thickness in the temporal, superior, nasal and inferior retinal quadrants. Circular scans were subsequently analyzed by including or excluding blood vessels from the RNFL thickness calculation, since blood vessels in rodents are almost completely embedded in the RNFL[235] and are included in automated RNFL measurement routines by all commercially available systems. Linear scans were also performed in the superio-temporal region of the retina (*area centralis)* in order to evaluate total retinal thickness, thickness of the photoreceptor layer and the RNFL thickness. Total of 25 linear scan lines were positioned in the superio-temporal retina. The most superior linear scan line was positioned 2.5 – 3 mm superior/1.5 – 2 mm temporal to the optic nerve head.

Statistical analysis

All statistical analyses were carried out using GraphPad Prism 5.0 (GraphPad software, San Diego, CA). Paired t-tests, one-way ANOVA with Bonferroni's post test, or repeated measures ANOVA with Bonferroni's post test analysis were used as described in the text. Differences between groups were considered statistically significant for $p < 0.05$.

Results

Pattern Electroretinography

Average pERG amplitudes were 9 ± 0.6 µV (N35-P50, mean ± SEM) and 11.2 ± 0.7 µV (P50-N95, Fig. 3A). Repeated measurement of pERG amplitudes in the same mice (four different recording sessions with a 7 day time interval between sessions for the same animal) revealed no significant inter-session difference compared to initial baseline recordings ($p=0.4$, Repeated Measures ANOVA with Bonferroni post test analysis, Fig. 3 B). The intra-animal variability across recording sessions was 1.9 ± 0.1 µV, with a 27.1 ± 2.7% coefficient of variation. Additionally, comparison of pERG amplitudes from the right and left eye revealed no significant interocular variability for the N35-P50 ($p = 0.5$, Paired t-test) or P50-N95 amplitudes ($p = 0.1$, Paired t-test). The pERG implicit times were: 29.3 ± 1.8 ms (N35), 78.4 ± 3.5 ms (P50) and 168.9 ± 6.6 ms (N95), with durations of 49.2 ± 3.2 ms (N35-P50) and 90.4 ± 5.4 ms (P50-N95, Fig. 3 C, D). In order to observe the effect of aging on the pERG response, recordings were conducted at 3 months, 11 months and 15 months of age on the same animals (Fig. 4). The average N35-P50 amplitude was 4.3 ± 0.9 µV, 6.6 ± 1.1 µV, and 6.2 ± 1.4 µV at 3 months, 11 months, and 15 months of age, respectively (Fig 4A). The average P50-N95 amplitude was 8.7 ± 1.3 µV, 7.9 ± 0.5 µV, 7.9 ± 1 µV at 3 months, 11 months, and 15 months of age, respectively (Fig. 4B). The average N35-P50 latency was 42.1 ± 5.3 ms, 58.5 ± 13.2 ms, and 56.7 ± 9.3 ms at 3 months, 11 months, and 15 months of age, respectively (Fig 4C). The average P50-N95 latency was 86 ± 14.3 ms, 137.4 ± 18.1 ms, and 123.9 ± 14.4 ms at 3 months, 11 months, and 15 months of age, respectively (Fig 4D). No statistically significant difference was observed in both amplitudes and latencies at different ages (Repeated Measures ANOVA with Bonferroni post test analysis: N35-P50

amplitude, p = 0.3; P50-N95 amplitude, p = 0.8; N35-P50 latency, p = 0.5; and P50-N95 latency, p = 0.1).

Chromatic Pupillography

The visual pigments present in the mouse retina (Fig. 5) have been previously characterized [236-238], and their differential contribution to the pupil light reflex has been utilized to characterize the functional properties of different retinal neuronal cells [211]. For red light stimulus the pupil constriction was 3.3 ± 0.4% of baseline size (0 log units), 6.6 ± 0.7% (0.6 log units), 14 ± 1.2% (1.2 log units), 21.13 ± 1.8% (1.8 log units), 25.9 ± 1.1% (2.4 log units), and 31.6 ± 0.9% (3.0 log units), respectively (Fig 6). However, blue light stimuli resulted in significantly greater pupil constriction for all tested light intensities (Fig 6): 0 log units, 20.3 ± 1.8% ($p < 0.0001$, Paired t-test); 0.6 log units, 30.3 ± 1.5% ($p < 0.0001$, Paired t-test); 1.2 log units, 42.6 ± 1.7% ($p < 0.0001$, Paired t-test); 1.8 log units, 51 ± 2% ($p = 0.0001$, Paired t-test); 2.4 log units, 60.6 ± 2.9% ($p < 0.0001$, Paired t-test); and 3.0 log units, 64 ± 3% ($p < 0.0001$, Paired t-test).

Pupil constriction in response to light of different wavelengths was also characterized with the Melan-100 instrument using higher light intensity (200 kcd/m^2). Baseline pupil diameters calculated prior to illumination in dim light conditions were 2.1 ± 0.05 mm (Fig. 7 A, D). The pupil diameter after constriction in response to red (630 nm) light stimulation was 1.1 ± 0.05 mm (Fig. 7 B, D). Stimulation with blue light induced significantly greater constriction of the pupil to a diameter of 0.56 ± 0.03 mm, compared to stimulation with red light (Fig. 7 C, D; $p < 0.001$, Paired t-test). The pupil constricted by 44.3 ± 3.3% (mean ± SEM) of the baseline value with red light stimulus, and the pupil constricted by 71.8 ± 1.9% of the baseline value with blue light stimulus.

Optical Coherence Tomography

Spectral-domain OCT was used to non-invasively analyze the RNFL and total retinal thickness *in vivo*. SD-OCT analysis revealed a total retinal thickness of 229.5 ± 1.7 µm (Fig. 8A, 9A; mean ± SEM) in the *area centralis* of healthy mouse eyes. The photoreceptor layer

thickness was 83.8 ± 0.7 µm, with RNFL thickness of 29 ± 0.5 µm in the region of the retina that corresponds to the *area centralis* (Fig. 8A, 9A). The thickness of the RNFL using circular scans and automated segmentation protocols was 46.7 ± 0.9 µm (temporal), 46.1 ± 0.9 µm (superior), 45.8 ± 0.9 µm (nasal) and 48.4 ± 1 µm (inferior) (Fig. 8, 9). The thickness of the RNFL did not vary between quadrants ($p = 0.1$, ANOVA with Bonferroni's post test). Analysis of RNFL thickness by excluding blood vessels thickness from the calculation was 22.8 ± 0.6 µm (temporal), 24.4 ± 0.5 µm (superior), 24.3 ± 0.6 µm (nasal) and 23.6 ± 0.8 µm (inferior) (Fig. 8B, 9C). The thickness of the RNFL did not vary between quadrants ($p = 0.2$, ANOVA with Bonferroni's post test). Exclusion of blood vessels from the analysis resulted in significantly decreased RNFL thickness for all tested quadrants when compared to values obtained with inclusion of blood vessels: temporal ($p<0.0001$, Paired t-test), superior ($p<0.0001$), nasal ($p<0.0001$) and inferior quadrant ($p<0.0001$).

Discussion

Repeated measurements of RGC structural and functional parameters are essential for following temporal disease progression or treatment effectiveness in different models of retina and optic nerve diseases. In this study we have characterized the normative values for healthy adult C57BL/6 mice using pattern electroretinography, chromatic pupillography and optical coherence tomography.

Pattern electroretinography has been successfully used in a rodent model of hereditary glaucoma (DBA/2J) to detect RGC deficits[239]. The baseline values reported for young DBA/2J mice prior to loss of RGCs were 8.15 ± 0.4 µV, which are similar to values obtained from adult healthy mice in our study. Repeatability is particularly important if pERG is to be used as a longitudinal tool to monitor RGC function for comparative purposes during disease progression or treatment effectiveness in the same animal. We have demonstrated that pERG recordings did not have significant intersession differences from baseline in our experimental conditions. The lateral eye position of rodents necessitates recording either one eye at a time or using two different stimulus monitors simultaneously; in our study, we have recorded one eye at a time using a single stimulus monitor, similar to previously published studies [239,240]. The experimental setup that we used did not result in a significant interocular difference of

pERG amplitudes or implicit times between right and left eyes, providing an opportunity to effectively monitor temporal RGC function in each eye. Furthermore, we have demonstrated that the RGC function does not vary significantly as mice age from 3 to 15 months. The pERG amplitudes and latencies at 11 months and 15 months of age did not change significantly from earlier recordings on the same mice at 3 months of age.

The PLR is an objective measure of retina and optic nerve function. The PLR has been used to monitor functional deficits caused by retina and optic nerve diseases in laboratory animals[195,196,241-243]. Recently, chromatic PLR analysis has been used in clinical settings in humans[244-246] and dogs[211] to monitor the rod-cone mediated and melanopsin mediated PLR responses. White light has been traditionally used for PLR analysis both clinically and experimentally. Since white light is a mixture of wavelengths of the visible spectrum (including red and blue), differentiation of rod-cone and ipRGC-mediated PLR activity cannot effectively be achieved with white light stimuli. As previously shown in healthy dogs[211], we have demonstrated that red light causes significantly less pupil constriction when compared to the blue light stimulation in healthy mouse eyes. Since blue light of 480 nm wavelength can activate all visual pigments in the mouse retina except the UV cone opsin, this type of stimulus provides the most robust activation of the PLR response. Based on the spectral properties of photosensitive pigments in mice, the red light (630 nm) can activate rhodopsin and M-cones, but not UV cones and the intrinsic photosensitive pigment melanopsin[247,248], which provides an opportunity for the specific evaluation of rod-cone mediated functional properties by measuring the red light mediated PLR responses. It has been previously shown that the ipRGCs project to midbrain structures and can mediate PLR activity and photopic blink response even in the complete absence of rod-cone input[249]. Furthermore, a subset of ipRGCs projects to the region of the lateral geniculate nucleus (LGN) and can mediate irradiance dependent firing rates of almost 40% of neurons in the LGN[250]. While the small number of ipRGCs in the mammalian retina does not suggest a primary role of ipRGCs in visual processing, a recent study has demonstrated that rod and cone deficient mice can still effectively recognize pattern gratings in a visual maze test using only melanopsin-mediated light processing [251]. Because the peak of melanopsin activation occurs near 480 nm (blue light)[247], and melanopsin cannot be activated by red light (630 nm),

red light based routines for evaluation of PLR can be effectively used to evaluate the status of RGC dendritic synaptic connections in cases where the rod and cone electrical activity is completely normal. A defect in the red light pupil response (rod-cone mediated signaling to ipRGCs) coupled with a normal blue light pupil response (suggestive of the normal ipRGC function) and normal scotopic and photopic ERG responses could be potentially indicative of a dysfunction in the RGC dendritic network. Chromatic PLR evaluation could be used for monitoring early retinal functional deficits in transgenic mouse models, or as an objective test for evaluation of the retina and RGC function as a result of experimental therapeutic treatments. Defects of the pupillary light reflex after illumination with the red and blue light in the presence of normal scotopic and photopic ERG responses would indicate a problem with the ipRGC soma, axons or higher processing areas of the brain (pretectum) or more distal nerve or iris muscle deficits. Considering that rod-cone mediated pupil input has to converge to ipRGCs which have large diameter axons, compressive optic nerve lesions and inflammatory optic nerve conditions theoretically could selectively impair this cell population resulting in decreased or absent PLR response while still sparing majority (or some) of smaller diameter RGCs resulting in the presence of some functional vision (Grozdanic et al, ACVO Abstract, San Antonio, TX, 2006). However, a majority of clinical and experimental conditions that we have evaluated during the last 5 years using chromatic PLR testing in different animal species are frequently characterized by an intact ipRGC mediated response to blue light illumination - even in cases where complete blindness based on visual behavior is already present[211].

While pERG and PLR are functional monitoring techniques that can detect functional deficits before any structural retina or retinal nerve fiber layer (RNFL) changes occur, observation of structural retina parameters remains a very frequently utilized measure of therapeutic outcome in animal models of ophthalmic diseases. Spectral domain OCT is a tool that has been extensively used to diagnose and monitor diseases of the eye and retina including glaucoma[6], retinitis pigmentosa[7], and macular degeneration[8]. Measurements of macular volume[252] and RNFL thickness[253] using OCT have also been used to estimate overall neuronal loss in patients with multiple sclerosis, while one recent clinical study has demonstrated inner retina thinning in patients with idiopathic Parkinson's disease[254].

Considering the diversity of transgenic mouse models for ophthalmic and neurodegenerative diseases, it is likely that SD-OCT imaging will become a useful technique for evaluation of structural optic nerve properties in many different animal disease models. Similar to recently published results with the use of adaptive optics and 78D lens[11], we have demonstrated that by using a 25-diopter lens, high quality OCT scans of the mouse retina can be obtained. It has been previously demonstrated that automated RNFL analysis routines overestimate RNFL thickness due to the inclusion of blood vessels in the RNFL thickness calculation[255]. We have also demonstrated a substantial increase in the RNFL thickness when blood vessels were included in the calculation. Since blood vessels are predominately embedded within the RNFL in a majority of animal species, a subtle increase or decrease in RNFL thickness could be potentially masked by change in the blood vessel diameter due to the overwhelming contribution of the blood vessels to the RNFL thickness calculations with conventional SD-OCT software.

There are several limitations which can decrease the effective use of the cPLR and SD-OCT responses for evaluation of the retina and optic nerve status. Mice with severe forms of iris atrophy or prominent intraocular inflammation can have significantly attenuated PLR responses, while the application of topical ocular medications with miotic or mydriatic action can also have a significant effect on the resting pupil diameter and overall pupil motility. Furthermore, CNS and peripheral nerve abnormalities, which can be frequently present in different transgenic mouse models affecting any of the subthalamic PLR centers or efferent PLR pathway components, can have significant effects on the quality of PLR responses, which may be a potentially limiting factor during cPLR testing routines. Similarly, limitations in pupil dilatation may have the potential effect on the quality of SD-OCT imaging. Presently, we are developing automated OCT segmentation software routines that are specific for mouse retina which are likely to improve further the application of OCT in mouse species.

Detailed *in vivo* analysis of functional and structural retina and RGC parameters can provide a significant advantage during evaluation of transgenic animal models of human ocular and neurodegenerative diseases. Introduction of these techniques may result in a significant

acceleration developing new therapeutic strategies, since all observed techniques are commonly utilized in human patients, which may allow for a rapid translation of animal study results to human patient population. Considering that the mouse is probably the most frequent experimental animal species encountered by veterinary ophthalmologists during toxicity and clinical safety/efficacy studies, the availability of normative pERG, chromatic PLR and OCT data may provide useful information for more specific evaluation of functional and structural retinal properties in this particular animal species.

Acknowledgements

This work was supported by the Department of Veterans Affairs Center for Prevention and Treatment of Vision Loss (CPTVL), VA RRD Grants C3919R and C4702R, Iowa Center for Advanced Neurotoxicology (ICAN) and the NIH (1R01EY019294).

Figures

Figure 1

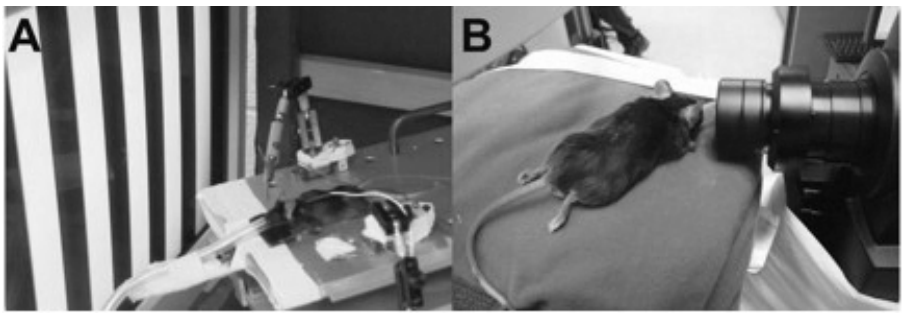

Figure 2

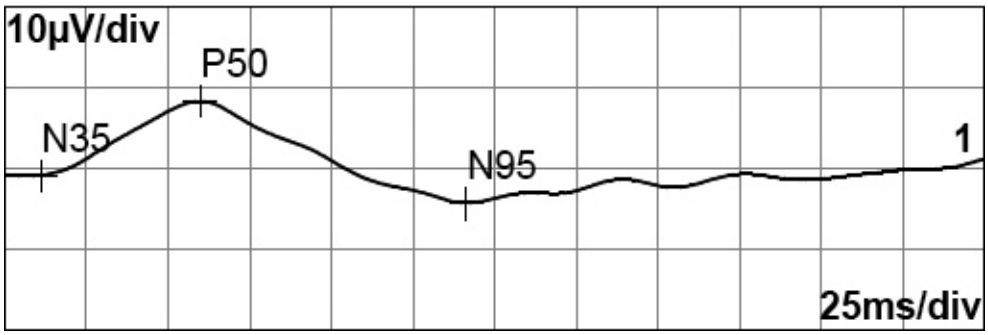

Figure 3

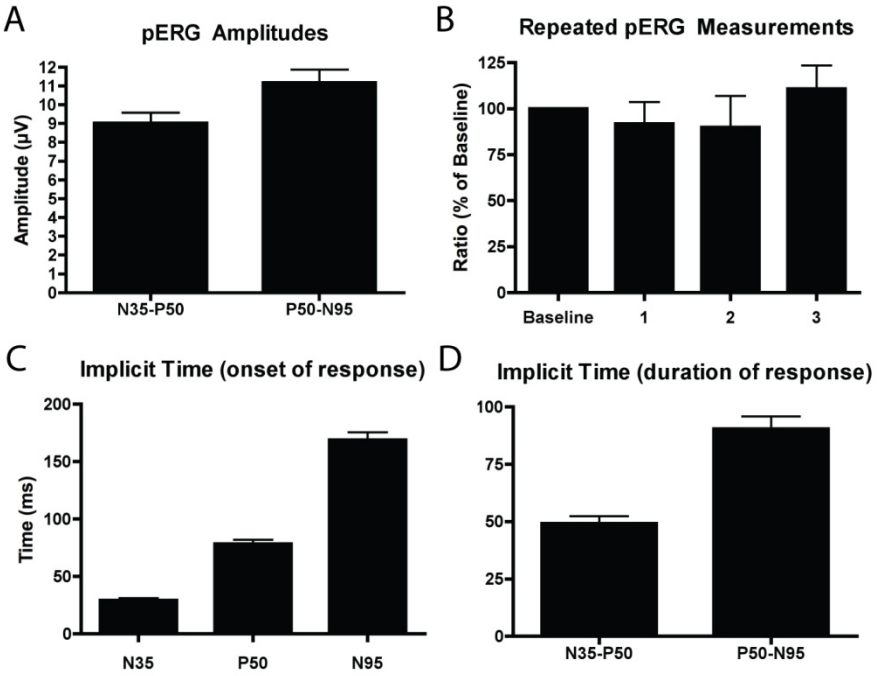

Figure 4

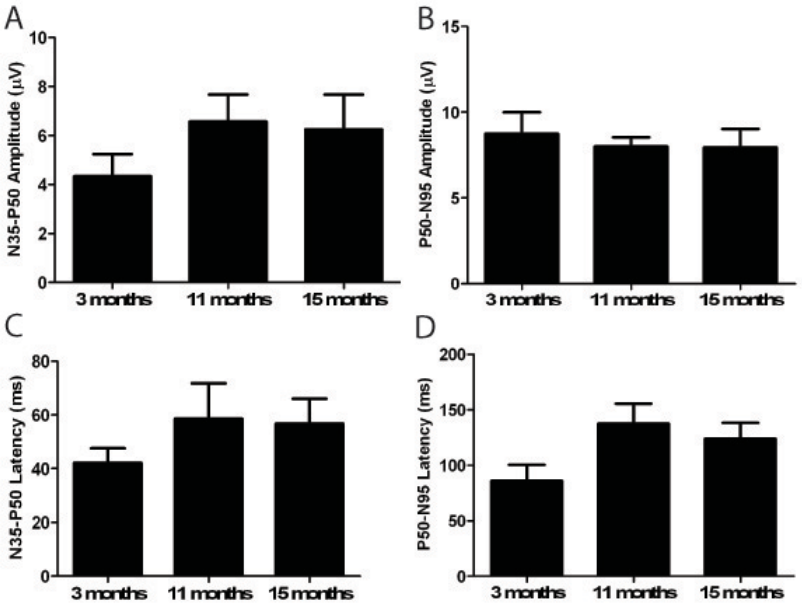

Figure 5

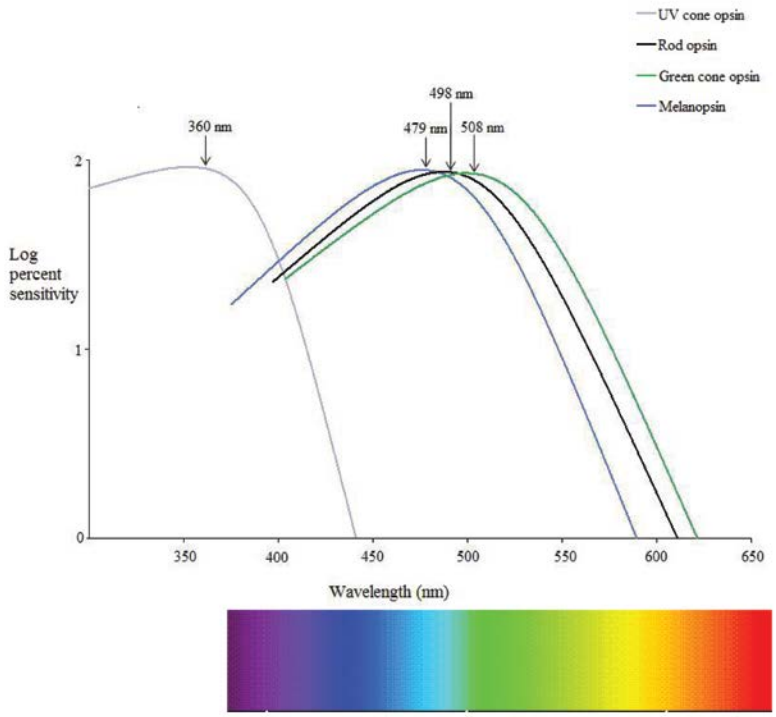

Figure 6

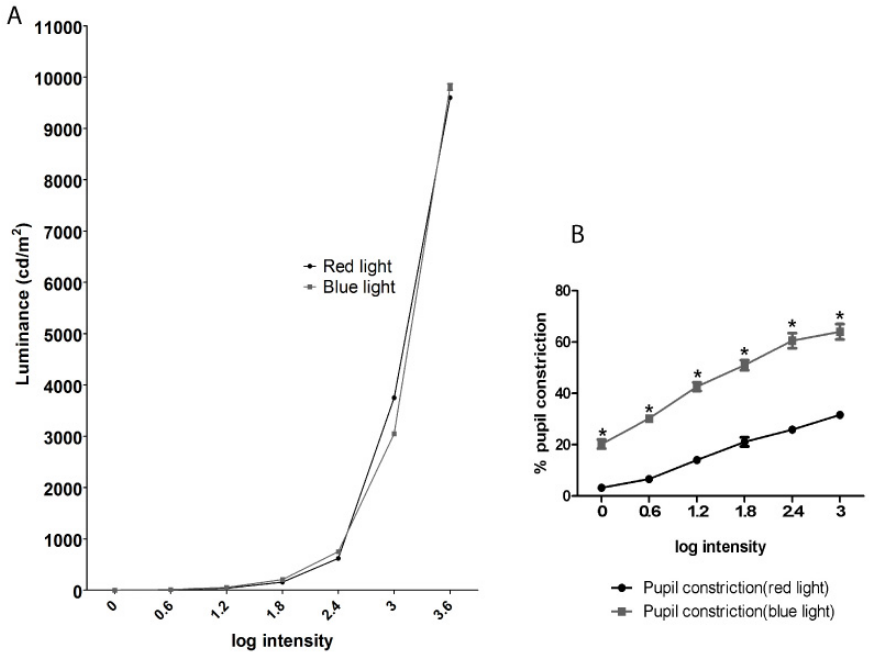

Figure 7

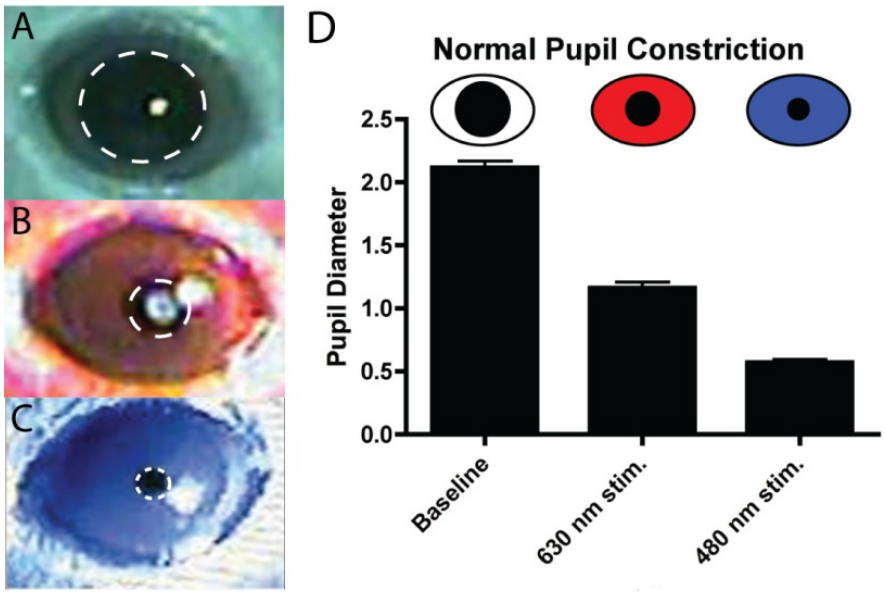

Figure 8

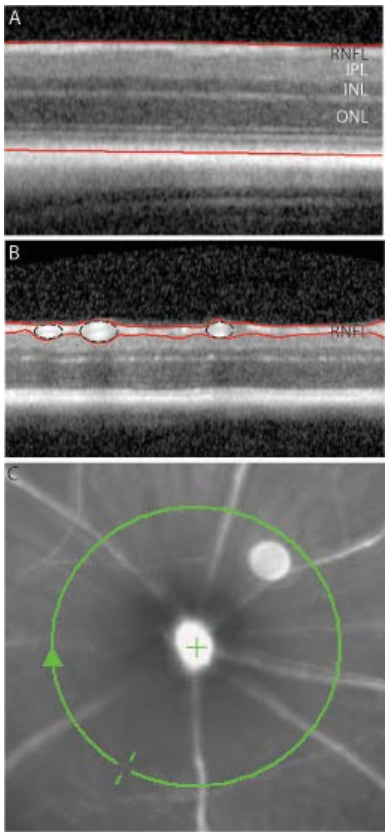

Figure 9

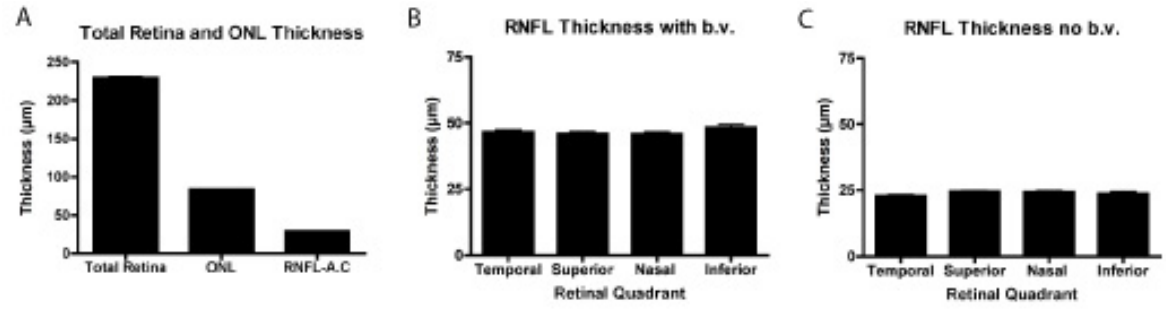

Figure Legends

Figure 1: A) Pattern ERG recording in mice. The mouse is positioned on a heated table and placed 20 cm from the stimulating screen. The position of the table and eye orientation is carefully controlled to provide consistent placement of the animal eye in front of the stimulating monitor. B) OCT recording in mice. A special 25D lens is attached to the SD-OCT Spectralis system for performing OCT imaging in mouse eyes. Anesthetized mice are kept warm by placement on a heating pad for the duration of the recording.

Figure 2: Representative mouse pERG tracing. Amplitudes are calculated for N35-P50 and P50-N95 intervals. It is considered that P50-N95 amplitude represents electrical activity of the retinal ganglion cell body and dendritic tree as a result of cell membrane depolarization.

Figure 3: Pattern ERG responses in healthy mice. A) Average pERG N35-P50 and P50-N95 amplitudes. B) Repeated measurement of pERG amplitude (amplitudes are presented as a ratio against the very first recording) in the same mice did not reveal significant differences ($p > 0.1$, Repeated Measures ANOVA). C, D) Analysis of implicit times showed higher implicit time for specific components of pERG waveform in mice when compared to previously reported values in humans and dogs.

Figure 4: Effect of age on pattern ERG responses in healthy mice. A, B, C, D) There was no statistically significant difference in amplitudes (A, N35-P50 amplitude; B, P50-N95 amplitude) and latencies (C, N35-P50 latency; D, P50-N95 latency) between 3, 11, and 15 month old mice.

Figure 5: Spectral properties of visual pigments in mice. Mouse retina has following visual pigments: rod opsin (λ_{max} at 498 nm), and two cone opsins (the UV cones with λ_{max} at 360 nm and the green cones with λ_{max} at 508 nm). In addition to these photoreceptor pigments, a specific subset of ganglion cells (intrinsically photosensitive retinal ganglion cells, ipRGC) contains the photopigment melanopsin, which has λ_{max} at 479 nm. Therefore, when red light of 620-630 nm wavelength is used as a stimulus, only the green cones and rods are activated. However, when blue light of wavelength 480 nm is directed on the retina, all retinal photopigments (with exception of UV cones) are activated. This difference in spectral properties can be utilized to identify functional deficits in specific cell types within the retina (Figure modified from Lucas, Douglas et al. 2001).

Figure 6: Chromatic pupil light reflex evaluation in mice using A-2000. A) Luminance of red and blue lights for different illumination parameters (0, 0.6, 1.2, 1.8, 2.4, 3 log (lux) units) was measured using a photometer. B) Significantly higher pupil constriction was observed following blue light stimulus when compared to the red light stimulus for all tested light intensities (* $p<0.0001$).

Figure 7: Chromatic pupil light reflex in mice using Melan-100. Representative images of pupil A) baseline diameter, and after stimulation with B) red (630 nm, 200 kcd/m^2) or C) blue (480 nm, 200 kcd/m^2) light. D) Pupil diameter variation from baseline following stimulation with red and blue light.

Figure 8: Optical coherence tomography. A) Retina linear scans were used to evaluate the total retinal thickness and to calculate the thickness of the outer nuclear layer (photoreceptor bodies) and the RNFL in the superior retina (*area centralis* region). B) Peripapillary scans were used to determine the RNFL thickness in the temporal, superior, nasal and inferior retinal quadrants. Area of blood vessels is demarcated with dashed circles. C) Fundus image of a mouse eye demonstrating area of the circular scan (grey circle). Abbreviations: RNFL – retinal nerve fiber layer; IPL– inner plexiform layer; INL – inner nuclear layer; ONL – outer nuclear layer.

Figure 9: SD-OCT retinal thickness parameters in healthy mice. A) Total retinal thickness, photoreceptor layer thickness, and RNFL thickness at the *area centralis* region, measured using SD-OCT. B) Circular scan analysis of the RNFL thickness with inclusion of blood vessels in the RNFL profile - there was no significant difference in RNFL thickness in different quadrants. C) Circular scan analysis of the RNFL thickness without inclusion of blood vessels in the RNFL profile showed significantly smaller thickness compared to values obtained by calculations performed by standard software routines (with inclusion of blood vessels) presented in image B. ONL – outer nuclear layer, AC – area centralis, b.v. – blood vessel.

CHAPTER III. PROTEIN KINASE C DELTA MEDIATES RETINAL GANGLION CELL FUNCTION LOSS FOLLOWING MPTP TREATMENT IN MICE

A manuscript prepared for submission to Investigative Ophthalmology and Visual Sciences, 2012

K. Mohan, M.M. Harper, A. Ghosh, V. Ananthram, A.G Kanthasamy, A. Kanthasamy, R.H. Kardon, S.D. Grozdanic

Abstract

Purpose: To characterize the functional and structural changes of the retina in a rodent model of Parkinson's disease (PD) using electroretinography (ERG), optical coherence tomography (OCT), and histology analysis and study the role of protein kinase C delta (PKCδ) in mediating these changes.

Methods: Pattern evoked electroretinography (pERG) and full field ERG were used to objectively evaluate retinal ganglion cell and total retinal function. Baseline amplitudes and latency were evaluated in wild type and PKCδ$^{-/-}$ mice prior and after induction of PD phenotype. A PD phenotype was created by injection of 1-methyl-4-phenyl-1,2,3,6-tetrahydropyridine (MPTP). OCT and histology analysis were used to evaluate retinal morphological changes.

Results: Analysis of the acute MPTP model of PD in wild-type mice revealed a significant decrease in the P50-N95 amplitude (4.42±0.4 µV) at 48 h post MPTP treatment when compared to baseline recordings (P50-N95 amplitude, 8.78±0.5 µV; $p<0.0001$, Paired t-test). Full field ERG analysis showed significant deficits in oscillatory potentials, however the maximum scotopic a- and b-wave amplitudes were not significantly reduced. A significant increase in the retinal nerve fiber layer thickness was observed by OCT analysis at 4 months after acute MPTP treatment. The P50-N95 amplitude (7.77±0.6 µV) in the MPTP-treated PKCδ$^{-/-}$ mice did not differ significantly from baseline (pre MPTP amplitudes) P50-N95 amplitudes (9.505±0.69 µV).

Conclusion: Visual dysfunction in the mouse MPTP model of PD is characterized by a significant loss of retinal ganglion cell function and structure, which may be partially mediated by PKCδ.

Introduction

Parkinson's disease (PD) is a progressive neurodegenerative disorder with clinical symptoms of tremor, rigidity, and akinesia[256]. A pathological hallmark of PD is the selective loss of dopaminergic neurons in the substantia nigra pars compacta (SNpc) with a concurrent reduction of dopamine in the striatum[62]. Although PD is predominantly associated with movement disorders, different types of visual deficits have been reported in human patients. A loss in visual contrast sensitivity[112] and spatiotemporal contrast sensitivity[113], [114] has been reported among PD patients. Additionally, visual acuity has been reported to decline progressively over time with disease progression in a small group of PD patients[111]. Delays in visual-evoked potentials were initially reported in PD patients by Bodis-Wollner and Yahr[257]. The full field electroretinogram (ERG) amplitudes have also been shown to be decreased in PD patients[258], while dopamine deficiency has been found to influence the multifocal ERG amplitudes[259]. Pattern-evoked electroretinography (pERG) is a sensitive, non-invasive tool for the measurement of retinal ganglion cell (RGC) function. Several studies have demonstrated a decrease in pERG amplitudes associated with early and advanced PD in human patients[260], [261], [262], in addition to alterations in the amplitudes and latencies of the pERG[130], [262]. It has been hypothesized that visual dysfunction in PD may be caused by disruption of the retinal dopaminergic neuronal system[263], [264]. A recent morphological study of the retina in PD patients using optical coherence tomography showed significant nerve fiber layer (NFL) loss even prior to the development of any visual deficits[265], further enhancing the need to more critically address functional and structural retina changes in PD patients.

The principal purpose of this study was to evaluate retinal changes in a rodent model of PD that develops clinical symptoms of PD as a result of exposure to 1-methyl-4-phenyl-1,2,3,6-tetrahydropyridine (MPTP). MPTP was identified to cause a PD-like phenotype in humans[63], and has been frequently used as a neurotoxin capable of destroying nigrostriatal

dopaminergic neurons and inducing PD phenotypes in different animal species[62]. Optical coherence tomography, full field electroretinography, pattern electroretinography and histology analysis were used to perform detailed retinal functional and structural analysis in this animal model with an ultimate goal of establishing a better understanding of the possible pathological effects of PD on the retina and optic nerve. Several recent studies have implicated protein kinase C delta in development of PD pathology[266-268]. We have evaluated the role of PKCδ the development of retinal abnormalities in the mouse model of MPTP induced PD.

Materials and Methods

Animals and MPTP treatment

A total of forty C57Bl/6 mice and eight PKCδ$^{-/-}$ mice were housed under standard conditions: constant temperature (22 ± 1°C), humidity (relative, 30%), and a 12 h light/dark cycle with access to food and water, *ad libitum*. PKCδ$^{-/-}$ animals were obtained from the animal breeding facility of Dr. Anumantha Kanthasamy's laboratory (Department of Biomedical Sciences, Iowa State University, Ames, Iowa). All animals were evaluated by pattern electroretinography, full-field electroretinography, and optical coherence tomography to rule out the presence of ocular diseases before inclusion in the study. For induction of acute MPTP toxicity mice received four intraperitoneal injections of MPTP-HCl (18 mg/kg of free base; Sigma-Aldrich) dissolved in saline at 2 h intervals as previously reported [269]. Control animals received only saline injections. Mice were euthanized and prepared for analysis 48-72 h post-treatment. The sub-chronic MPTP treatment involved one dose of MPTP (30 mg/kg), repeated daily over 5 days. Mice were sacrificed 16 days after the first injection. All animal studies were conducted in accordance with the ARVO Statement for the Use of Animals in Ophthalmic and Vision Research and were approved by the Iowa State University Institutional Animal Care and Use Committee.

Pattern electroretinography

Pattern evoked electroretinography (pERG) was used to objectively measure the function of RGCs by recording the amplitudes and latency of N35-P50 and P50-N95 pERG waveforms.

Mice (Acute MPTP, wild-type n = 22, PKCδ$^{-/-}$ n = 8; Sub-chronic MPTP, wild-type n = 10) were anesthetized with a mixture of 75% oxygen, 25% nitrous oxide and 3.5% halothane. After induction, mice were placed on a stainless steel recording table equipped with a hot-water based warming platform to maintain body temperature and the halothane concentration was decreased to 1.75%. Mice were positioned 20 cm from the stimulus monitor with their head angle tilted at 45 degrees to provide direct exposure of the pattern stimulus to the visual axis of the recorded eye. Pattern ERG responses were evoked using alternating, reversing, black and white vertical stimuli delivered on a CRT monitor with a Roland Consult ERG system (Roland Consult, Brandenburg, Germany). Each animal was placed at the same fixed position in front of the monitor to prevent recording variability due to animal placement. Stimuli (9° full field pattern, 1 Hz frequency, 200 averaged signals with cut off filter frequencies of 1-30 Hz) were delivered in photopic conditions, since slow stimulation speed in mesopic and scotopic conditions can elicit rod-mediated full field ERG responses, which can completely conceal the pERG responses in rodents. Visually evoked responses were evaluated by measuring the amplitudes (N35-P50 and P50-N95) and corresponding implicit times (latency) of the waveform.

Spectral domain optical coherence tomography

Spectral domain optical coherence tomography (SD-OCT) analysis was performed on anesthetized mice using Spectralis SD-OCT (Heidelberg Engineering, Vista, CA) imaging system, coupled with a 25D lens for mouse ocular imaging (Heidelberg Engineering, Vista, CA). Mice (n = 8) were anesthetized using 2.5% halothane and 100% oxygen mixture on a heating pad to maintain body temperature. Pupils were dilated using a 1% tropicamide solution. The cornea was moisturized with a saline solution, which was applied every 20-30 seconds. Linear scans were collected from the superior-temporal region of the retina, which corresponds to the *macular region* in primates in order to evaluate the RNFL thickness.

Full-field electroretinography

Mice (n = 4) were dark adapted for 12 h prior to recordings. Mice were anesthetized with a mixture of 75% oxygen, 25% nitrous oxide and 3.5% halothane, while anesthesia was

maintained using a mixture of 75% oxygen, 25% nitrous oxide and 1.75% halothane. After induction, mice were placed on a stainless steel recording table equipped with a hot-water based warming platform to maintain body temperature. The mice were positioned inside a Ganzfeld stimulating globe. The luminance in all globe quadrants was 1600 ± 200 cd/m^2. A Roland Consult (Brandenburg, Germany) ERG system was used to deliver stimuli triggered output to the flash stimulator and to collect signals from both eyes using custom made mouse gold ring lens electrodes (Roland Consult, Brandenburg, Germany). The maximum scotopic rod-cone response was recorded, with the stimulus delivered at 0.07 Hz frequency (low-cut amplifier frequency, 1 Hz; high-cut amplifier frequency, 300 Hz; 8 averaged responses per recording session). Oscillatory potentials (OPs) were recorded by delivering light stimuli at a 0.07 Hz frequency (low-cut amplifier frequency, 200 Hz; high-cut amplifier frequency, 500 Hz;]; *n* = 8 stimuli were averaged). The photopic flicker response was recorded using from light adapted animals by delivering light stimuli at a 20 Hz frequency (low-cut amplifier frequency, 1 Hz; high-cut amplifier frequency, 300 Hz; *n* = 50 stimuli were averaged).

HPLC analysis

The striatal and ocular dopamine (DA) levels were quantified using high-performance liquid chromatography (HPLC) with electrochemical detection. Samples were prepared and quantified as described previously [270], [271]. Briefly, 48 h after MPTP injection, control (n = 4) and treated mice (n = 10) were sacrificed, striata and eyes were collected and stored at -80°C. Dopamine from tissues was extracted in 0.1 M perchloric acid solutions containing 0.05% Na_2EDTA and 0.1% $Na_2S_2O_5$). Isoproterenol was used as an internal standard. Extracts were filtered in 0.22 µm spin tubes and 20 µl of the sample was loaded for analysis. Dopamine was separated isocratically in a reversed-phase C-18 column using a flow rate of 0.7 ml/min. An HPLC system (ESA Inc., Bedford, MA, USA) with an automatic sampler equipped with a refrigerated temperature control (model 542; ESA Inc.) was used for these experiments. The electrochemical detection system consisted of a Coulochem model 5100A with a microanalysis cell (model 5014A) and a guard cell (model 5020) (ESA Inc.). Standard stock solutions of catecholamines (1 mg/ml) were prepared in perchloric acid solution and further

diluted to a final working concentration of 50 pg/µl prior to injection. The data acquisition and analysis were performed using the EZStart HPLC Software (ESA Inc.).

FluoroJade B analysis for dying neurons

FluoroJade B (HistoChem Inc., USA) is an anionic fluorescein derivative that stains dying neurons with high specificity. The FluoroJade B working solution (0.0008% in 0.1% acetic acid) was prepared fresh before use. Tissue sections embedded in paraffin (Control, n = 9; WT MPTP, n = 19; PKC$\delta^{-/-}$, n = 7) were initially warmed for 15 min at 50°C and washed in xylene for 5 min. This was followed by graded ethanol series (100% - 5 min, 90% - 5 min, 70% - 5 min) and a 5-min wash in bidistilled water. The slides were then incubated with shaking in a 0.06% potassium permanganate solution for 30 min. Following a 2 min wash with bidistilled water, slides were incubated in .0004% FluoroJade solution for 30 min. Slides were washed thrice with bidistilled water for 1 minute. Excess water was removed, and the slides were dried at room temperature for 5 min, followed by incubation in xylene for 1 min. The slides were then coated using DPX mounting media (Sigma-Aldrich, USA) and microscopy analysis was carried out after 24 h. Cell numbers in the retina were quantified by blinded observers.

Rotarod analysis

The coordinated sensorimotor function (Acute MPTP, n = 19; Sub-chronic MPTP, n = 6) was evaluated using the rotarod test after MPTP injection. The time spent on the rod was observed at two different speeds: 18 rpm - mimicking walking pace, and 26 rpm - mimicking jogging pace. The activity of the mice was recorded prior to and 48 h after MPTP treatment. If the mice remained on the rod for 20 min, the trial was terminated. The average time spent on the rod over 3 trials was recorded. The mice were rested for at least 5-7 minutes in between trials to exclude fatigue.

Open Field test for locomotor activity

The locomotor activity of the mice (acute MPTP, n = 18; sub-chronic MPTP, n = 6) was observed using the VersaMax animal activity monitors (Model RXYZCM-16; Accuscan

Instruments Inc., Columbus, OH). The mice were recorded prior to and following MPTP treatment. The open field maze consists of 4 chambers, each measuring 40 × 40 × 30.5 cm. Infrared monitoring sensors are evenly placed (one every 2.54 cm, to a total of 16 infrared beams) along the perimeter of the maze, at a height of 2.5 cm above the floor. In order to monitor the vertical activity, two additional sets of 16 sensors, 8.0 cm high from the floor, are present on opposite sides. The entire maze, including a ventilated lid, is constructed of clear Plexiglas. Recording was carried out over a 10-minute time interval. The data collected from the test was analyzed using the accompanying VersaMax analyzer (model CDA-8; Accuscan Instruments Inc.).

Statistical analysis

All statistical analyses were carried out using GraphPad Prism 5.0 (GraphPad software, San Diego, CA). Paired t-tests were used to compare pretreatment with post-MPTP treatment values. Student's t-tests, one-way ANOVA with Bonferroni's post-test or Dunnet's multiple comparison tests were used as described in the text. Differences between groups were considered statistically significant for $p < 0.05$.

Results

Characterization of the Parkinsonian phenotype in wild type MPTP treated mice

Coordinated motor activity testing: Prior to MPTP treatment, mice (n = 19) remained on the rod for 889.7 ± 83.47 s (mean ± SEM) and 753.5 ± 100.9 s at 18 rpm and 26 rpm speeds, respectively (Fig 1A). At 48 h following acute MPTP treatment, there was a significant reduction in the time spent on the rotarod, both at 18 rpm (345.6 ± 73.24 s; $p < 0.0001$, Paired t-test) and 26 rpm (166.1 ± 48.77 s; $p < 0.0001$, Paired t-test). In addition, we tested unrestricted movement of the mice in an open field maze (simple motor activity) and recorded their horizontal and vertical activities (Fig 1B, C). Similar to the rotarod, the recordings on the mice were performed at least 2 days prior to MPTP injection. Prior to MPTP treatment, mice (n = 18) had horizontal and vertical activities of 1938 ± 60.25 and 78.06 ± 6.531, respectively. At 48 h after acute MPTP treatment, the horizontal and vertical

activities were significantly reduced to 756.8 ± 129.9 ($p < 0.0001$, Paired t-test) and 13.06 ± 5.237 ($p = 0.0001$, Paired t-test), respectively.

Dopamine quantification: The establishment of the Parkinsonian phenotype was further confirmed by the quantification of striatal and ocular dopamine content using HPLC analysis (Fig 2A). We observed a significant reduction ($p < 0.0001$, Student's t-test) in total dopamine content in the striatum following MPTP treatment (0.8547 ± 0.1857 ng/ml, n = 10) when compared to control tissue (40.63 ± 1.949 ng/ml, n = 4). HPLC analysis was also conducted for dopamine content in the eyes of MPTP treated animals (Fig 2B). Control eyes had 0.0729 ± 0.02449 ng/ml (n = 4) dopamine, while acute MPTP-treated wild-type mice had 0.02913 ± 0.0026 ng/ml (n = 8) dopamine. This reduction in the dopamine content was significant ($p = 0.0048$, Student's t-test).

Pattern ERG analysis of MPTP treated mice

The pERG (representative pERG graph, Fig 3) from all mice (n = 22) was recorded at least 2 days prior to MPTP treatment, and their baseline amplitudes and latencies were recorded (Fig 4). The pretreatment (control) N35-P50 amplitude was 7.039 ± 0.56 µV (mean ± SEM) and the P50-N95 amplitude was 8.78 ± 0.50 µV; the N35-P50 latency was 44 ± 2.21 ms, and the P50-N95 latency was 78.84 ± 4.35 ms. Following acute MPTP treatment (48 h post final injection), pERGs were recorded and we observed significant deficits in both amplitudes and latencies when compared to baseline recording values (Fig 3). We observed N35-P50 amplitude of 4.38 ± 0.43 µV ($p < 0.0001$, Paired t-test) and P50-N95 amplitude of 4.42 ± 0.40 µV ($p < 0.0001$, Paired t-test); the N35-P50 latency was 32.47 ± 2.04 ms ($p = 0.0005$, Paired t-test) and the P50-N95 latency was 53.23 ± 3.47 ms ($p < 0.0001$, Paired t-test).

Sub chronic MPTP treatment

To study the effect of less acute toxic insult, we induced a sub chronic MPTP exposure in wild type mice (n = 10). After baseline values were recorded, the pERG amplitudes in these mice were recorded starting on day 1, 3, 4, 9 and 16 after initiation of MPTP treatment (Fig 5). The baseline N35-P50 amplitude was 5.17 ± 0.65 µV and the P50-N95 amplitude was 7.76 ± 0.82 µV. On day 3, the N35-P50 amplitude was 5.87 ± 0.75 µV and the P50-N95

amplitude was 7.03 ± 0.91 µV. On day 5, N35-P50 amplitude was 4.18 ± 0.49 µV and the P50-N95 amplitude was 4.07 ± 0.36 µV. On day 9, N35-P50 amplitude was 4.44 ± 0.71 µV and the P50-N95 amplitude was 4.68 ± 0.67 µV. On day 16, N35-P50 amplitude was 3.48 ± 0.58 µV and P50-N95 amplitude was 4.02 ± 0.44 µV. We observed a statistically significant reduction in P50-N95 amplitudes at days 9 and 16 (Fig 5 B), when compared to pretreatment values ($p = 0.001$, One-way ANOVA with Dunnet's multiple comparison test). However, only the P50-N95 amplitudes (on these days) were significantly smaller when compared to pretreatment values ($p = 0.001$, One-way ANOVA with Bonferroni's post-test). No significant changes were observed in the rotarod and open field tests following subchronic MPTP treatment (data not shown).

Full field ERG analysis of MPTP treated mice

Analysis of the full-field ERG was carried out using the ISCEV protocol. Baseline recordings were obtained on all mice at least 2 days prior to acute MPTP treatment. Full field ERGs were then recorded again 48 h post acute MPTP treatment. We observed baseline amplitudes of 144 ± 21 µV ($n = 4$) for the scotopic combined a-wave, 903.9 ± 45.5 µV ($n = 4$) for the scotopic combined b-wave, and 693.2 ± 30.19 µV ($n = 4$) for oscillatory potentials (Fig 6). Following acute MPTP treatment, we observed a significant reduction of oscillatory potentials (551.8 ± 25.17 µV; $p = 0.0112$, Paired t-test). However, the amplitudes of the scotopic combined a-wave (114.6 ± 25.33 µV; $p = 0.3899$, Paired t-test) and b-wave (796.4 ± 47.72 µV; $p = 0.1274$, Paired t-test) did not differ significantly from pretreatment values.

Optical coherence tomography analysis of RNFL thickness in MPTP treated mice

The structural retinal integrity following the acute MPTP treatment was evaluated using optical coherence tomography. The linear scans of the superior-temporal retina (area centralis) from the region corresponding to macula in primates were analyzed for thickness of the retinal nerve fiber layer (RNFL, Fig 7A). Baseline recordings were obtained at least 2 days before initiating the acute MPTP treatment. The pretreatment RNFL thickness were 42.05 ± 0.97 µm ($n = 4$). At 4 months post acute MPTP treatment, we observed a significant increase in the RNFL thickness (47.95 ± 1.38 µm; $p = 0.0277$, Paired t-test) (Fig 7B).

RGC function is significantly preserved in protein kinase Cδ deficient mice after MPTP treatment

In order to evaluate whether PKCδ has a role in the RGC deficits induced by the MPTP treatment, we evaluated mice genetically deficient for PKCδ ($PKC\delta^{-/-}$) (n = 8). Baseline pERG amplitudes (before MPTP treatment) were not significantly different in $PKC\delta^{-/-}$ mice when compared to wild type animals (N35-P50 = 8.48 ± 0.51 µV, p = 0.053, Student's t-test; P50-N95 = 9.50 ± 0.69 µV, p = 0.3113, Student's t-test; data not shown). Significantly better pERG amplitudes were observed in $PKC\delta^{-/-}$ mice when compared to the pERG recordings from wild type mice after MPTP treatment. Following acute MPTP treatment, the $PKC\delta^{-/-}$ mice had N35-P50 amplitude of 6.877 ± 0.722 µV, which was significantly higher compared to wild type mice which had N35-P50 amplitudes of 4.38 ± 0.43 µV (p = 0.002, Student's t-test, Fig 8A). Similar results were observed with the P50-N95 amplitude: $PKC\delta^{-/-}$ mice had P50-N95 amplitude of 7.77 ± 0.599 µV, which was significantly higher compared to wild type mice (p = 0.0002, Student's t-test, Fig 8B). We did not observe significant reduction in P50-N95 pERG amplitudes in the $PKC\delta^{-/-}$ mice after MPTP treatment when compared to pretreatment values (p = 0.0585, Paired t-test; data not shown).

Quantification of positively stained cells in the RGC layer (Fig 8C) revealed 3.4 ± 1.07 cells in wild-type control mice (n = 5), 4.7 ± 1.16 cells (n = 7) in wild-type mice treated with MPTP, and 4 ± 1.22 cells (n = 4) in $PKC\delta^{-/-}$ mice treated with MPTP; no significant difference in cell numbers were observed (p = 0.4, One-way ANOVA) among the groups.

A comparison of the coordinated motor activity (rotarod test; Fig 8D) was performed in wild-type and $PKC\delta^{-/-}$ mice. Prior to MPTP treatment, $PKC\delta^{-/-}$ mice spent 680.44 ± 228.16 s (18 rpm) and 306.33 ± 98.81 s (26 rpm) on the rotarod. The acute MPTP treatment resulted in a decrease of rotarod time in wild type and $PKC\delta^{-/-}$ mice. However, $PKC\delta^{-/-}$ mice spent 531.3 ± 38.23 s (18 rpm) and 194.3 ± 23.52 s (26 rpm) on the rotarod, which was significantly better compared to MPTP treated wild type mice: 87.6 ± 17.19 s (18 rpm, $p < 0.0001$, Student's t-test) and 12.5 ± 3.29 s (26 rpm, $p < 0.0001$, Student's t-test).

Discussion

A significant body of literature has described the effects of PD on the retina and higher visual centers, which result in visual abnormalities such as visual hallucinations, decreased visual acuity, decreased color and contrast sensitivity and decreased motion perception [115,264,272-280]. While PD diagnostic and therapeutic strategies are focused on the central nervous system, there is a growing need for a better understanding of PD effects on the retina and optic nerve in PD patients. Data from several studies have described visual abnormalities as a cause for a decreased quality of life in PD patients. This necessitates the development of therapeutic treatments for retina and optic nerve abnormalities for this patient population[264,272].

We have used the well-accepted mouse model of MPTP exposure in order to evaluate the retina and optic nerve abnormalities associated with an experimentally induced PD. Systemically administered MPTP is converted to its toxic cation 1-methyl-4-phenylpyridinium (MPP+) by nondopaminergic neurons and glial cells. Following conversion MPP+ is exported to the extracellular space where it is actively transported in dopaminergic neurons by dopamine transporter system (DAT)[62]. After incorporation in dopaminergic neurons, MPP+ causes mitochondrial impairment, which results in degeneration and death of dopaminergic neurons, a decrease in striatal dopamine levels and a PD phenotype[281].

We have demonstrated that MPTP treatment in mice results in a dramatic reduction of striatal and ocular dopamine levels and also causes significant sensorimotor deficits. Similar results have been previously reported in monkeys and rabbits after acute MPTP exposure[282,283]. We have performed a detailed characterization of retinal ganglion cell function and structure using pERG and OCT analysis and demonstrated significant retina functional and structural deficits as previously reported in human PD patients and an experimentally induced PD-like condition in animals[254,284-286]. It has been previously demonstrated that PD impairs function of the retina dopaminergic system, which primarily results in abnormalities of amacrine cells and retinal ganglion cells dependent on dopamine as a neurotransmitter[132,286-288]. Electrophysiological studies from human patients and experimental PD models showed deficits in oscillatory potentials (generated by amacrine cells) and the P50-N95 component of

the pERG amplitude (generated by retinal ganglion cells)[259,262,287-289]. Histological analysis of human and experimental animal retinal tissue showed degenerative changes and intracellular inclusion accumulation associated with cells in the GCL and INL [283,290,291]. Our functional and structural studies confirmed that a similar type of change exists in a mouse model of MPTP exposure. Furthermore, we have also demonstrated that sub chronic MPTP treatment results in much milder damage. Similar patterns of retinal damage have been described in a primate model of MPTP induced PD[292].

Several studies using OCT analysis of the RNFL in PD patients have shown significant thinning of the inferior peripapillary RNFL[285 254]. Furthermore, an early decrease in RNFL thickness has been reported in PD patients with early clinical signs of the disease, even before the onset of any visual deficits [265]. However, a recent study on 32 patients with PD did not find significant difference in RNFL or macular thickness when compared to healthy control[293]. In our experimental study, we have observed a significant increase in the RNFL thickness at 4 months after acute MPTP treatment. Further, Fluoro-Jade analysis for dying neurons at acute time-points did not reveal significant cell death in the retina. We hypothesize that such an increase in RNFL thickness could be a result of early gliosis at the optic nerve, which could eventually lead to RNFL thinning. Since evaluation of the retina and optic nerve function and structure can be objectively achieved using OCT and ERG, this methodology could also provide a sensitive and objective assessment of therapeutic value of novel PD drugs administered systemically[294,295], especially in the light of recent data which has shown a good correlation between retinal morphological and functional findings and clinical severity scores in Parkinson's disease[284]. These techniques coupled with the power of transgenic mouse models could dramatically accelerate the discovery and objective evaluation of novel drug candidate compounds for treatment of PD.

An important finding of this study is the lack of retinal deficits in PKCδ$^{-/-}$ mice exposed to acute MPTP administration. Previous studies have demonstrated a strong role of PKCδ in dopaminergic neuronal death[266,296,297]. PKCδ is a member of a family of serine- and threonine-specific protein kinases, and may have pro-apoptotic or pro-survival properties[298]. Proteolytic cleavage of PKCδ due to increased activation of caspase-3 (most frequently as a

result of increased oxidative stress) results in the auto-regulatory enhancement of caspase-3 activity and strong pro-apoptotic activity that has been implicated in the degeneration of dopaminergic neurons [266,298]. Furthermore, cleaved PKCδ can phosphorylate phosphatase 2A (PP2A), which results in a dephosphorylation and inhibition of tyrosine hydroxylase and an ultimate decrease in dopamine production.

Our experimental results are strongly suggestive of the important role of PKCδ in retinal deficits, since PKCδ$^{-/-}$ mice had significantly better RGC function observed by pERG analysis when compared to wild-type after MPTP exposure. Considering increased PKCδ expression in brain tissue of human PD patients (A. Kanthasamy, unpublished observation), it is likely that pharmacological targeting of this particular kinase may be a therapeutic strategy for treatment of PD patients[296]. While the goal of any PD treatment remains systemic treatment, which should result in adequate drug levels in the brain, targeting of PKCδ by using topical (eye drop) administration or intravitreal drug delivery may become an important additional therapeutic approach for treatment of PD associated retina and optic nerve abnormalities. Considering that targeted ocular drug delivery could be safely utilized for different pharmacological agents, which may not have adequate systemic therapeutic effects, or have unacceptable side effects after systemic administration, ocular therapeutics may be a relatively safe approach for treatment of PD patients suffering from visual abnormalities.

In conclusion, we have demonstrated that the MPTP inducible model of PD in mice is characterized by significant functional and structural retinal deficits, which correspond well to changes seen in human PD population. Furthermore, we have demonstrated that PKCδ may have an important role in retinal neuronal dysfunction and death in a Parkinson's-like pathology. Considering the availability of different transgenic animals and the extensive molecular tools for mouse studies, it is likely that mouse based studies may provide an opportunity for better understanding of visual system abnormalities associated with PD and the development of novel therapeutic strategies in the future.

Acknowledgements

This work was supported in part by the Department of Veterans Affairs Center for Prevention and Treatment of Visual Loss and a Rehabilitation Research and Development Career Development Award (MMH).

Figures

Figure 1

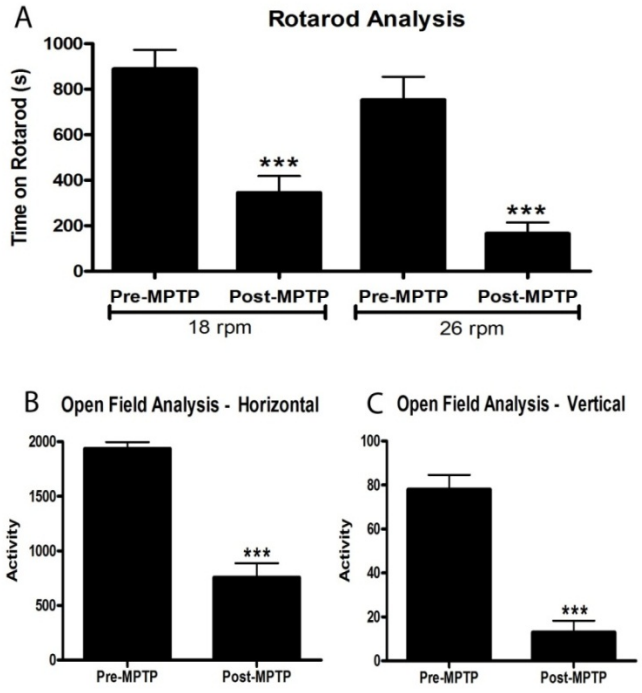

Figure 2

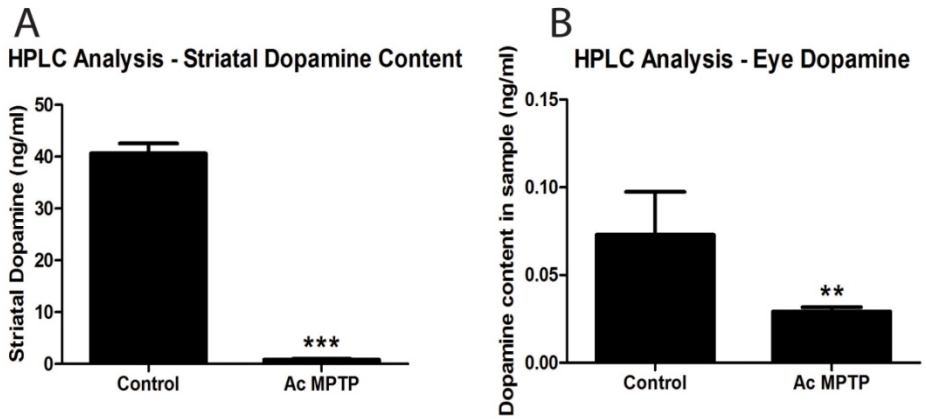

Figure 3

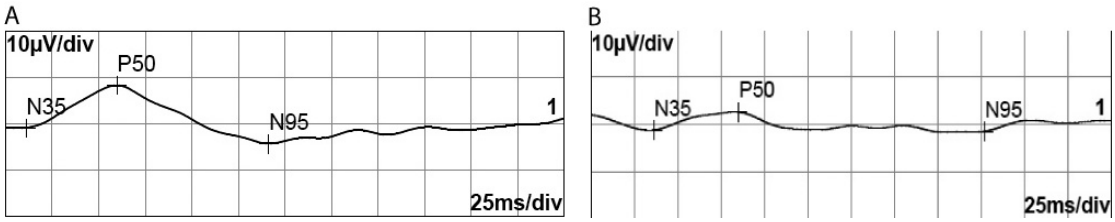

Figure 4

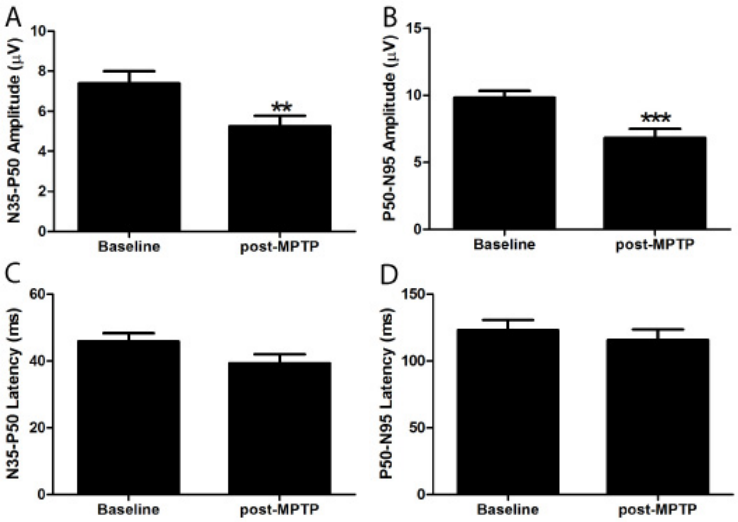

Figure 5

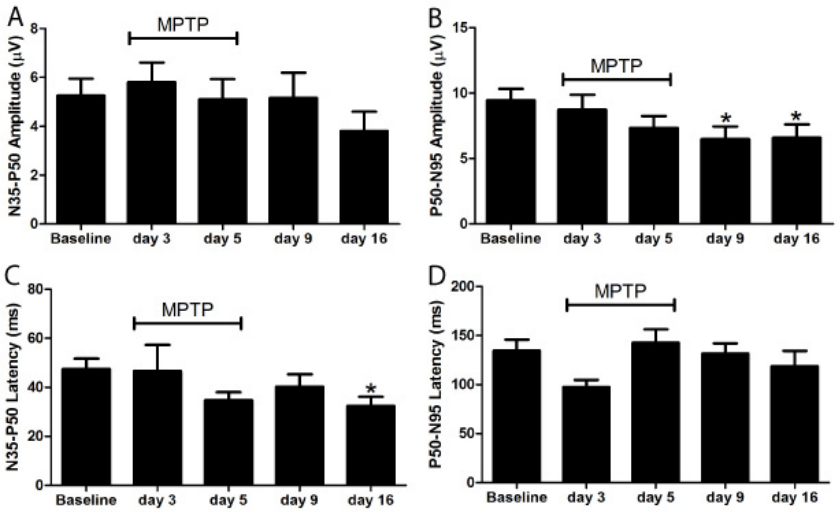

Figure 6

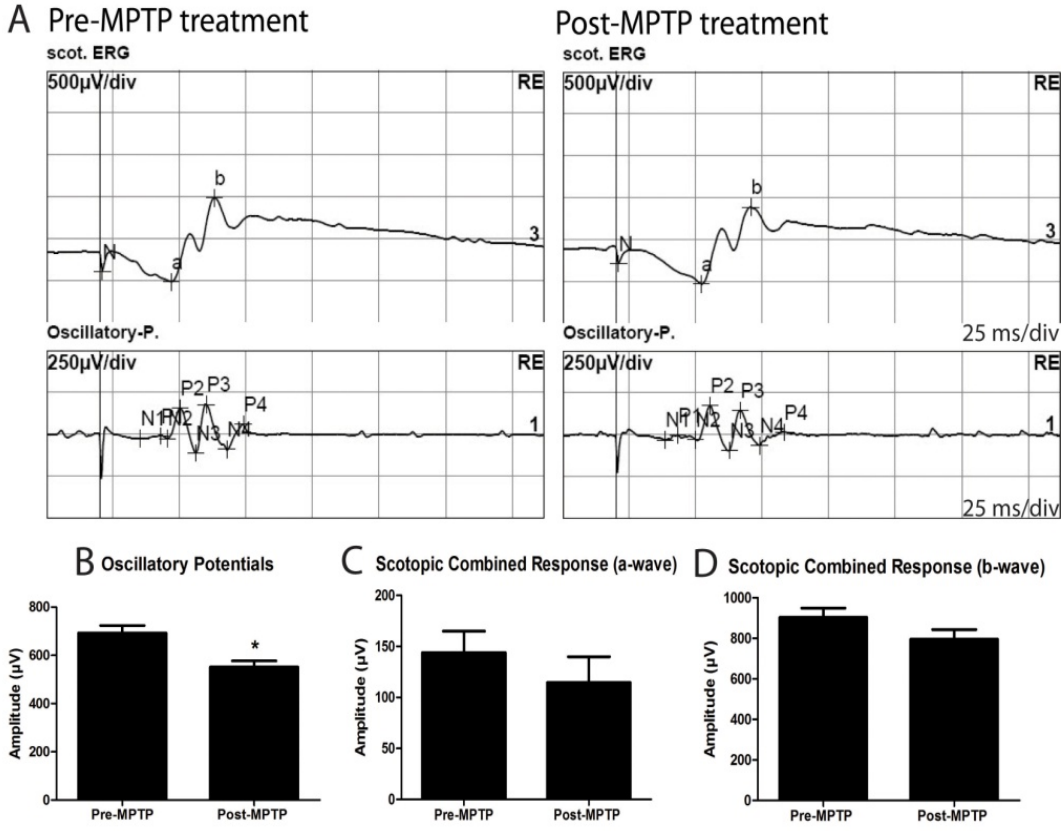

Figure 7

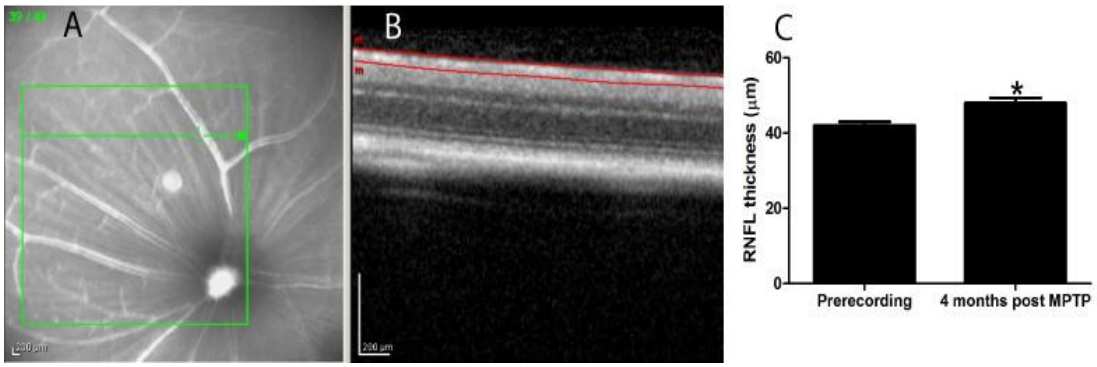

Figure 8

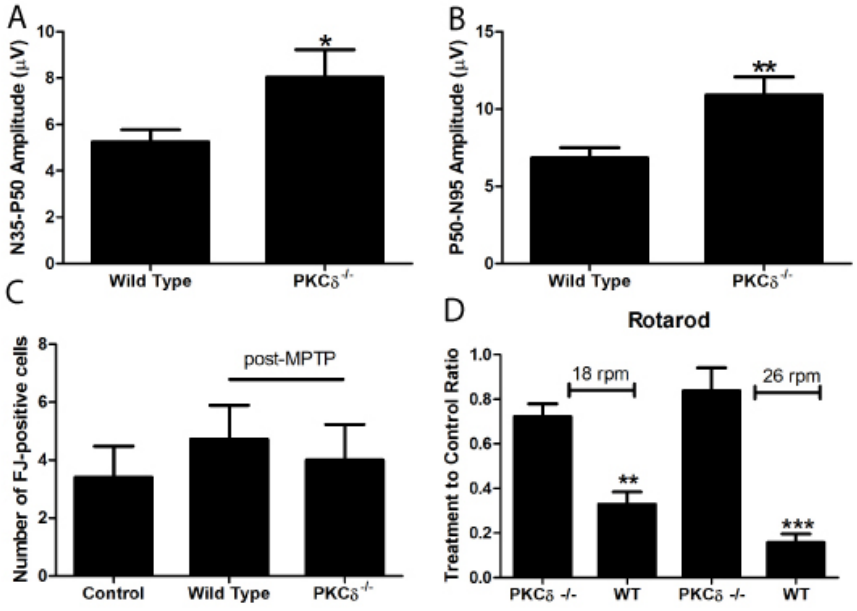

Figure Legends

Figure 1: The establishment of a Parkinsonian phenotype was determined by behavioral tests for the coordinated (A) and simple motor activity (B, C). MPTP treatment caused significant deficits in both tested parameters .Bars represent mean ± SEM.

Figure 2: A reduction in dopamine content is a well-recognized feature of PD. The dopamine content in the striatal region of the brain (A) and in the eye (B) of control and MPTP-treated mice was evaluated. When compared to control tissue, a significant reduction in total dopamine content in the striatum and in the eyes following MPTP treatment was observed.

Figure 3: Representative pattern-evoked electroretinography (pERG) results from control (A) and MPTP treated (B) C57Bl/6 mice.

Figure 4: At 48 h post acute MPTP treatment, we observed significant deficits in both N35-P50 and P50-N95 amplitudes; however, no significant differences were observed in the latencies when compared to baseline recordings.

Figure 5: The sub-chronic MPTP treatment is a less acute insult that helps better mimic actual degeneration that occurs in PD. Recordings were performed out on days 3, 5, 9, and 16 post injection. A reduction in the P50-N95 amplitude was observed on days 9 and 16, and the N35-P50 latency was significantly reduced on day 16 (B, C). No significant differences were observed in the other parameters on the measured days.

Figure 6: Representative full-field ERG results from control and MPTP treated C57Bl/6 mice (A). Following MPTP treatment, a significant deficit in the amplitude of the oscillatory potentials was observed (B). The amplitudes of the scotopic combined response a-wave and b-wave (C, D) did not differ significantly from pretreatment values.

Figure 7: OCT scan analysis of the RNFL revealed a significant thickening in MPTP-treated mice. The OCT scan was recorded from the superior-temporal region, the region of the retina corresponding to the *area centralis* in higher mammals (A). Demarcation of the layers of the retina with a RNFL being delineated with red lines (B). At 4 months post acute MPTP treatment, we observed a significant increase in the RNFL thickness (C).

Figure 8: PKCδ knockout mice exposed to acute MPTP treatment had significantly better N35-P50 (A) and P50-95 amplitudes (B) compared to wild type mice. Quantification of cell death in the RGC layer (C) revealed no significant difference in the number of dying neurons in MPTP-treated wild type mice retina when compared to control and PKC$\delta^{-/-}$ retina. Significant preservation of motor activity, evidenced by performance on the rotarod, was observed.

CHAPTER IV. FUNCTIONAL AND STRUCTURAL EVALUATION OF RETINA AND OPTIC NERVE IN AN EXPERIMENTAL RODENT MODEL OF BLAST EXPOSURE

A manuscript prepared for submission to Investigative Ophthalmology and Visual Sciences, 2012

K. Mohan, M.M. Harper, H. Kecova, E. Hernandez-Merino, S.D. Grozdanic, T. Lazic

Abstract

Purpose: To evaluate retina and optic nerve function and structure after blast exposure.

Methods: Healthy adult male C57/Bl6 mice were exposed to a blast wave (137 kPa) within a blast chamber. Retina and optic nerve function and structure were evaluated using the chromatic pupil light reflex (cPLR), full-field and pattern electroretinography (ERG) and spectral-domain optical coherence tomography (SD-OCT). Histological analysis of the retina and optic nerve was performed at the termination of the study.

Results: A significant decrease in pattern ERG (P50-N95) amplitudes was observed in 1-year-old mice exposed to blast at 2 months (n=9, 6.2±0.6 µV,mean±SEM), 4 months (n=9, 5.5±0.6 µV) and 8 months (n=11, 6.2±0.6 µV) of age when compared to healthy 1-year-old control animals (n=20, 8.5±0.5 µV; p=0.003, one-way ANOVA with Dunnet's multiple comparison test). Assessment of the cPLR demonstrated decreased maximum pupil constriction diameter in blast-injured mice (n=12) using red light (ctrl=1.12±0.05 mm; blast=1.38±0.07 mm; p=0.0063, Student's t-test) or blue light stimuli (ctrl=0.57±0.03 mm; blast=0.71±0.03 mm; p=0.0008, Student's t-test) 24h after blast exposure compared to control mice (n=9). Three months following blast exposure a significant thinning of the superior-temporal peripapillary retinal nerve fiber layer was observed (n=5) compared to control animals (n=11) using SD-OCT (ctrl=61.1±0.9 µm, blast=56.4±1.7 µm; p=0.0217, Student's t-test).

Conclusions: Blast exposure in mice is associated with a mild, but persistent functional and structural optic nerve deficits. Utilization of non-invasive functional and structural

examination techniques may be a useful approach for early detection of visual system abnormalities in blast-exposed subjects.

Introduction

The widespread use of improvised explosive devices (IEDs) in recent military conflicts has increased the prevalence of blast-mediated injuries in soldiers. Blast-mediated injuries are the leading cause of combat-related injuries in Operations Enduring and Iraqi Freedom (OEF/OIF), leading them to be designated as the signature injury of these conflicts[141]. Residual physical symptoms reported after blast exposure include headache, nausea, light and noise sensitivity, and visual disturbances, among others[175]. In addition to the cognitive and neurobehavioral symptoms experienced by soldiers following TBI, a number of somatosensory abnormalities have been documented, with visual and auditory disturbances being predominantly observed[142-145].

Many blast exposed subjects suffer from damage to the visual system[150] and similar visual disturbances have been described also in civilian population after mild, moderate or severe TBI episodes. Lachapelle et al[190] carried out a long-term analysis of visual event-related potentials (VERPs) in 17 patients with mild TBI, who presented deficits in complex visual integrative tests. A significantly delayed latency was observed in texture segregation paradigms by TBI patients. Furthermore, reduced amplitude and delayed latency of the VERP P300 component has been observed in patients with moderate TBI[191]. Recently, chronic visual dysfunction has been documented in subjects with TBI caused by exposure to blast waves[147,299-301]. Cockerham et al[302] reported that 20 of 46 patients with blast-mediated injuries had evidence of closed-globe eye injuries, although the visual acuity of most eyes remained normal. Other visual system disorders in these patients include photosensitivity, oculomotor difficulties, and binocular vision deficits[147-149], which have been found to persist up to one year post-injury[303].

The primary purpose of this study was to characterize retina and optic nerve deficits in a rodent model of blast injury. To achieve this, we have utilized a battery of tools to analyze structure and function of the retina and optic nerve. We have also characterized the

expression of oxidative stress markers in the retina to better understand the molecular consequences of blast exposure.

Methods

Animals

All animal studies were conducted in accordance with the ARVO Statement for the Use of Animals in Ophthalmic and Vision Research and were approved by the Iowa City Veterans Affairs Institutional Animal Care and Use Committee. Adult healthy male C57BL/6 mice (8 weeks old) were used for the purpose of this study.

Blast injury

Mice were anesthetized using the 4% halothane with 0.8 L/min oxygen flow using the custom made blast chamber (BioMed Vision Technologies, Ames, IA). The blast chamber had two parts divided by opening which was fitted with a plastic mylar membrane that ruptures at 20 ± 0.2 psi (mean ± SEM) pressure. Once when one part of the chamber is pressurized and reaches the pressure of 20 psi, the mylar membrane ruptures, resulting in the blast wave propagation in the chamber. Mice were subsequently positioned in the animal holder, which was padded to prevent blunt head injury against the rigid walls of the animal holder. The animal holder is fixed within the blast chamber with the left side of the head oriented toward the blast opening at a distance of 30 cm (Fig. 1). A continuous flow of 4% halothane anesthesia was maintained while the mouse was in the chamber using a soft flexible nose cone connected through a one-way port in the side of the blast chamber. Only the head of the mouse was exposed, with the rest of body was shielded from the blast wave, with a goal of preventing interaction of blast wave with any body structures beside the head region. Immediately following exposure to the blast wave animals were placed on a heating pad and provided with 100% oxygen to facilitate recovery from general anesthesia and to prevent hypothermia. Analgesic agent (buprenorphine – 0.01 mg/ml) was provided in drinking water for 5 days after blast exposure.

Pattern electroretinography

Pattern evoked electroretinography (pERG) was used to objectively measure the function of the retinal ganglion cells by recording the amplitude and latency of the pERG waveform. Mice (n=79) were initially anesthetized with 3.5% halothane and 0.8 L/min oxygen until unresponsive to the righting reflex. They were subsequently maintained using 1.75% halothane, 0.8 L/min oxygen, and 0.4 L/min nitrous oxide for the duration of recording. The mice were placed on a stainless steel recording table equipped with a hot-water based warming platform to maintain body temperature. Pupils were dilated using a 1% tropicamide solution. The mice were positioned 20 cm from the stimulus monitor with the head angle tilted at 45 degrees to provide direct exposure of the stimulus to the visual axis of the recorded eye. Pattern ERG responses were evoked using alternating, reversing, black and white vertical stimuli delivered on a monitor with a Roland Consult ERG system (Roland Consult, Brandenburg, Germany). Each animal was placed at the same fixed position in front of the monitor to prevent recording variability due to animal placement. Stimuli (9° full field pattern, 1 Hz frequency, 200 averaged signals with cut off filter frequencies of 1-30 Hz, 98% contrast, 80 cd/m^2 monitor illumination intensity) were delivered under photopic conditions, since slower stimulation rates in mesopic and scotopic conditions can elicit rod-mediated full field ERG responses, which can completely conceal the pERG response. The pERG response was evaluated by measuring the amplitude (N35-P50 and P50-N95) and implicit time of the waveform. Implicit times were calculated for the N35-P50 and P50-N95 components.

Full-Field Electroretinography

Mice (n=17) were dark adapted for 12 hours prior to recording the full-field ERG. Animals were initially anesthetized with 3.5% halothane and 0.8 L/min oxygen until unresponsive to the righting reflex. Animals were subsequently maintained using 1.75% halothane, 0.8 L/min oxygen, and 0.4 L/min nitrous oxide for the duration of recording. Pupils were dilated using 2.5% phenylephrine and 1% tropicamide applied to the cornea. Animals were positioned on a heated stage to maintain body temperature during anesthesia and recording sessions. Ground and reference electrodes were placed subcutaneously in the tail and forehead of the animal, respectively. A solid recording electrode (Roland Consult) was

placed on each eye in contact with the cornea, and a thin layer of methylcellulose was used to maintain contact between the cornea and electrode and to decrease the recording noise. Following placement of the electrodes, animals were dark adapted for an additional 30 minutes prior to recording. An automated ERG protocol was used to evaluate the electroretinographic parameters. The ERG recordings were performed using the Reti-Port system (Roland Consult). Scotopic rod responses (illumination 0.22 cd/m^2, cut off frequency 1-300Hz, n = 8 responses were averaged) were collected first, followed by the scotopic maximum combined response (78 cd/m^2, 1-300 Hz, n = 8 responses were averaged), oscillatory potentials (78 cd/m^2, 200-500 Hz, n=8 responses were averaged), photopic cone response (21 cd/m^2 rod bleaching background light in combination with 78 cd/m^2 stimulation, 1-300 Hz, n = 8 responses were averaged), and the flicker ERG response (78 cd/m^2, 1-300 Hz, n = 50 responses were averaged). The ERG responses were subsequently analyzed using the RETIport32 software (Roland Consult).

Phenol red thread tear test

Zone-Quick (Showa Yakuhin Kako Co. Ltd., Japan) phenol red thread (PRT) test (n=9) was used to analyze tear production. The test uses a sterilized PRT that changes color from yellow to red when in contact with tears. With one end bent, the thread can be placed onto the palpebral conjunctiva. Once the thread was placed on the lower eyelid, 30 seconds were counted, following which, the thread was removed. The length of color change from yellow to red was recorded.

Chromatic Pupil Light Reflex

The chromatic pupil light reflex (cPLR) evaluation was performed using a Melan-100 instrument (BioMed Vision Technologies, Ames, IA,). Mice (n=35) were awake during the recording session and were held still using minimal manual restraint. Recording sessions in most animals lasted less than one minute. The intensity of the diode based light sources were: 630 ± 3 nm for red light, luminance 200 kcd/m^2, and 480 ± 3 nm for blue light, luminance 200 kcd/m^2. Baseline pupil diameter measurements in mice were taken in darkness prior to illumination using an infrared video camera (Sony Handycam, Sony Corporation). A red light stimulus with a two second duration was used to illuminate one

eye of the mouse at a distance of 4 cm from the ocular surface. The direct pupil constriction responses were recorded from the illuminated eye with a digital infrared camera. Prior to performing illumination with the blue light, pupils were allowed to completely dilate to baseline diameter. Captured digital movies of pupil responses were analyzed using Adobe Photoshop (v. 10.0.1, Adobe Systems, Inc.). A calibrated dot grid with dot sizes of 0.5, 1, 1.5, 2 and 3 mm in diameter was recorded from a distance of 4cm to calculate a regression equation so calculation of the absolute pupil diameter from the recorded image could be performed.

Spectral domain optical coherence tomography

Spectral domain optical coherence tomography (SD-OCT) analysis was performed on anesthetized mice (n=16) using a Spectralis SD-OCT (Heidelberg Engineering, Vista, CA) imaging system, coupled with a 25D lens for mouse ocular imaging (Heidelberg Engineering, Vista, CA) 3 months following blast injury. Mice were anesthetized using a 3% halothane and 0.8 L/min oxygen mixture on a heating pad to maintain body temperature. Pupils were dilated using a 1% tropicamide solution. The cornea was moisturized with a saline solution, which was applied every 20-30 seconds. Circular scans around the optic nerve region were performed to quantify the retinal nerve fiber layer (RNFL) thickness. Circular scans were subsequently analyzed by including or excluding blood vessels from the RNFL thickness calculation, since blood vessels in rodents are almost completely embedded in the RNFL[235] and are included in automated RNFL measurement routines.

Histopathology and morphology analysis of the retina and optic nerve

Immunohistochemical procedures were used to examine the expression profile of proteins associated with oxidative and endoplasmic reticulum stress in the retina after blast-mediated injury. Briefly, paraffin embedded sections of the retina were re-hydrated using xylene and decreasing concentrations of ethanol followed by a final rinse with potassium phosphate buffered solution (KPBS). Heat-mediated antigen retrieval was performed using citrate buffer. Tissue was incubated in a blocking solution containing 0.1% bovine serum albumin (BSA, A9647, Sigma), 0.04% Triton X-100 (Fisher), and 5% normal donkey serum (NDS,

017-000-121, Jackson ImmunoResearch, West Grove, PA) in KPBS. Primary antibodies (Table 1) were diluted in blocking solution and incubated overnight at room temperature. Tissue was rinsed with KPBS containing Triton X-100, and incubated with Cy-3 conjugated secondary antibodies for 2 hours. Following rinses, 4', 6'-diamidino-2-phenylindole, dilactate (DAPI, 1 µg/ mL, D3571, Sigma) was applied for 30 min at room temperature in order to visualize nuclei. Slides were mounted with an anti-fade mounting media and sealed. Negative controls were processed in parallel by omission of the primary or secondary antibody. Tissue was examined using a Leica DM5000B microscope. Micrographs were prepared using Adobe Photoshop (CS3, Adobe, San Jose, CA) and Adobe Illustrator (CS3).

Ultrathin sections of optic nerves were examined by electron microscopy. Briefly, optic nerves (dissected 1 mm posterior to the sclera) were postfixed in a solution containing 2% paraformaldehyde-2% glutaraldehyde in 0.1 M phosphate buffer (pH 7.4) and then rinsed in cacodylate buffer, postfixed in 2% osmium tetroxide in cacodylate buffer, dehydrated in alcohol, and embedded in epoxy resin. Cross sections (1 µm thick) were cut with an ultramicrotome, mounted on glass slides and stained with 1% toluidine blue.

Results

Blast exposure

The method of blast injury described here (Fig. 1) resulted in 3% mortality of mice exposed to the blast wave within the first two minutes after injury. All surviving animals had physiologically normal appearance 60 minutes after blast exposure, including normal motility, grooming and behavior. We did not observe delayed mortality at later times due to blast exposure.

Pattern Electroretinography

For analysis of the pERG parameters acutely following blast exposure, the baseline pERG response amplitudes and latencies from all mice (n =30) were recorded at least 2 days prior to blast exposure (Fig 2). Animals were euthanized at each time point after pERG recording and tissue collected for histological analysis. The pre-recorded baseline N35-P50 amplitude

was 5.6 ± 0.44 µV (Fig 2A; mean ± SEM). Following blast exposure, pERGs were recorded at 1 hour (n=11), 12 hours (n=9), and 24 hours (n=10) post injury. A statistically significant reduction was observed in the N35-P50 amplitude at 1 hour (3.5 ± 0.4 µV; p=0.01, Student's t-test) and 12 hours (3.1 ± 0.5 µV; p=0.002, Student's t-test) post injury, when compared to baseline values. However, this N35-P50 amplitude recovered to the baseline amplitude values at 24 hours (6.8 ± 1.2 µV; p = 0.5022, Student's t-test) after injury (Fig. 2 A). The baseline P50-N95 amplitude was 9.3 ± 0.5 µV (Fig. 2 B). Following blast exposure, significantly reduced P50-N95 amplitudes of 6 ± 0.7 µV (p = 0.0012, Student's t-test) and 5.7 ± 0.9 µV (p = 0.0007, Student's t-test) were observed at 1 hour and 12 hours post blast, respectively, when compared to the pre-recorded baseline amplitude. No significant difference in the P50-N95 amplitude was observed at 24 hours (9.4 ± 0.9 µV; p = 0.9, Student's t-test) post injury.

The baseline N35-P50 latency was 52.3 ± 3.4 ms (Fig. 2 C, mean ± SEM). The N35-P50 latency was significantly decreased at 1 hour (39.8 ± 6.9 ms; p = 0.02, Student's t-test) and 12 hours (33.8 ± 3.9 ms; p = 0.005, Student's t-test) following blast exposure, when compared to baseline latency. However, no statistically significant reduction was observed at 24 hours post injury (46.7 ± 4 ms; p = 0.51, Student's t-test). The baseline P50-N95 latency was 123.8 ± 6.8 ms (Fig. 2 D). There was not a significant difference in the P50-N95 latency at 1 hour (130.8 ± 15 ms; p = 0.86, Student's t-test), 12 hours (116.8 ± 16.1 ms; p = 0.5, Student's t-test) or 24 hours (124.2 ± 14.2 ms; p = 0.98, Student's t-test) post injury, when compared to the baseline value.

In order to observe the effect of aging on chronic pERG parameters, mice were exposed to blast at different ages and their pERG was recorded at 1 year of age (Fig 3). Mice were randomly selected to be exposed to blast at either 2 months (n = 9), 4 months (n = 9), or 8 months (n = 11) of age; pERG recordings were then carried out at 10 months, 8 months, or 4 months post blast exposure, respectively. At 1 year of age, the N35-P50 amplitude was 6.2 ± 0.7 µV in healthy control mice (n = 20; mean ± SEM). The N35-P50 amplitudes of the 1-year-old blast-exposed mice (4 months post blast, 4.6 ± 0.7 µV; 8 months post blast, 5.6 ± 0.7 µV; 10 months post blast, 5.4 ± 0.8 µV) were not significantly reduced when compared

to age-matched controls (Fig 3A; p = 0.47, ANOVA with Dunnet's multiple comparison test). Healthy 1-year-old control mice had P50-N95 amplitude of 8.5 ± 0.5 µV. However, the P50-N95 amplitudes of the 1-year-old blast-exposed mice (4 months post blast, 6.2 ± 0.6 µV; 8 months post blast, 5.5 ± 0.6 µV; 10 months post blast, 6.2 ± 0.6 µV) were significantly reduced when compared to age-matched controls (Fig 3B; p = 0.003, ANOVA with Dunnet's multiple comparison test).

The N35-P50 latency in healthy 1-year-old control mice was 52.7 ± 5.7 ms (mean ± SEM). The N35-P50 latency of 1-year-old blast-exposed mice (4 months post blast, 43.1 ± 5.8 ms; 8 months post blast, 49.8 ± 5.3 ms; 10 months post blast, 44.1 ± 9 ms) were not significantly different from age-matched controls (Fig 3C; p = 0.61, ANOVA with Dunnet's multiple comparison test). The P50-N95 latency in healthy 1-year-old control mice was 122.9 ± 10.3 ms. The P50-N95 latency of 1-year-old blast-exposed mice (4 months post blast, 123.1 ± 13.2 ms; 8 months post blast, 88.6 ± 8.8 ms; 10 months post blast, 116.7 ± 19.1 ms) were not significantly different from age-matched controls (Fig 3D; p = 0.35, ANOVA with Dunnet's multiple comparison test).

Full field ERG

The baseline amplitudes of healthy control mice (n=7) were 146.0 ± 35.95 µV for the scotopic maximum combined a-wave, 274.5 ± 67.31 µV for the scotopic maximum combined b-wave, 253.2 ± 54.42 µV oscillatory potential summation, and 20.57 ± 4.69 µV for the flicker response (P1-N3 amplitude) (Fig 4). There was not a significant difference in the full-field ERG response 7 days after blast exposure (n=10) for the scotopic maximum combined a-wave (Fig. 4 A; 214.9 ± 22.68 µV, p = 0.1088, Student's t-test) or b-wave (Fig 4 B; 427.4 ± 45.60 µV, p = 0.0694, Student's t-test). Additionally, we did not detect significant differences in the oscillatory potentials (Fig 4 C; 332.7 ± 49.83 µV, p = 0.3060, Student's t-test) or P1-N3 flicker response amplitude (Fig 4 D; 24.62 ± 3.64 µV, p=0.5000, Student's t-test) seven days after injury.

Tear production

Tear production was tested using the phenol red thread (PRT) test in blast-exposed mice (9 months post blast, n = 4) and age-matched healthy control mice (n = 5). The length of color change on the PRT was 10.3 ± 1.1 mm (Fig. 5, mean ± SEM) and 10.5 ± 1.3 mm in healthy controls and blast-exposed mice, respectively. No significant difference was observed between both groups (p = 0.99, Student's t-test).

Chromatic Pupil Light Reflex

The cPLR was used to determine the effects of blast exposure on the retina and optic nerve using red (630 nm) or blue (480 nm) light one day post-injury. The resting baseline pupil diameter in scotopic conditions was not significantly different between control (n=9) and blast injured (n=12) animals (Fig. 6 A, ctrl = 2.11 ± 0.05 mm; blast = 2.11 ± 0.04 mm; p = 0.9914). The pupil diameter in healthy control mice decreased to 1.12 ± 0.05 mm and 0.57 ± 0.03 mm after stimulation with red (630 nm) or blue (480 nm) light, respectively (mean ± SEM). Blast exposure caused a significantly weaker pupillary constriction after stimulation with red (Fig 6 B, 1.38 ± 0.07mm, p = 0.0063, Student's t-test) and blue (Fig. 6 C, 0.71 ± 0.03, p = 0.0008, Student's t-test) light compared to healthy control mice.

To observe whether cPLR deficits persisted chronically following blast exposure, a similar analysis was carried out at 10 months post blast injury. The resting baseline pupil diameter in scotopic conditions was not significantly different between age-matched control (n=5) and blast injured (n=9) mice (Fig. 6 D, control = 2.5 ± 0.06 mm; 10 months post blast = 2.6 ± 0.04 mm; p = 0.74, Student's t-test). Following stimulation with red (630 nm) or blue (480 nm) light, the pupil diameter in healthy control mice decreased to 1.2 ± 0.07 mm and 0.7 ± 0.08 mm, respectively (mean ± SEM). No statistically significant difference was observed in the pupillary constriction of blast-exposed mice after stimulation with red (Fig 6 E, 1.3 ± 0.06 mm, p = 0.36, Student's t-test) and blue (Fig. 6 F, 0.68 ± 0.04, p = 0.41, Student's t-test) light compared to age-matched healthy control mice.

Optical Coherence Tomography

Optical coherence tomography (OCT) was used to analyze the thickness of the retinal nerve fiber layer (RNFL) from the superior-temporal region of the retina (Fig. 7). Age-matched healthy control mice (n = 11) were compared to mice that were 3 months post blast exposure (n = 5). The RNFL thickness in control mice was 61.1 ± 0.9 µm (mean ± SEM). Three months after blast exposure, there was a significant decrease in the RNFL thickness (56.4 ± 1.7 µm, p = 0.0217, Student's t-test) when compared to control.

Histological analysis of the retina and optic nerve

Pathologic analysis of the retina demonstrated a reduction in cellularity in the GCL following blast injury when compared to healthy control mice (Fig. 8). Analysis of ultrastructural optic nerve integrity using electron microscopy revealed decreased axon density and glial scarring 10 months after blast injury in mice (Fig. 9).

Immunohistochemistry

Blast injury resulted in an acute upregulation of proteins associated with oxidative stress. Analysis of 4-HNE (a marker for oxidative stress and lipid peroxidation) showed significantly increased immunoreactivity in the retina of animals exposed to blast (n=12) as compared to healthy controls (n=4) (Fig. 10 A; Control - $1.2 \times 10^{-6} \pm 2.5 \times 10^{-7}$ (mean ± SEM); 1 hour post blast - 0.6 ± 0.1; p = 0.04, Student's t-test). Evaluation of iNOS expression showed a trend toward increased immunoreactivity in blast-injured mice (n=12) when compared to controls (n=21) (Fig. 10 B; control - 0.57 ± 0.16, 1 hour post blast - 0.91 ± 0.19), however the difference was not statistically significant (p = 0.08, Student's t-test). One hour post blast injury, beta amyloid immunoreactivity was significantly increased in the retina of animals exposed to blast injury (n=10) when compared to healthy control eyes (n=20) (Fig. 10 C, control - 0.4 ± 0.11, 1 hour post blast - 1.0 ± 0.2, p=0.03, Student's t-test). However, no statistically significant difference was observed when 12 hours (n=6) and 24 hours (n=10) post blast exposure were included in the analysis (12 hours post blast - 0.6 ± 0.2; 24 hours post blast – 0.8 ± 0.2; p = 0.18, One-way ANOVA with Dunnet's multiple comparison test).

Discussion

Many retrospective studies conducted on soldiers returning from the recent wars have found increased incidence of visual disturbances following exposure to blast wave[150,151,155,178,303]. A recent study by Brahm et al [150] found 33% of all returning veterans to have some form of visual dysfunction primarily due to blast exposure. Commonly reported visual symptoms include diplopia, fixation instability, nystagmus, and blurred vision; in addition, abnormal vestibular ocular reflex, convergence insufficiencies, corneal injury, and oculomotor palsies have been observed clinically[149].

In our study we have demonstrated that a single blast exposure episode results in the mild functional and structural damage to the optic nerve. Subsequent histological analysis demonstrated very minimal and focal axonal damage in optic nerves of mice exposed to the blast. We have demonstrated that functional recording (pERG) of optic nerve function seems to be the most sensitive test for detection of blast-induced optic nerve abnormalities.

Previous studies showed that functional evaluation of evoked potentials (EP) and event-related potentials (ERP) can be potentially utilized in the assessment of the CNS functional status and prediction of ultimate clinical outcome after TBI[181]. Of these, visual ERP (VERP) are valuable indicators of visual pathway integrity and cognitive function. In a VERP study on 17 patients with mild TBI [190], TBI patients presented with deficits in complex visual integrative tests and significantly delayed latencies in texture segregation paradigms compared to control subjects. Several studies have also documented abnormalities in the visual P300 component in patients with mild and moderate TBI[189,191,192].

While the vast majority of studies in human patient population described visual disturbances in blast patients, which could be predominantly attributed to the damage in the brain centers or efferent pathways controlling the oculo-motor control, there are relatively sparse data about the effect of blast exposure on the retina and optic nerve function. In this study we have demonstrated that even single episode of relatively mild blast exposure may result in detectable damage to the optic nerve. Our experimental design could not effectively address the possible mechanism of the optic nerve injury after blast exposure, however previous studies suggested that rapid propagation of the blast wave results in shearing forces, which can particularly damage long axonal tracts. This notion is potentially supported by previous studies which demonstrated diffuse axonal injury (particularly in long axonal tracts) in

experimental animal models of blast exposure by using the shock tube [161-165]. Two experimental studies looks specifically in the morphological properties of the optic nerve after TBI. In one study, rats exposed to blast overpressure of 129-173 kPa had extensive axonal degeneration of the optic nerve, optic tracts, lateral geniculate body, and superior colliculus[170]. A recent study using the fluid percussion model of TBI has demonstrated possible damage to the optic nerve vasculature at the level of bony canal resulting in Wallerian degeneration within 48 hours of injury[171].

Our study has several important findings related to the mechanism of blast-induced optic nerve injury. It seems that even relatively mild blast exposure can result in the minimal, but detectable optic nerve damage, which creates the concern about the optic nerve status in individuals exposed to the multiple blasts over the course of active duty. Our study is also suggestive of the possible immediate nature of the optic nerve injury, which does not seem to have a progressive nature. Our molecular data support this notion, since it seems that the most prominent change occurs in the early period post blast exposure (1 h post blast) with gradual normalization of changes over the course of 12-24h post exposure. Most importantly, our study demonstrated that age of the subject does not change the predisposition to the optic nerve injury after blast exposure (young and old mice had almost identical level of functional optic nerve deficits). Results of this study further support the critical need for the careful and thorough evaluation of the optic nerve function and structure in individuals exposed to the blast effects.

Considering that the last decade resulted in significantly increased activities resulting in the massive civilian and military exposure to the action of explosive devices, there is a significant concern that blast-induced CNS and visual system pathology may become more frequently encountered entity by ophthalmologists. Probably the most critical care has to be dedicated to the visual examination and rehabilitation of returning veterans, which were exposed to the multiple blast episodes, and may be at risk of having the significant long term consequences for their visual system function.

Conclusion

It has been demonstrated in previous studies that the acute symptoms of blast injury typically resolve rapidly, although chronic, progressive cognitive, somatic and affective disorders may manifest months to years after the initial injury. Our results are supportive of these previous findings. We observed chronic optic nerve dysfunction following exposure to a single blast wave. This is also accompanied by mild structural abnormalities, predominantly at the level of the ganglion cell layer, retinal nerve fiber layer, and the optic nerve. These results argue for diffuse axonal injury as the primary pathology of the optic nerve following blast exposure. Utilization of non-invasive analyses of visual function may allow for better identification of individuals with TBIs.

Acknowledgements

This work was supported in part by the Department of Veterans Affairs Center for Prevention and Treatment of Visual Loss, a Rehabilitation Research and Development Career Development Award (MMH) and a Rehabilitation Research and Development Merit Award (TL).

Tables

Table 1: Antibodies used in this study

Primary Antibody	Source	Dilution
anti-4HNE	Abcam (ab48506)	1:150
anti-Beta Amyloid	Abcam (ab2539)	1:100
anti-iNOS	Abcam (ab15323)	1:200

Figures

Figure 1

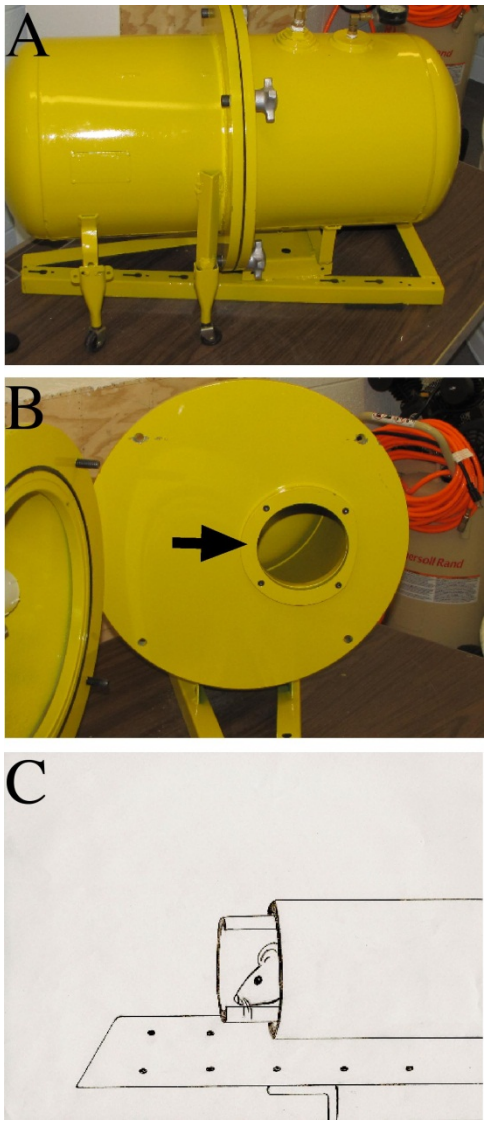

Figure 2

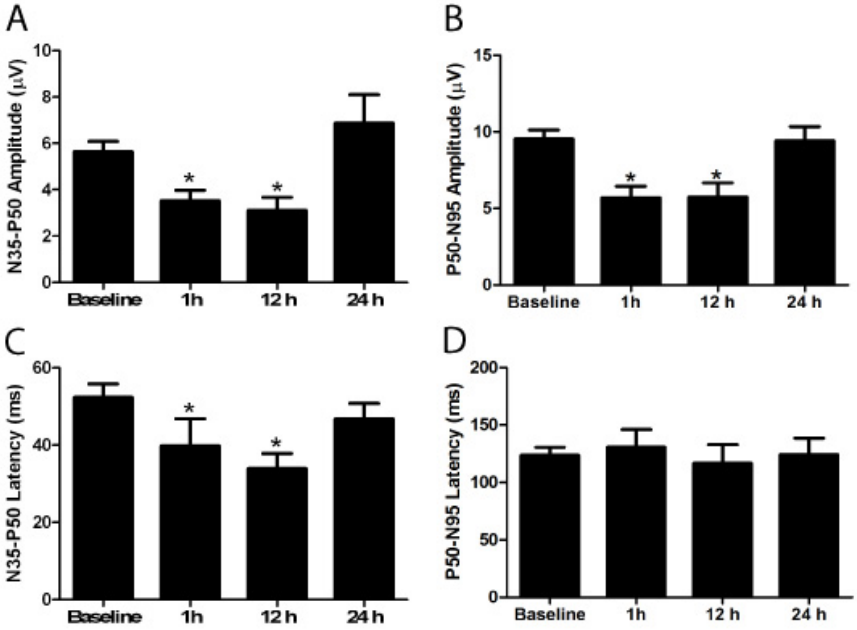

Figure 3

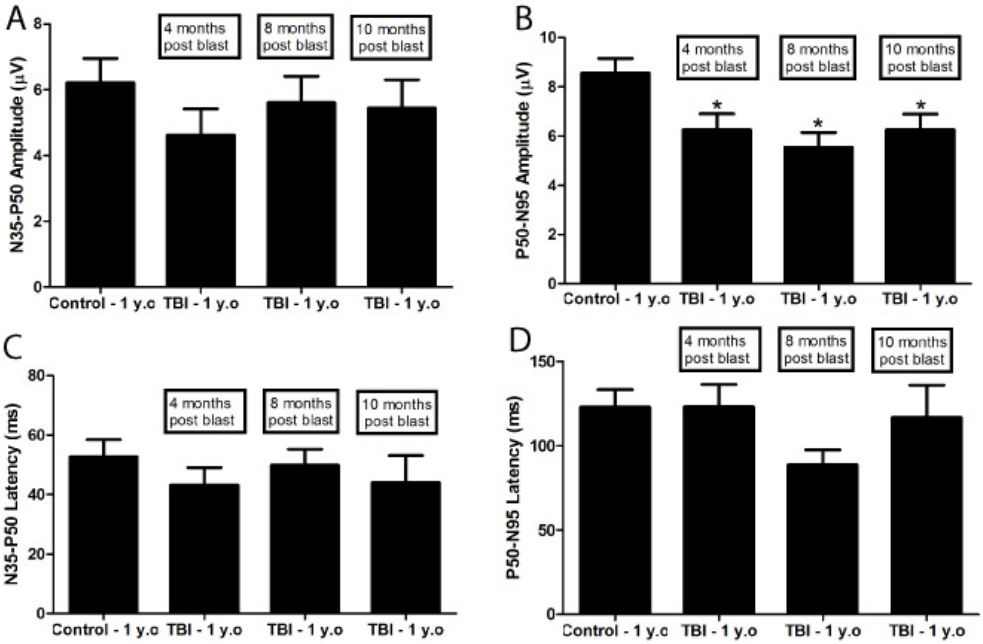

Figure 4

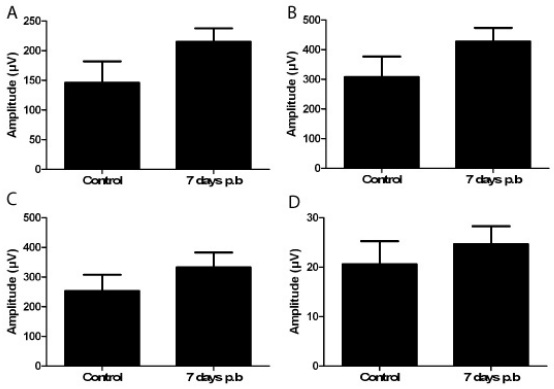

Figure 5

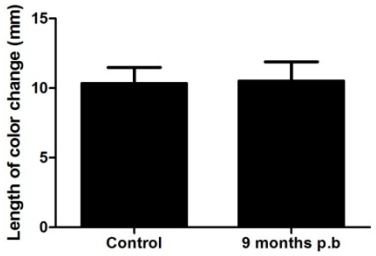

Figure 6

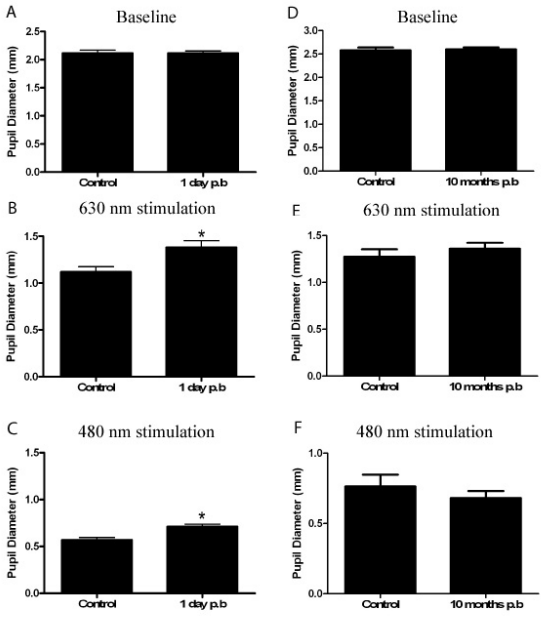

Figure 7

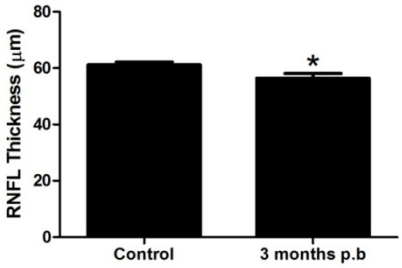

Figure 8

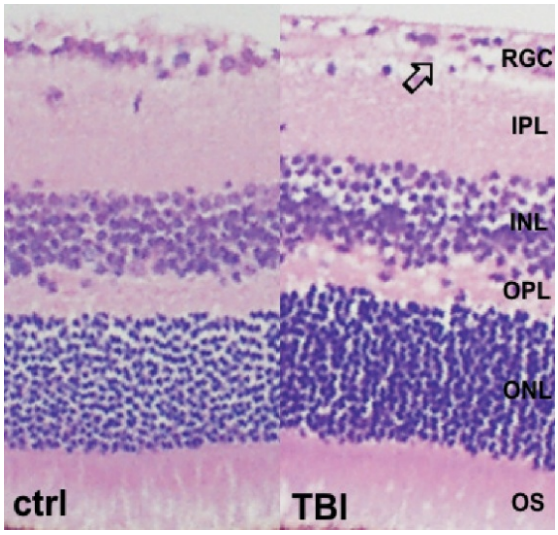

Figure 9

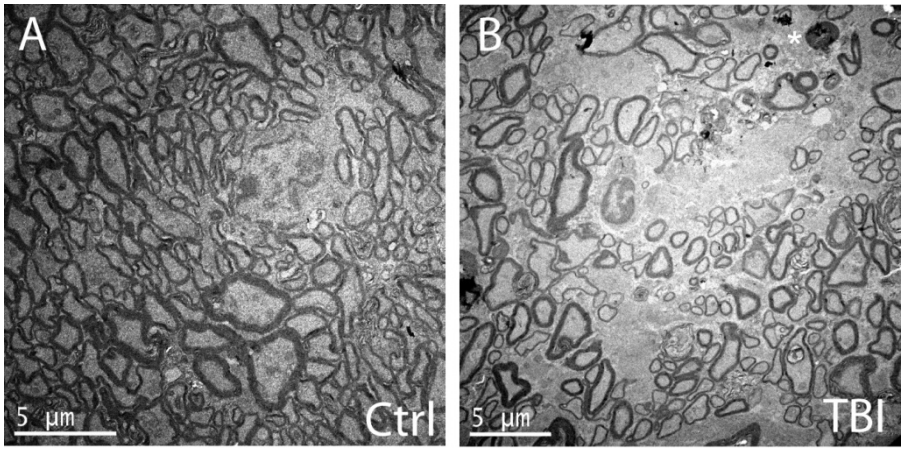

Figure 10

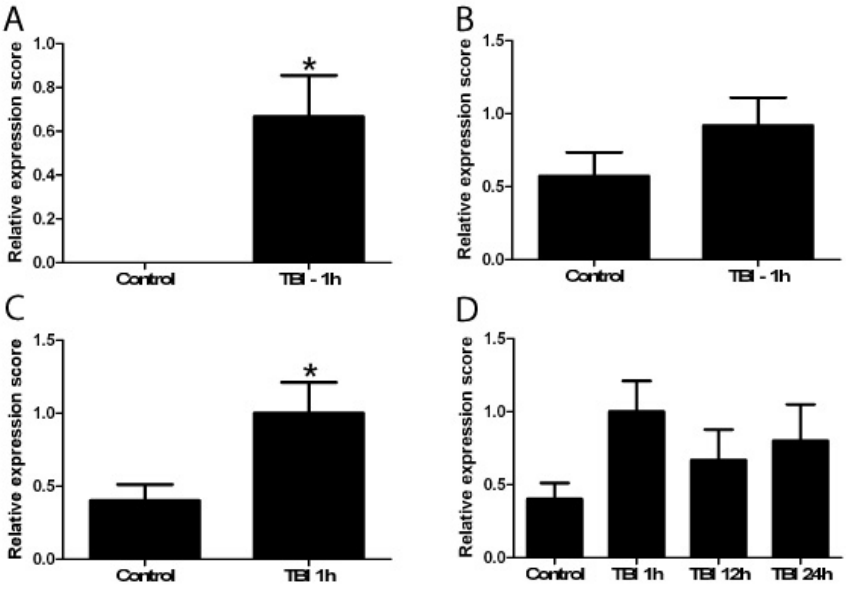

Figure Legends

Figure 1: A schematic of the blast chamber showing (A) the two halves of the tank closed together. A small port in one half of the tank is covered with a mylar membrane to generate the blast wave, which is sealed in place using a locking metal ring (B). The anesthetized mouse is held securely in a padded animal holder, with the left side of the head facing the blast wave at a distance of 30 cm from the mylar membrane and the rest of the body shielded from the blast wave.

Figure 2: Acute pERG deficits following blast injury. pERG was recorded at 1 h (n=11), 12 h (n=9), and 24 h (n=10) post blast. Significant deficits were observed in the N35-P50 amplitude at 1 h and 12 h compared to baseline parameters that recovered by 24 hours post injury (A). Similarly, a significant reduction was observed in the P50-N95 amplitude at 1 h and 12 h following blast injury; by 24 h, the P50-N95 amplitude was not significantly different from baseline parameters (2B). In the N35-P50 latency parameter, there was a significant deficit at 1 h and12 h, which recovered by 24 h (2C). No significant changes were observed in the P50-N95 latency values before and after blast injury (2D).

Figure 3: Chronic pERG deficits occur following blast injury, regardless of the age of the animal when injury was induced. Two month old mice (n=9), 4 month old mice (n=9) and 8 month (n=11) old mice were exposed to the identical blast injury and their pERG function was evaluated at 1 year of age, with a goal of evaluating possible age related susceptibility to the optic nerve damage. A significant reduction of the P50-N95 amplitude was observed in all groups of blast exposed mice at 1 year of age when compared to age-matched controls (n=20) (3B). The deficit at this time point occurred regardless of the age at which they were subjected to the blast injury. No significant deficits were observed in the other pERG parameters.

Figure 4: Full-field ERG responses are not affected by blast exposure. At 7 days post blast (n=10), no significant difference was observed in the maximum combined scotopic ERG a-wave (4A) and b-wave (4B), when compared to age-matched control mice (n=7). Additionally, there was no significant difference in the amplitudes of the summated oscillatory potential component (4C) and P1-N3 flicker response (4D) between control and blast-exposed mice.

Figure 5: Tear production analysis. Tear production was measured 10 months post blast exposure. No statistically significant difference was observed in the tear production between blast exposed mice (n=4) and age-matched controls (n=5).

Figure 6: Chromatic PLR analysis in blast-exposed mice. Chromatic PLR analysis of blast exposed mice (n=12) showed significant deficits 24 h after blast exposure, using the red (630 nm) and blue (480 nm) light compared to age-matched controls (n=9) (Fig 6 B, C). Chromatic PLR analysis of blast-exposed mice at 10 months post blast exposure (n=9) did not show statistically significant difference compared to response obtained from healthy (control) age-matched mice (n=5) (Fig 6 E, F). There was not a statistically significant difference in the resting pupil diameter of control or blast-exposed mice in scotopic conditions (Fig 6 A, D).

Figure 7: OCT analysis following blast exposure showed mild but statistically significant loss in the peripapillary RNFL thickness (superior-temporal quadrant) in blast exposed mice

(n=5) when compared to the age matched controls (n=11). There was not statistically significant difference in the RNFL thickness for all other peripapillary quadrants, total retinal thickness or RNFL thickness in the area centralis region. Recordings were performed 3 months post blast exposure.

Figure 8: Histological evaluation of the retina from control and blast-injured mice show a near normal appearance. A reduction in cellularity of the retinal ganglion cell layer was observed, while all other retinal layers had a normal appearance.

Figure 9: Electron microscopy of the optic nerve in healthy control mice demonstrates normal axonal appearance (A). Electron microscopy of the optic nerves of mice chronically after blast exposure (10 months post blast) shows reduced axon density (B).

Figure 10: Proteins associated with oxidative stress are increased acutely after blast exposure. At 1 hour post blast, a significant increase in the expression of 4HNE was observed in the retina of blast-exposed mice (n=4) compared to age-matched controls (n=12) (A). At 1 hour post blast (n=12), there was a trend toward an increase in the expression of iNOS in blast-exposed animals compared to healthy control mice (n=21), although this change was not statistically significant (B). At 1 hour post blast, retinal expression of beta amyloid in blast-exposed mice (n=10) was significantly increased (p=0.03) compared to age matched controls (n=20) (C). No statistically significant difference was observed when 12 h (n=6) and 24 h (n=10) post blast exposure were added to the analysis.

CHAPTER V. GENERAL CONCLUSION

The major findings of each research chapter included in this dissertation have been described and interpreted in the discussion section of each individual chapter. This section presents an overview of the results and findings of this dissertation. Comprehensively, we have successfully characterized optic nerve structure and function in healthy C57/bl6 mice, and we have applied similar techniques to study disease progression as a result of direct and indirect injury to the optic nerve. We have also confirmed that pERG is a sensitive and reliable tool to non-invasively study the functional progression of optic neuropathy in two different experimental models.

Optic nerve structure and function in C57/bl6 mice

We have longitudinally characterized the optic nerve function in healthy mice using pERG. Pattern ERG has been extensively used to study glaucoma[24-28], and recently, in Parkinson's disease [304]. In our study, no significant changes were observed in the pERG amplitudes and latencies of healthy mice at 3 months and 15 months of age. Chromatic PLR is a sensitive technique that can be used for monitoring early functional deficits in the retina/optic nerve. The utility of cPLR in association with ERG techniques may be a powerful method to accurately localize the source of retinal dysfunction. We have described in detail the normal pupil constriction values in C57/bl6 mice following exposure to red/blue light. We have also demonstrated that photopically matched blue light induces stronger pupil constriction compared to red light. These results are consistent with previously published data in different animal species[34,247] and in humans[212]. Early SD-OCT studies used custom-made modifications to improve imaging for rodent retinas [305,306]. However, with the advent of adaptive optics technology and the utility of 78D lens in SD-OCT [11], rodent retinal imaging can be performed with better resolution and sensitivity. In our study, SD-OCT analysis using 25D lens consistently provided high resolution images of the fundus and the retinal layers. However, the automated segmentation of RNFL by the Spectralis software does not anatomically correlate for rodent retina, and manual segmentation is required to accurately reflect RNFL thickness. We have measured total retinal thickness and RNFL thickness in healthy mice, and our values for retinal thickness are consistent with previously published

mouse data using different OCT techniques and histology analysis [307]. Altogether, these techniques can provide a good representation of retina/optic nerve structure and function.

Optic nerve deficits in the experimentally induced PD mouse model

We have observed significant deficits in pERG function with acute and sub-chronic treatments of MPTP, a toxin that has been previously reported to induce PD symptoms in humans [63] and animal models[62]. Furthermore, we have observed decreased amplitude of the oscillatory potentials (OP) in MPTP-treated mice using full-field ERG, although the combined scotopic responses of the ERG were normal. Reductions in OP amplitudes are likely a consequence of amacrine cell dysfunction or membrane damage to the dendritic processes of RGC[308]. Previous studies have demonstrated impairment of the retinal dopaminergic system in PD, which primarily results in abnormalities of amacrine cells and retinal ganglion cells dependent on dopamine as a neurotransmitter[132,286-288]. These observations, in combination with reduced dopamine content observed in the eyes of MPTP-treated mice in our study, strongly suggest dysfunction of the anterior visual pathway as a result of dopaminergic impairment.

The most interesting aspect of the study is a nearly complete protection of pERG function in PKCδ$^{-/-}$ mice treated with MPTP. PKCδ is an enzyme activated in response to oxidative stress events leading to an increased activation of caspase-3 and the subsequent pro-apoptotic cascade, which has been implicated in the degeneration of dopaminergic neurons [266,298]. Further, a recent study has demonstrated that microglial activation also proceeds via a PKCδ-mediated caspase pathway [309]. These suggest the potential utility of PKCδ inhibitors in the treatment of PD-induced visual system abnormalities. In order to avoid the systemic side effects associated with current PKCδ inhibitors such as rottlerin, topical ocular treatment may provide an effective alternate toward the treatment of retina and optic nerve abnormalities in PD patients.

Our results suggest that the pERG can be used as a sensitive diagnostic tool to monitor disease progression related to Parkinson's disease in the retina. Furthermore, this approach

can be used to test the efficacy of therapeutic interventions targeting the retina and optic nerve in experimental animal models and human PD patients.

Optic nerve deficits following blast exposure in mice

Acutely following blast exposure, we have observed significant deficits in cPLR and pERG analyses, which resolve soon afterwards. cPLR may be therefore be a useful technique for early screening of blast-exposed subjects exhibiting clinical signs of optic nerve injury. No significant changes were detected in the full field ERG parameters following blast exposure in our study. However, an interesting observation was that regardless of the age at which the mice were exposed to blast, mild but significant deficits in pERG P50-N95 amplitude persisted at 1 year of age. These results are contrary to the assumption that the effect of blast injury would be amplified by aging-associated dysfunction. However, it has been well-established in ischemic stroke literature that although ischemic events are more prevalent in an aged population, tolerance for such events is also higher in this population[310]. It is believed that short, sub-lethal ischemic events can lead to the activation of protective mechanisms that provide tolerance to longer ischemic events which are normally lethal. Such adaptive defense mechanisms have been shown to involve genomic reprogramming[311] and metabolic downregulation[312] in the affected region. It is possible that similar tolerance mechanisms prevent the escalation of blast injury damage in aged animals. Identification of the underlying molecular events could potentially provide targets for therapeutic intervention. In addition to function loss, we have observed RNFL thinning 3 months post blast exposure. Many studies have reported visual dysfunction in veterans, which persists many years after exposure to blast injury [148,303]. Our results support these findings, and based on our observations, it appears that the RGC and the optic nerve are the most susceptible ocular structures to blast exposure. We have also observed increased expression of oxidative stress-associated markers immediately following blast exposure. Altogether, these results suggest a role for mitochondrial dysfunction as a result of blast exposure, which can affect the optic nerve function due to its greater energy needs. Further, from our results, it appears that pERG and cPLR together are potentially useful diagnostic tools for the detection of blast-mediated optic neuropathy.

Future studies

Based on the findings elaborated in this dissertation, undertaking the following studies could lead to the development of early diagnostic tools and therapeutic interventions for different forms of optic neuropathy.

- Topical ocular treatment of PKCδ inhibitors in experimental PD models to study possible protective effects on retinal function
- Testing the clinical utility of pERG as an early diagnostic parameter for PD patients
- Testing the clinical utility of cPLR and pERG as screening tools for blast exposed subjects
- Elucidation of compensatory mechanisms to protect retina/optic nerve function following blast exposure

REFERENCES

1. Newman NJ. Optic neuropathy. *Neurology* 1996;46:315-322.
2. Newman NJ, Biousse V. Hereditary optic neuropathies. *Eye* 2004;18:1144-1160.
3. Huang D, Swanson EA, Lin CP, et al. Optical coherence tomography. *Science* 1991;254:1178-1181.
4. Frohman EM, Fujimoto JG, Frohman TC, et al. Optical coherence tomography: a window into the mechanisms of multiple sclerosis. *Nature clinical practice Neurology* 2008;4:664-675.
5. Sakata LM, Deleon-Ortega J, Sakata V, et al. Optical coherence tomography of the retina and optic nerve - a review. *Clinical & experimental ophthalmology* 2009;37:90-99.
6. Forte R, Ambrosio L, Bonavolonta P, et al. Pattern electroretinogram optimized for glaucoma screening (PERGLA) and retinal nerve fiber thickness in suspected glaucoma and ocular hypertension. *Doc Ophthalmol* 2009.
7. Huang Q, Chowdhury V, Coroneo MT. Evaluation of patient suitability for a retinal prosthesis using structural and functional tests of inner retinal integrity. *J Neural Eng* 2009;6:035010.
8. Freeman SR, Kozak I, Cheng L, et al. Optical coherence tomography-raster scanning and manual segmentation in determining drusen volume in age-related macular degeneration. *Retina* 2009.
9. van Velthoven ME, Faber DJ, Verbraak FD, et al. Recent developments in optical coherence tomography for imaging the retina. *Progress in retinal and eye research* 2007;26:57-77.
10. Fisher JB, Jacobs DA, Markowitz CE, et al. Relation of visual function to retinal nerve fiber layer thickness in multiple sclerosis. *Ophthalmology* 2006;113:324-332.
11. Fischer MD, Huber G, Beck SC, et al. Noninvasive, in vivo assessment of mouse retinal structure using optical coherence tomography. *PLoS One* 2009;4:e7507.
12. Mendoza-Santiesteban CE, Gonzalez-Garcia A, Hedges TR, 3rd, et al. Optical coherence tomography for neuro-ophthalmologic diagnoses. *Seminars in ophthalmology* 2010;25:144-154.
13. Kolappan M, Henderson AP, Jenkins TM, et al. Assessing structure and function of the afferent visual pathway in multiple sclerosis and associated optic neuritis. *J Neurol* 2009;256:305-319.
14. Naismith RT, Xu J, Tutlam NT, et al. Diffusion tensor imaging in acute optic neuropathies: predictor of clinical outcomes. *Arch Neurol* 2012;69:65-71.
15. Smith SA, Williams ZR, Ratchford JN, et al. Diffusion tensor imaging of the optic nerve in multiple sclerosis: association with retinal damage and visual disability. *AJNR American journal of neuroradiology* 2011;32:1662-1668.
16. Wang MY, Qi PH, Shi DP. Diffusion tensor imaging of the optic nerve in subacute anterior ischemic optic neuropathy at 3T. *AJNR American journal of neuroradiology* 2011;32:1188-1194.

17. Wang Q, Vlkolinsky R, Xie M, et al. Diffusion tensor imaging detected optic nerve injury correlates with decreased compound action potentials after murine retinal ischemia. *Investigative ophthalmology & visual science* 2012;53:136-142.

18. Zhang X, Sun P, Wang J, et al. Diffusion tensor imaging detects retinal ganglion cell axon damage in the mouse model of optic nerve crush. *Investigative ophthalmology & visual science* 2011;52:7001-7006.

19. Kupersmith MJ, Kardon RH, Durbin MK, et al. Scanning Laser Polarimetry Reveals Status of Retinal Nerve Fiber Layer (RNFL) Integrity in Eyes with Optic Nerve Head Swelling by OCT. *Investigative ophthalmology & visual science* 2012.

20. Medeiros FA, Zangwill LM, Alencar LM, et al. Rates of progressive retinal nerve fiber layer loss in glaucoma measured by scanning laser polarimetry. *American journal of ophthalmology* 2010;149:908-915.

21. Alencar LM, Zangwill LM, Weinreb RN, et al. A comparison of rates of change in neuroretinal rim area and retinal nerve fiber layer thickness in progressive glaucoma. *Investigative ophthalmology & visual science* 2010;51:3531-3539.

22. Lemij HG, Reus NJ. New developments in scanning laser polarimetry for glaucoma. *Current opinion in ophthalmology* 2008;19:136-140.

23. Townsend KA, Wollstein G, Schuman JS. Imaging of the retinal nerve fibre layer for glaucoma. *The British journal of ophthalmology* 2009;93:139-143.

24. Ventura LM, Golubev I, Feuer WJ, et al. Pattern Electroretinogram Progression in Glaucoma Suspects. *Journal of glaucoma* 2011.

25. Bode SF, Jehle T, Bach M. Pattern electroretinogram in glaucoma suspects: new findings from a longitudinal study. *Investigative ophthalmology & visual science* 2011;52:4300-4306.

26. Tafreshi A, Racette L, Weinreb RN, et al. Pattern electroretinogram and psychophysical tests of visual function for discriminating between healthy and glaucoma eyes. *American journal of ophthalmology* 2010;149:488-495.

27. Bowd C, Vizzeri G, Tafreshi A, et al. Diagnostic accuracy of pattern electroretinogram optimized for glaucoma detection. *Ophthalmology* 2009;116:437-443.

28. Hood DC, Xu L, Thienprasiddhi P, et al. The pattern electroretinogram in glaucoma patients with confirmed visual field deficits. *Investigative ophthalmology & visual science* 2005;46:2411-2418.

29. Holder GE. Pattern electroretinography (PERG) and an integrated approach to visual pathway diagnosis. *Progress in retinal and eye research* 2001;20:531-561.

30. Viswanathan S, Frishman LJ, Robson JG. The uniform field and pattern ERG in macaques with experimental glaucoma: removal of spiking activity. *Invest Ophthalmol Vis Sci* 2000;41:2797-2810.

31. Maffei L, Fiorentini A, Bisti S, et al. Pattern ERG in the monkey after section of the optic nerve. *Exp Brain Res* 1985;59:423-425.

32. Mafei L, Fiorentini A. Electroretinographic responses to alternating gratings before and after section of the optic nerve. *Science* 1981;211:953-955.

33. Ben-Shlomo G, Bakalash S, Lambrou GN, et al. Pattern electroretinography in a rat model of ocular hypertension: functional evidence for early detection of inner retinal damage. *Exp Eye Res* 2005;81:340-349.

34. Grozdanic S, Kecova H, Harper MM, et al. Functional and structural changes in a canine model of hereditary primary angle-closure glaucoma. *Invest Ophthalmol Vis Sci* 2009.

35. Ofri R, Samuelson DA, Strubbe DT, et al. Altered retinal recovery and optic nerve fiber loss in primary open-angle glaucoma in the beagle. *Exp Eye Res* 1994;58:245-248.

36. Nagaraju M, Saleh M, Porciatti V. IOP-dependent retinal ganglion cell dysfunction in glaucomatous DBA/2J mice. *Invest Ophthalmol Vis Sci* 2007;48:4573-4579.

37. Hokazono K, Oyamada MK, Monteiro ML. Pattern-reversal electroretinograms for the diagnosis and management of disorders of the anterior visual pathway. *Arquivos brasileiros de oftalmologia* 2011;74:222-226.

38. Kardon R, Anderson SC, Damarjian TG, et al. Chromatic pupil responses: preferential activation of the melanopsin-mediated versus outer photoreceptor-mediated pupil light reflex. *Ophthalmology* 2009;116:1564-1573.

39. Grozdanic SD, Matic M, Sakaguchi DS, et al. Evaluation of retinal status using chromatic pupil light reflex activity in healthy and diseased canine eyes. *Investigative ophthalmology & visual science* 2007;48:5178-5183.

40. Grozdanic SD, Harper MM, Kecova H. Antibody-mediated retinopathies in canine patients: mechanism, diagnosis, and treatment modalities. *Vet Clin North Am Small Anim Pract* 2008;38:361-387, vii.

41. Thurtell MJ, Bala E, Yaniglos SS, et al. Evaluation of optic neuropathy in multiple sclerosis using low-contrast visual evoked potentials. *Neurology* 2009;73:1849-1857.

42. Weinstock-Guttman B, Baier M, Stockton R, et al. Pattern reversal visual evoked potentials as a measure of visual pathway pathology in multiple sclerosis. *Multiple sclerosis* 2003;9:529-534.

43. Hood DC, Odel JG, Winn BJ. The multifocal visual evoked potential. *Journal of neuro-ophthalmology : the official journal of the North American Neuro-Ophthalmology Society* 2003;23:279-289.

44. Thienprasiddhi P, Greenstein VC, Chen CS, et al. Multifocal visual evoked potential responses in glaucoma patients with unilateral hemifield defects. *American journal of ophthalmology* 2003;136:34-40.

45. Gutierrez-Diaz E, Perez-Rico C, de Atauri MJ, et al. Evaluation of the visual function in obstructive sleep apnea syndrome patients and normal-tension glaucoma by means of the multifocal visual evoked potentials. *Graefe's archive for clinical and experimental ophthalmology = Albrecht von Graefes Archiv fur klinische und experimentelle Ophthalmologie* 2012.

46. Wangsupadilok B, Greenstein VC, Kanadani FN, et al. A method to detect progression of glaucoma using the multifocal visual evoked potential technique. *Documenta ophthalmologica Advances in ophthalmology* 2009;118:139-150.

47. Wirdefeldt K, Adami HO, Cole P, et al. Epidemiology and etiology of Parkinson's disease: a review of the evidence. *Eur J Epidemiol* 2011;26 Suppl 1:S1-58.

48. Parkinson J. An essay on the shaking palsy. 1817. *J Neuropsychiatry Clin Neurosci* 2002;14:223-236; discussion 222.

49. Chaudhuri KR, Schapira AH. Non-motor symptoms of Parkinson's disease: dopaminergic pathophysiology and treatment. *Lancet Neurol* 2009;8:464-474.

50. Banerjee R, Starkov AA, Beal MF, et al. Mitochondrial dysfunction in the limelight of Parkinson's disease pathogenesis. *Biochimica et biophysica acta* 2009;1792:651-663.

51. Martin I, Dawson VL, Dawson TM. Recent advances in the genetics of Parkinson's disease. *Annual review of genomics and human genetics* 2011;12:301-325.

52. Lesage S, Brice A. Parkinson's disease: from monogenic forms to genetic susceptibility factors. *Human molecular genetics* 2009;18:R48-59.

53. Giasson BI, Duda JE, Murray IV, et al. Oxidative damage linked to neurodegeneration by selective alpha-synuclein nitration in synucleinopathy lesions. *Science* 2000;290:985-989.

54. Spillantini MG, Crowther RA, Jakes R, et al. alpha-Synuclein in filamentous inclusions of Lewy bodies from Parkinson's disease and dementia with lewy bodies. *Proceedings of the National Academy of Sciences of the United States of America* 1998;95:6469-6473.

55. Jellinger KA. Lewy body-related alpha-synucleinopathy in the aged human brain. *Journal of neural transmission* 2004;111:1219-1235.

56. Braak H, Bohl JR, Muller CM, et al. Stanley Fahn Lecture 2005: The staging procedure for the inclusion body pathology associated with sporadic Parkinson's disease reconsidered. *Mov Disord* 2006;21:2042-2051.

57. Braak H, Del Tredici K, Rub U, et al. Staging of brain pathology related to sporadic Parkinson's disease. *Neurobiol Aging* 2003;24:197-211.

58. Langston JW. The Parkinson's complex: parkinsonism is just the tip of the iceberg. *Ann Neurol* 2006;59:591-596.

59. Obeso JA, Rodriguez-Oroz MC, Goetz CG, et al. Missing pieces in the Parkinson's disease puzzle. *Nature medicine* 2010;16:653-661.

60. Schapira AH, Gegg M. Mitochondrial contribution to Parkinson's disease pathogenesis. *Parkinson's disease* 2011;2011:159160.

61. Schapira AH, Jenner P. Etiology and pathogenesis of Parkinson's disease. *Mov Disord* 2011;26:1049-1055.

62. Dauer W, Przedborski S. Parkinson's disease: mechanisms and models. *Neuron* 2003;39:889-909.

63. Langston JW, Ballard P, Tetrud JW, et al. Chronic Parkinsonism in humans due to a product of meperidine-analog synthesis. *Science* 1983;219:979-980.

64. Nicklas WJ, Vyas I, Heikkila RE. Inhibition of NADH-linked oxidation in brain mitochondria by 1-methyl-4-phenyl-pyridine, a metabolite of the neurotoxin, 1-methyl-4-phenyl-1,2,5,6-tetrahydropyridine. *Life sciences* 1985;36:2503-2508.

65. Miller GW, Gainetdinov RR, Levey AI, et al. Dopamine transporters and neuronal injury. *Trends in pharmacological sciences* 1999;20:424-429.

66. Vila M, Perier C, Feger J, et al. Evolution of changes in neuronal activity in the subthalamic nucleus of rats with unilateral lesion of the substantia nigra assessed by metabolic and electrophysiological measurements. *Eur J Neurosci* 2000;12:337-344.

67. Fearnley JM, Lees AJ. Ageing and Parkinson's disease: substantia nigra regional selectivity. *Brain : a journal of neurology* 1991;114 (Pt 5):2283-2301.

68. Eric Kandel JS, Thomas Jessell *Principles of Neural Science*. 4th ed. ed: McGraw-Hill Medical, 2000.

69. Javoy-Agid F, Agid Y. Is the mesocortical dopaminergic system involved in Parkinson disease? *Neurology* 1980;30:1326-1330.

70. Patrick RL, Snyder TE, Barchas JD. Regulation of dopamine synthesis in rat brain striatal synaptosomes. *Molecular pharmacology* 1975;11:621-631.

71. Elsworth JD, Roth RH. Dopamine synthesis, uptake, metabolism, and receptors: relevance to gene therapy of Parkinson's disease. *Experimental neurology* 1997;144:4-9.

72. Ciliax BJ, Heilman C, Demchyshyn LL, et al. The dopamine transporter: immunochemical characterization and localization in brain. *The Journal of neuroscience : the official journal of the Society for Neuroscience* 1995;15:1714-1723.

73. Thobois S, Guillouet S, Broussolle E. Contributions of PET and SPECT to the understanding of the pathophysiology of Parkinson's disease. *Neurophysiologie clinique = Clinical neurophysiology* 2001;31:321-340.

74. Stoessl AJ, Martin WW, McKeown MJ, et al. Advances in imaging in Parkinson's disease. *Lancet Neurol* 2011;10:987-1001.

75. Antonini A, Schwarz J, Oertel WH, et al. Long-term changes of striatal dopamine D2 receptors in patients with Parkinson's disease: a study with positron emission tomography and [11C]raclopride. *Mov Disord* 1997;12:33-38.

76. Lefaucheur JP. Motor cortex dysfunction revealed by cortical excitability studies in Parkinson's disease: influence of antiparkinsonian treatment and cortical stimulation. *Clinical neurophysiology : official journal of the International Federation of Clinical Neurophysiology* 2005;116:244-253.

77. Colebatch JG. Bereitschaftspotential and movement-related potentials: origin, significance, and application in disorders of human movement. *Mov Disord* 2007;22:601-610.

78. Hauber W. Involvement of basal ganglia transmitter systems in movement initiation. *Progress in neurobiology* 1998;56:507-540.

79. Albanese A, Altavista MC, Rossi P. Organization of central nervous system dopaminergic pathways. *Journal of neural transmission Supplementum* 1986;22:3-17.

80. Goldstein DS, Sewell L, Sharabi Y. Autonomic dysfunction in PD: a window to early detection? *Journal of the neurological sciences* 2011;310:118-122.

81. Ziemssen T, Reichmann H. Non-motor dysfunction in Parkinson's disease. *Parkinsonism Relat Disord* 2007;13:323-332.

82. Martinez-Castrillo JC, Vela L, del Val J, et al. Nonmotor disorders and their correlation with dopamine: can they be treated by currently available methods? *The neurologist* 2011;17:S9-17.

83. Calabresi P, Picconi B, Parnetti L, et al. A convergent model for cognitive dysfunctions in Parkinson's disease: the critical dopamine-acetylcholine synaptic balance. *Lancet Neurol* 2006;5:974-983.

84. Remy P, Doder M, Lees A, et al. Depression in Parkinson's disease: loss of dopamine and noradrenaline innervation in the limbic system. *Brain : a journal of neurology* 2005;128:1314-1322.

85. Halliday GM, Blumbergs PC, Cotton RG, et al. Loss of brainstem serotonin- and substance P-containing neurons in Parkinson's disease. *Brain research* 1990;510:104-107.

86. Harding AJ, Broe GA, Halliday GM. Visual hallucinations in Lewy body disease relate to Lewy bodies in the temporal lobe. *Brain : a journal of neurology* 2002;125:391-403.

87. Owen AM, Doyon J, Dagher A, et al. Abnormal basal ganglia outflow in Parkinson's disease identified with PET. Implications for higher cortical functions. *Brain : a journal of neurology* 1998;121 (Pt 5):949-965.

88. Owen AM, James M, Leigh PN, et al. Fronto-striatal cognitive deficits at different stages of Parkinson's disease. *Brain : a journal of neurology* 1992;115 (Pt 6):1727-1751.

89. Sawamoto N, Piccini P, Hotton G, et al. Cognitive deficits and striato-frontal dopamine release in Parkinson's disease. *Brain : a journal of neurology* 2008;131:1294-1302.

90. Chaudhuri KR, Healy DG, Schapira AH. Non-motor symptoms of Parkinson's disease: diagnosis and management. *Lancet Neurol* 2006;5:235-245.

91. Chaudhuri KR, Naidu Y. Early Parkinson's disease and non-motor issues. *J Neurol* 2008;255 Suppl 5:33-38.

92. Polak T, Weise D, Metzger F, et al. Vagus nerve somatosensory evoked potentials in Parkinson's disease. *J Neurol* 2011;258:2276-2277.

93. Katzenschlager R, Lees AJ. Olfaction and Parkinson's syndromes: its role in differential diagnosis. *Current opinion in neurology* 2004;17:417-423.

94. Ponsen MM, Stoffers D, Booij J, et al. Idiopathic hyposmia as a preclinical sign of Parkinson's disease. *Ann Neurol* 2004;56:173-181.

95. Gagnon JF, Bedard MA, Fantini ML, et al. REM sleep behavior disorder and REM sleep without atonia in Parkinson's disease. *Neurology* 2002;59:585-589.

96. Boeve BF, Silber MH, Parisi JE, et al. Synucleinopathy pathology and REM sleep behavior disorder plus dementia or parkinsonism. *Neurology* 2003;61:40-45.

97. Alves G, Larsen JP, Emre M, et al. Changes in motor subtype and risk for incident dementia in Parkinson's disease. *Mov Disord* 2006;21:1123-1130.

98. Burn DJ, Rowan EN, Allan LM, et al. Motor subtype and cognitive decline in Parkinson's disease, Parkinson's disease with dementia, and dementia with Lewy bodies. *Journal of neurology, neurosurgery, and psychiatry* 2006;77:585-589.

99. Halliday GM, Li YW, Blumbergs PC, et al. Neuropathology of immunohistochemically identified brainstem neurons in Parkinson's disease. *Ann Neurol* 1990;27:373-385.

100. Sharabi Y, Imrich R, Holmes C, et al. Generalized and neurotransmitter-selective noradrenergic denervation in Parkinson's disease with orthostatic hypotension. *Mov Disord* 2008;23:1725-1732.

101. Abbott RD, Petrovitch H, White LR, et al. Frequency of bowel movements and the future risk of Parkinson's disease. *Neurology* 2001;57:456-462.

102. Abbott RD, Ross GW, Petrovitch H, et al. Bowel movement frequency in late-life and incidental Lewy bodies. *Mov Disord* 2007;22:1581-1586.

103. Frederick JM, Rayborn ME, Laties AM, et al. Dopaminergic neurons in the human retina. *The Journal of comparative neurology* 1982;210:65-79.

104. Djamgoz MB, Hankins MW, Hirano J, et al. Neurobiology of retinal dopamine in relation to degenerative states of the tissue. *Vision research* 1997;37:3509-3529.

105. Rodnitzky RL. Visual dysfunction in Parkinson's disease. *Clinical neuroscience* 1998;5:102-106.

106. Wink B, Harris J. A model of the Parkinsonian visual system: support for the dark adaptation hypothesis. *Vision research* 2000;40:1937-1946.

107. Archibald NK, Clarke MP, Mosimann UP, et al. The retina in Parkinson's disease. *Brain : a journal of neurology* 2009;132:1128-1145.

108. Bloomfield SA, Volgyi B. The diverse functional roles and regulation of neuronal gap junctions in the retina. *Nat Rev Neurosci* 2009;10:495-506.

109. Hutton JT, Morris JL. Vision in Parkinson's disease. *Adv Neurol* 2001;86:279-288.

110. Armstrong RA. Visual signs and symptoms of Parkinson's disease. *Clinical & experimental optometry : journal of the Australian Optometrical Association* 2008;91:129-138.

111. Repka MX, Claro MC, Loupe DN, et al. Ocular motility in Parkinson's disease. *J Pediatr Ophthalmol Strabismus* 1996;33:144-147.

112. Bodis-Wollner I, Marx MS, Mitra S, et al. Visual dysfunction in Parkinson's disease. Loss in spatiotemporal contrast sensitivity. *Brain* 1987;110 (Pt 6):1675-1698.

113. Masson G, Mestre D, Blin O. Dopaminergic modulation of visual sensitivity in man. *Fundam Clin Pharmacol* 1993;7:449-463.

114. Mestre D, Blin O, Serratrice G, et al. Spatiotemporal contrast sensitivity differs in normal aging and Parkinson's disease. *Neurology* 1990;40:1710-1714.

115. Biousse V, Skibell BC, Watts RL, et al. Ophthalmologic features of Parkinson's disease. *Neurology* 2004;62:177-180.

116. Buttner T, Kuhn W, Muller T, et al. Visual hallucinosis: the major clinical determinant of distorted chromatic contour perception in Parkinson's disease. *Journal of neural transmission* 1996;103:1195-1204.

117. Diederich NJ, Goetz CG, Raman R, et al. Poor visual discrimination and visual hallucinations in Parkinson's disease. *Clinical neuropharmacology* 1998;21:289-295.

118. Diederich NJ, Goetz CG, Stebbins GT. Repeated visual hallucinations in Parkinson's disease as disturbed external/internal perceptions: focused review and a new integrative model. *Mov Disord* 2005;20:130-140.

119. Price MJ, Feldman RG, Adelberg D, et al. Abnormalities in color vision and contrast sensitivity in Parkinson's disease. *Neurology* 1992;42:887-890.

120. Buttner T, Kuhn W, Klotz P, et al. Disturbance of colour perception in Parkinson's disease. *Journal of neural transmission Parkinson's disease and dementia section* 1993;6:11-15.

121. Leigh RJ, Riley DE. Eye movements in parkinsonism: it's saccadic speed that counts. *Neurology* 2000;54:1018-1019.

122. MacAskill MR, Anderson TJ, Jones RD. Adaptive modification of saccade amplitude in Parkinson's disease. *Brain : a journal of neurology* 2002;125:1570-1582.

123. Tan A, Salgado M, Fahn S. Rapid eye movement sleep behavior disorder preceding Parkinson's disease with therapeutic response to levodopa. *Mov Disord* 1996;11:214-216.

124. Peppe A, Stanzione P, Pierelli F, et al. Low contrast stimuli enhance PERG sensitivity to the visual dysfunction in Parkinson's disease. *Electroencephalography and clinical neurophysiology* 1992;82:453-457.

125. Ikeda H, Head GM, Ellis CJ. Electrophysiological signs of retinal dopamine deficiency in recently diagnosed Parkinson's disease and a follow up study. *Vision research* 1994;34:2629-2638.

126. Bodis-Wollner I, Marx MS, Mitra S, et al. Visual dysfunction in Parkinson's disease. Loss in spatiotemporal contrast sensitivity. *Brain : a journal of neurology* 1987;110 (Pt 6):1675-1698.

127. Calzetti S, Franchi A, Taratufolo G, et al. Simultaneous VEP and PERG investigations in early Parkinson's disease. *Journal of neurology, neurosurgery, and psychiatry* 1990;53:114-117.

128. Aaker GD, Myung JS, Ehrlich JR, et al. Detection of retinal changes in Parkinson's disease with spectral-domain optical coherence tomography. *Clinical ophthalmology* 2010;4:1427-1432.

129. Moschos MM, Tagaris G, Markopoulos I, et al. Morphologic changes and functional retinal impairment in patients with Parkinson disease without visual loss. *European journal of ophthalmology* 2011;21:24-29.

130. Peppe A, Stanzione P, Pierelli F, et al. Visual alterations in de novo Parkinson's disease: pattern electroretinogram latencies are more delayed and more reversible by levodopa than are visual evoked potentials. *Neurology* 1995;45:1144-1148.

131. Ghilardi MF, Chung E, Bodis-Wollner I, et al. Systemic 1-methyl,4-phenyl,1-2-3-6-tetrahydropyridine (MPTP) administration decreases retinal dopamine content in primates. *Life sciences* 1988;43:255-262.

132. Ghilardi MF, Marx MS, Bodis-Wollner I, et al. The effect of intraocular 6-hydroxydopamine on retinal processing of primates. *Ann Neurol* 1989;25:357-364.

133. Nguyen-Legros J, Botteri C, Phuc LH, et al. Morphology of primate's dopaminergic amacrine cells as revealed by TH-like immunoreactivity on retinal flat-mounts. *Brain research* 1984;295:145-153.

134. Harnois C, Di Paolo T. Decreased dopamine in the retinas of patients with Parkinson's disease. *Investigative ophthalmology & visual science* 1990;31:2473-2475.

135. Castelo-Branco M, Mendes M, Silva F, et al. Motion integration deficits are independent of magnocellular impairment in Parkinson's disease. *Neuropsychologia* 2009;47:314-320.

136. Bazarian JJ, McClung J, Shah MN, et al. Mild traumatic brain injury in the United States, 1998--2000. *Brain injury : [BI]* 2005;19:85-91.

137. Bradshaw BD. TBI Task Force Report, January 2008.

138. Bazarian JJ, Blyth B, Cimpello L. Bench to bedside: evidence for brain injury after concussion--looking beyond the computed tomography scan. *Acad Emerg Med* 2006;13:199-214.

139. Ponsford J, Cameron P, Fitzgerald M, et al. Long-term outcomes after uncomplicated mild traumatic brain injury: a comparison with trauma controls. *Journal of neurotrauma* 2011;28:937-946.

140. Vanderploeg RD, Curtiss G, Luis CA, et al. Long-term morbidities following self-reported mild traumatic brain injury. *Journal of clinical and experimental neuropsychology* 2007;29:585-598.

141. . State of the Art IX: Traumatic Brain Injury Research 2008.

142. Halbauer JD, Ashford JW, Zeitzer JM, et al. Neuropsychiatric diagnosis and management of chronic sequelae of war-related mild to moderate traumatic brain injury. *Journal of rehabilitation research and development* 2009;46:757-796.

143. Xydakis MS, Fravell MD, Nasser KE, et al. Analysis of battlefield head and neck injuries in Iraq and Afghanistan. *Otolaryngology--head and neck surgery : official journal of American Academy of Otolaryngology-Head and Neck Surgery* 2005;133:497-504.

144. Fausti SA, Wilmington DJ, Gallun FJ, et al. Auditory and vestibular dysfunction associated with blast-related traumatic brain injury. *Journal of rehabilitation research and development* 2009;46:797-810.

145. Lew HL, Garvert DW, Pogoda TK, et al. Auditory and visual impairments in patients with blast-related traumatic brain injury: Effect of dual sensory impairment on Functional Independence Measure. *Journal of rehabilitation research and development* 2009;46:819-826.

146. Thach AB, Johnson AJ, Carroll RB, et al. Severe eye injuries in the war in Iraq, 2003-2005. *Ophthalmology* 2008;115:377-382.

147. Lew HL, Poole JH, Vanderploeg RD, et al. Program development and defining characteristics of returning military in a VA Polytrauma Network Site. *J Rehabil Res Dev* 2007;44:1027-1034.

148. Goodrich GL, Kirby J, Cockerham G, et al. Visual function in patients of a polytrauma rehabilitation center: A descriptive study. *J Rehabil Res Dev* 2007;44:929-936.

149. Cockerham GC, Goodrich GL, Weichel ED, et al. Eye and visual function in traumatic brain injury. *J Rehabil Res Dev* 2009;46:811-818.

150. Brahm KD, Wilgenburg HM, Kirby J, et al. Visual impairment and dysfunction in combat-injured servicemembers with traumatic brain injury. *Optom Vis Sci* 2009;86:817-825.

151. Taber KH, Warden DL, Hurley RA. Blast-related traumatic brain injury: what is known? *J Neuropsychiatry Clin Neurosci* 2006;18:141-145.

152. Mott D. Blast-Induced Pressure Fields Beneath a Military Helmet for Non-Lethal Threats. American Physical Society 2008.

153. Wightman JM, Gladish SL. Explosions and blast injuries. *Annals of emergency medicine* 2001;37:664-678.

154. Moore DF, Jerusalem A, Nyein M, et al. Computational biology - modeling of primary blast effects on the central nervous system. *NeuroImage* 2009;47 Suppl 2:T10-20.

155. Wolf SJ, Bebarta VS, Bonnett CJ, et al. Blast injuries. *Lancet* 2009;374:405-415.

156. Phillips YY. Primary blast injuries. *Annals of emergency medicine* 1986;15:1446-1450.

157. Ling G, Bandak F, Armonda R, et al. Explosive blast neurotrauma. *Journal of neurotrauma* 2009;26:815-825.

158. Kocsis JD, Tessler A. Pathology of blast-related brain injury. *Journal of rehabilitation research and development* 2009;46:667-672.

159. Yilmaz S, Pekdemir M. An unusual primary blast injury Traumatic brain injury due to primary blast injury. *The American journal of emergency medicine* 2007;25:97-98.

160. Warden DL, French LM, Shupenko L, et al. Case report of a soldier with primary blast brain injury. *NeuroImage* 2009;47 Suppl 2:T152-153.

161. Cernak I, Wang Z, Jiang J, et al. Ultrastructural and functional characteristics of blast injury-induced neurotrauma. *The Journal of trauma* 2001;50:695-706.

162. Wang Y, Wei Y, Oguntayo S, et al. Tightly coupled repetitive blast-induced traumatic brain injury: development and characterization in mice. *Journal of neurotrauma* 2011;28:2171-2183.

163. Garman RH, Jenkins LW, Switzer RC, 3rd, et al. Blast exposure in rats with body shielding is characterized primarily by diffuse axonal injury. *Journal of neurotrauma* 2011;28:947-959.

164. Koliatsos VE, Cernak I, Xu L, et al. A mouse model of blast injury to brain: initial pathological, neuropathological, and behavioral characterization. *Journal of neuropathology and experimental neurology* 2011;70:399-416.

165. Long JB, Bentley TL, Wessner KA, et al. Blast overpressure in rats: recreating a battlefield injury in the laboratory. *Journal of neurotrauma* 2009;26:827-840.

166. Lu J, Ng KC, Ling G, et al. Effect of Blast Exposure on the Brain Structure and Cognition in Macaca fascicularis. *Journal of neurotrauma* 2011.

167. Cernak I, Wang Z, Jiang J, et al. Cognitive deficits following blast injury-induced neurotrauma: possible involvement of nitric oxide. *Brain injury : [BI]* 2001;15:593-612.

168. Leonardi AD, Bir CA, Ritzel DV, et al. Intracranial pressure increases during exposure to a shock wave. *Journal of neurotrauma* 2011;28:85-94.

169. Saljo A, Svensson B, Mayorga M, et al. Low-level blasts raise intracranial pressure and impair cognitive function in rats. *Journal of neurotrauma* 2009;26:1345-1352.

170. Petras JM, Bauman RA, Elsayed NM. Visual system degeneration induced by blast overpressure. *Toxicology* 1997;121:41-49.

171. Wang J, Hamm RJ, Povlishock JT. Traumatic axonal injury in the optic nerve: evidence for axonal swelling, disconnection, dieback, and reorganization. *Journal of neurotrauma* 2011;28:1185-1198.

172. Sullivan PG, Keller JN, Bussen WL, et al. Cytochrome c release and caspase activation after traumatic brain injury. *Brain research* 2002;949:88-96.

173. Conti AC, Raghupathi R, Trojanowski JQ, et al. Experimental brain injury induces regionally distinct apoptosis during the acute and delayed post-traumatic period. *The Journal of neuroscience : the official journal of the Society for Neuroscience* 1998;18:5663-5672.

174. Schwab KA, Ivins B, Cramer G, et al. Screening for traumatic brain injury in troops returning from deployment in Afghanistan and Iraq: initial investigation of the usefulness of a short screening tool for traumatic brain injury. *J Head Trauma Rehabil* 2007;22:377-389.

175. Defense and Veterans Brain Injury Center Working Group on the Acute Management of Mild Traumatic Brain Injury in Military Operational Settings: Clinical Practice Guideline and Recommendations In: Defense DoVADo, ed, December 2006.

176. Dikmen SS, Corrigan JD, Levin HS, et al. Cognitive outcome following traumatic brain injury. *The Journal of head trauma rehabilitation* 2009;24:430-438.

177. Matsushita M, Hosoda K, Naitoh Y, et al. Utility of diffusion tensor imaging in the acute stage of mild to moderate traumatic brain injury for detecting white matter lesions and predicting long-term cognitive function in adults. *Journal of neurosurgery* 2011;115:130-139.

178. Mac Donald CL, Johnson AM, Cooper D, et al. Detection of blast-related traumatic brain injury in U.S. military personnel. *The New England journal of medicine* 2011;364:2091-2100.

179. Sidaros A, Engberg AW, Sidaros K, et al. Diffusion tensor imaging during recovery from severe traumatic brain injury and relation to clinical outcome: a longitudinal study. *Brain : a journal of neurology* 2008;131:559-572.

180. Levin HS, Wilde E, Troyanskaya M, et al. Diffusion tensor imaging of mild to moderate blast-related traumatic brain injury and its sequelae. *Journal of neurotrauma* 2010;27:683-694.

181. Folmer RL, Billings CJ, Diedesch-Rouse AC, et al. Electrophysiological assessments of cognition and sensory processing in TBI: applications for diagnosis, prognosis and rehabilitation. *International journal of psychophysiology : official journal of the International Organization of Psychophysiology* 2011;82:4-15.

182. Carter BG, Butt W. Are somatosensory evoked potentials the best predictor of outcome after severe brain injury? A systematic review. *Intensive care medicine* 2005;31:765-775.

183. Robinson LR, Micklesen PJ, Tirschwell DL, et al. Predictive value of somatosensory evoked potentials for awakening from coma. *Critical care medicine* 2003;31:960-967.

184. Lew HL, Dikmen S, Slimp J, et al. Use of somatosensory-evoked potentials and cognitive event-related potentials in predicting outcomes of patients with severe traumatic brain injury. *American journal of physical medicine & rehabilitation / Association of Academic Physiatrists* 2003;82:53-61; quiz 62-54, 80.

185. Wirsen A, Stenberg G, Rosen I, et al. Quantified EEG and cortical evoked responses in patients with chronic traumatic frontal lesions. *Electroencephalography and clinical neurophysiology* 1992;84:127-138.

186. Fischer C, Luaute J, Adeleine P, et al. Predictive value of sensory and cognitive evoked potentials for awakening from coma. *Neurology* 2004;63:669-673.

187. Marmarou A, Lu J, Butcher I, et al. Prognostic value of the Glasgow Coma Scale and pupil reactivity in traumatic brain injury assessed pre-hospital and on enrollment: an IMPACT analysis. *Journal of neurotrauma* 2007;24:270-280.

188. Theriault M, De Beaumont L, Gosselin N, et al. Electrophysiological abnormalities in well functioning multiple concussed athletes. *Brain injury : [BI]* 2009;23:899-906.

189. Gaetz M, Weinberg H. Electrophysiological indices of persistent post-concussion symptoms. *Brain injury : [BI]* 2000;14:815-832.

190. Lachapelle J, Bolduc-Teasdale J, Ptito A, et al. Deficits in complex visual information processing after mild TBI: electrophysiological markers and vocational outcome prognosis. *Brain injury : [BI]* 2008;22:265-274.

191. Lew HL, Poole JH, Chiang JY, et al. Event-related potential in facial affect recognition: potential clinical utility in patients with traumatic brain injury. *Journal of rehabilitation research and development* 2005;42:29-34.

192. Gaetz M, Goodman D, Weinberg H. Electrophysiological evidence for the cumulative effects of concussion. *Brain injury : [BI]* 2000;14:1077-1088.

193. Maruta J, Suh M, Niogi SN, et al. Visual tracking synchronization as a metric for concussion screening. *The Journal of head trauma rehabilitation* 2010;25:293-305.

194. Galetta KM, Barrett J, Allen M, et al. The King-Devick test as a determinant of head trauma and concussion in boxers and MMA fighters. *Neurology* 2011.

195. Grozdanic S, Betts DM, Allbaugh RA, et al. Characterization of the pupil light reflex, electroretinogram and tonometric parameters in healthy mouse eyes. *Curr Eye Res* 2003;26:371-378.

196. Grozdanic S, Sakaguchi DS, Kwon YH, et al. Characterization of the pupil light reflex, electroretinogram and tonometric parameters in healthy rat eyes. *Curr Eye Res* 2002;25:69-78.

197. Grozdanic SD, Matic M, Betts DM, et al. Recovery of canine retina and optic nerve function after acute elevation of intraocular pressure: implications for canine glaucoma treatment. *Vet Ophthalmol* 2007;10 Suppl 1:101-107.

198. Panagakis E, Moschos M. Pattern ERG changes in suspected glaucoma. *Ophthalmologica* 1998;212:112-114.

199. Mierdel P, Zenker HJ, Marre E. The pattern ERG in glaucoma: effect of pattern reversal time. *Int Ophthalmol* 1992;16:211-214.

200. Price MJ, Drance SM, Price M, et al. The pattern electroretinogram and visual-evoked potential in glaucoma. *Graefes Arch Clin Exp Ophthalmol* 1988;226:542-547.

201. van den Berg TJ, Riemslag FC, de Vos GW, et al. Pattern ERG and glaucomatous visual field defects. *Doc Ophthalmol* 1986;61:335-341.

202. Papst N, Bopp M, Schnaudigel OE. Pattern electroretinogram and visually evoked cortical potentials in glaucoma. *Graefes Arch Clin Exp Ophthalmol* 1984;222:29-33.

203. Wanger P, Persson HE. Pattern-reversal electroretinograms in unilateral glaucoma. *Invest Ophthalmol Vis Sci* 1983;24:749-753.

204. Porciatti V, Nagaraju M. Head-up tilt lowers IOP and improves RGC dysfunction in glaucomatous DBA/2J mice. *Exp Eye Res* 2009.

205. Porciatti V. The mouse pattern electroretinogram. *Doc Ophthalmol* 2007;115:145-153.

206. Miura G, Wang MH, Ivers KM, et al. Retinal pathway origins of the pattern ERG of the mouse. *Exp Eye Res* 2009;89:49-62.

207. Porciatti V, Ventura LM. Adaptive changes of inner retina function in response to sustained pattern stimulation. *Vision Res* 2009;49:505-513.

208. Hull BM, Thompson DA. A review of the clinical applications of the pattern electroretinogram. *Ophthalmic & physiological optics : the journal of the British College of Ophthalmic Opticians* 1989;9:143-152.

209. Bach M. Electrophysiological approaches for early detection of glaucoma. *European journal of ophthalmology* 2001;11 Suppl 2:S41-49.

210. Ventura LM, Porciatti V. Pattern electroretinogram in glaucoma. *Current opinion in ophthalmology* 2006;17:196-202.

211. Grozdanic SD, Matic M, Sakaguchi DS, et al. Evaluation of retinal status using chromatic pupil light reflex activity in healthy and diseased canine eyes. *Invest Ophthalmol Vis Sci* 2007;48:5178-5183.

212. Park JC, Moura AL, Raza AS, et al. Toward a clinical protocol for assessing rod, cone, and melanopsin contributions to the human pupil response. *Investigative ophthalmology & visual science* 2011;52:6624-6635.

213. McDougal DH, Gamlin PD. The influence of intrinsically-photosensitive retinal ganglion cells on the spectral sensitivity and response dynamics of the human pupillary light reflex. *Vision research* 2010;50:72-87.

214. McNeill DS, Sheely CJ, Ecker JL, et al. Development of melanopsin-based irradiance detecting circuitry. *Neural development* 2011;6:8.

215. Tsujimura S, Ukai K, Ohama D, et al. Contribution of human melanopsin retinal ganglion cells to steady-state pupil responses. *Proceedings Biological sciences / The Royal Society* 2010;277:2485-2492.

216. Tsujimura S, Tokuda Y. Delayed response of human melanopsin retinal ganglion cells on the pupillary light reflex. *Ophthalmic & physiological optics : the journal of the British College of Ophthalmic Opticians* 2011;31:469-479.

217. Benarroch EE. The melanopsin system: Phototransduction, projections, functions, and clinical implications. *Neurology* 2011;76:1422-1427.

218. Markwell EL, Feigl B, Zele AJ. Intrinsically photosensitive melanopsin retinal ganglion cell contributions to the pupillary light reflex and circadian rhythm. *Clinical & experimental optometry : journal of the Australian Optometrical Association* 2010;93:137-149.

219. Do MT, Yau KW. Intrinsically photosensitive retinal ganglion cells. *Physiological reviews* 2010;90:1547-1581.

220. Schmidt TM, Kofuji P. Novel insights into non-image forming visual processing in the retina. *Cellscience* 2008;5:77-83.

221. Kankipati L, Girkin CA, Gamlin PD. Post-illumination pupil response in subjects without ocular disease. *Investigative ophthalmology & visual science* 2010;51:2764-2769.

222. Zele AJ, Feigl B, Smith SS, et al. The circadian response of intrinsically photosensitive retinal ganglion cells. *PloS one* 2011;6:e17860.

223. Kocaoglu OP, Uhlhorn SR, Hernandez E, et al. Simultaneous fundus imaging and optical coherence tomography of the mouse retina. *Invest Ophthalmol Vis Sci* 2007;48:1283-1289.

224. Fingler J, Readhead C, Schwartz DM, et al. Phase-contrast OCT imaging of transverse flows in the mouse retina and choroid. *Invest Ophthalmol Vis Sci* 2008;49:5055-5059.

225. Srinivasan VJ, Ko TH, Wojtkowski M, et al. Noninvasive volumetric imaging and morphometry of the rodent retina with high-speed, ultrahigh-resolution optical coherence tomography. *Invest Ophthalmol Vis Sci* 2006;47:5522-5528.

226. Strouthidis NG, Grimm J, Williams GA, et al. A Comparison of Optic Nerve Head Morphology Viewed by Spectral Domain Optical Coherence Tomography and By Serial Histology. *Invest Ophthalmol Vis Sci* 2009;29:29.

227. Wang M, Hood DC, Cho JS, et al. Measurement of local retinal ganglion cell layer thickness in patients with glaucoma using frequency-domain optical coherence tomography. *Arch Ophthalmol* 2009;127:875-881.

228. Abramoff MD, Lee K, Niemeijer M, et al. Automated segmentation of the cup and rim from spectral domain OCT of the optic nerve head. *Invest Ophthalmol Vis Sci* 2009;50:5778-5784.

229. Garvin MK, Abramoff MD, Kardon R, et al. Intraretinal layer segmentation of macular optical coherence tomography images using optimal 3-D graph search. *IEEE Trans Med Imaging* 2008;27:1495-1505.

230. Kim KH, Puoris'haag M, Maguluri GN, et al. Monitoring mouse retinal degeneration with high-resolution spectral-domain optical coherence tomography. *J Vis* 2008;8:17 11-11.

231. Xu J, Molday LL, Molday RS, et al. In vivo imaging of the mouse model of X-linked juvenile retinoschisis with fourier domain optical coherence tomography. *Invest Ophthalmol Vis Sci* 2009;50:2989-2993.

232. Cebulla CM, Ruggeri M, Murray TG, et al. Spectral domain optical coherence tomography in a murine retinal detachment model. *Exp Eye Res*;90:521-527.

233. Huber G, Beck SC, Grimm C, et al. Spectral domain optical coherence tomography in mouse models of retinal degeneration. *Invest Ophthalmol Vis Sci* 2009;50:5888-5895.

234. Sho K, Takahashi K, Fukuchi T, et al. Quantitative evaluation of ischemia-reperfusion injury by optical coherence tomography in the rat retina. *Jpn J Ophthalmol* 2005;49:109-113.

235. Connolly SE, Hores TA, Smith LE, et al. Characterization of vascular development in the mouse retina. *Microvascular Research* 1988;36:275-290.

236. Bowes C, Li T, Danciger M, et al. Retinal degeneration in the rd mouse is caused by a defect in the beta subunit of rod cGMP-phosphodiesterase. *Nature* 1990;347:677-680.

237. Lucas RJ, Douglas RH, Foster RG. Characterization of an ocular photopigment capable of driving pupillary constriction in mice. *Nat Neurosci* 2001;4:621-626.

238. Sun H, Macke JP, Nathans J. Mechanisms of spectral tuning in the mouse green cone pigment. *Proc Natl Acad Sci U S A* 1997;94:8860-8865.

239. Porciatti V, Saleh M, Nagaraju M. The pattern electroretinogram as a tool to monitor progressive retinal ganglion cell dysfunction in the DBA/2J mouse model of glaucoma. *Invest Ophthalmol Vis Sci* 2007;48:745-751.

240. Ben-Shlomo G, Ofri R. Development of inner retinal function, evidenced by the pattern electroretinogram, in the rat. *Exp Eye Res* 2006;83:417-423.

241. Trejo LJ, Cicerone CM. Retinal sensitivity measured by the pupillary light reflex in RCS and albino rats. *Vision Res* 1982;22:1163-1171.

242. Aleman TS, Jacobson SG, Chico JD, et al. Impairment of the transient pupillary light reflex in Rpe65(-/-) mice and humans with leber congenital amaurosis. *Invest Ophthalmol Vis Sci* 2004;45:1259-1271.

243. Whiteley SJ, Young MJ, Litchfield TM, et al. Changes in the pupillary light reflex of pigmented royal college of surgeons rats with Age. *Exp Eye Res* 1998;66:719-730.

244. Kardon R, Anderson SC, Damarjian TG, et al. Chromatic pupillometry in patients with retinitis pigmentosa. *Ophthalmology* 2011;118:376-381.

245. de Zavalia N, Plano SA, Fernandez DC, et al. Effect of experimental glaucoma on the non-image forming visual system. *Journal of neurochemistry* 2011;117:904-914.

246. Kankipati L, Girkin CA, Gamlin PD. The post-illumination pupil response is reduced in glaucoma patients. *Investigative ophthalmology & visual science* 2011;52:2287-2292.

247. Hattar S, Lucas RJ, Mrosovsky N, et al. Melanopsin and rod-cone photoreceptive systems account for all major accessory visual functions in mice. *Nature* 2003;424:76-81.

248. Fu Y, Zhong H, Wang M-HH, et al. Intrinsically photosensitive retinal ganglion cells detect light with a vitamin A-based photopigment, melanopsin. *Proc Natl Acad Sci U S A* 2005;102:10339-10344.

249. Hattar S, Kumar M, Park A, et al. Central projections of melanopsin-expressing retinal ganglion cells in the mouse. *J Comp Neurol* 2006;497:326-349.

250. Brown TM, Wynne J, Piggins HD, et al. Multiple hypothalamic cell populations encoding distinct visual information. *J Physiol* 2011.

251. Ecker JL, Dumitrescu ON, Wong KY, et al. Melanopsin-expressing retinal ganglion-cell photoreceptors: cellular diversity and role in pattern vision. *Neuron* 2010;67:49-60.

252. Burkholder BM, Osborne B, Loguidice MJ, et al. Macular volume determined by optical coherence tomography as a measure of neuronal loss in multiple sclerosis. *Arch Neurol* 2009;66:1366-1372.

253. Garcia-Martin E, Pueyo V, Martin J, et al. Progressive changes in the retinal nerve fiber layer in patients with multiple sclerosis. *Eur J Ophthalmol* 2009.

254. Hajee ME, March WF, Lazzaro DR, et al. Inner retinal layer thinning in Parkinson disease. *Arch Ophthalmol* 2009;127:737-741.

255. Hood DC, Salant JA, Arthur SN, et al. The Location of the Inferior and Superior Temporal Blood Vessels and Interindividual Variability of the Retinal Nerve Fiber Layer Thickness. *J Glaucoma* 2009.

256. Lang AE, Lozano AM. Parkinson's disease. First of two parts. *N Engl J Med* 1998;339:1044-1053.

257. Bodis-Wollner I, Yahr MD. Measurements of visual evoked potentials in Parkinson's disease. *Brain* 1978;101:661-671.

258. Ikeda H, Head GM, Ellis CJ. Electrophysiological signs of retinal dopamine deficiency in recently diagnosed Parkinson's disease and a follow up study. *Vision Res* 1994;34:2629-2638.

259. Palmowski-Wolfe AM, Perez MT, Behnke S, et al. Influence of dopamine deficiency in early Parkinson's disease on the slow stimulation multifocal-ERG. *Doc Ophthalmol* 2006;112:209-215.

260. Sartucci F, Orlandi G, Lucetti C, et al. Changes in pattern electroretinograms to equiluminant red-green and blue-yellow gratings in patients with early Parkinson's disease. *J Clin Neurophysiol* 2003;20:375-381.

261. Sartucci F, Orlandi G, Bonuccelli U, et al. Chromatic pattern-reversal electroretinograms (ChPERGs) are spared in multiple system atrophy compared with Parkinson's disease. *Neurol Sci* 2006;26:395-401.

262. Langheinrich T, Tebartz van Elst L, Lagreze WA, et al. Visual contrast response functions in Parkinson's disease: evidence from electroretinograms, visually evoked potentials and psychophysics. *Clin Neurophysiol* 2000;111:66-74.

263. Djamgoz MB, Hankins MW, Hirano J, et al. Neurobiology of retinal dopamine in relation to degenerative states of the tissue. *Vision Res* 1997;37:3509-3529.

264. Rodnitzky RL. Visual dysfunction in Parkinson's disease. *Clin Neurosci* 1998;5:102-106.

265. Moschos MM, Tagaris G, Markopoulos I, et al. Morphologic changes and functional retinal impairment in patients with Parkinson disease without visual loss. *Eur J Ophthalmol* 2010.

266. Kaul S, Anantharam V, Yang Y, et al. Tyrosine phosphorylation regulates the proteolytic activation of protein kinase Cdelta in dopaminergic neuronal cells. *J Biol Chem* 2005;280:28721-28730.

267. Kanthasamy AG, Kitazawa M, Kaul S, et al. Proteolytic activation of proapoptotic kinase PKCdelta is regulated by overexpression of Bcl-2: implications for oxidative stress and environmental factors in Parkinson's disease. *Ann N Y Acad Sci* 2003;1010:683-686.

268. Anantharam V, Kitazawa M, Wagner J, et al. Caspase-3-dependent proteolytic cleavage of protein kinase Cdelta is essential for oxidative stress-mediated dopaminergic cell death after exposure to methylcyclopentadienyl manganese tricarbonyl. *J Neurosci* 2002;22:1738-1751.

269. Ghosh A, Roy A, Liu X, et al. Selective inhibition of NF-kappaB activation prevents dopaminergic neuronal loss in a mouse model of Parkinson's disease. *Proc Natl Acad Sci U S A* 2007;104:18754-18759.

270. Ghosh A, Roy A, Matras J, et al. Simvastatin inhibits the activation of p21ras and prevents the loss of dopaminergic neurons in a mouse model of Parkinson's disease. *J Neurosci* 2009;29:13543-13556.

271. Zhang D, Anantharam V, Kanthasamy A, et al. Neuroprotective effect of protein kinase C delta inhibitor rottlerin in cell culture and animal models of Parkinson's disease. *J Pharmacol Exp Ther* 2007;322:913-922.

272. Archibald NK, Clarke MP, Mosimann UP, et al. The retina in Parkinson's disease. *Brain* 2009;132:1128-1145.

273. Bodis-Wollner I. Retinopathy in Parkinson Disease. *J Neural Transm* 2009;116:1493-1501.

274. Holroyd S, Wooten GF. Preliminary FMRI evidence of visual system dysfunction in Parkinson's disease patients with visual hallucinations. *J Neuropsychiatry Clin Neurosci* 2006;18:402-404.

275. Holroyd S, Currie L, Wooten GF. Prospective study of hallucinations and delusions in Parkinson's disease. *J Neurol Neurosurg Psychiatry* 2001;70:734-738.

276. Matsui H, Udaka F, Tamura A, et al. Impaired visual acuity as a risk factor for visual hallucinations in Parkinson's disease. *J Geriatr Psychiatry Neurol* 2006;19:36-40.

277. Matsui H, Udaka F, Oda M, et al. [Two cases of Parkinson's disease in which visual hallucinations disappeared after cataract surgery]. *No To Shinkei* 2004;56:351-354.

278. Pieri V, Diederich NJ, Raman R, et al. Decreased color discrimination and contrast sensitivity in Parkinson's disease. *J Neurol Sci* 2000;172:7-11.

279. Diederich NJ, Goetz CG, Raman R, et al. Poor visual discrimination and visual hallucinations in Parkinson's disease. *Clin Neuropharmacol* 1998;21:289-295.

280. Buttner T, Kuhn W, Muller T, et al. Visual hallucinosis: the major clinical determinant of distorted chromatic contour perception in Parkinson's disease. *J Neural Transm* 1996;103:1195-1204.

281. Jackson-Lewis V, Przedborski S. Protocol for the MPTP mouse model of Parkinson's disease. *Nat Protoc* 2007;2:141-151.

282. Ghilardi MF, Bodis-Wollner I, Onofrj MC, et al. Spatial frequency-dependent abnormalities of the pattern electroretinogram and visual evoked potentials in a parkinsonian monkey model. *Brain* 1988;111 (Pt 1):131-149.

283. Wong C, Ishibashi T, Tucker G, et al. Responses of the pigmented rabbit retina to NMPTP, a chemical inducer of parkinsonism. *Exp Eye Res* 1985;40:509-519.

284. Altintas O, Iseri P, Ozkan B, et al. Correlation between retinal morphological and functional findings and clinical severity in Parkinson's disease. *Doc Ophthalmol* 2008;116:137-146.

285. Inzelberg R, Ramirez JA, Nisipeanu P, et al. Retinal nerve fiber layer thinning in Parkinson disease. *Vision Res* 2004;44:2793-2797.

286. Ghilardi MF, Chung E, Bodis-Wollner I, et al. Systemic 1-methyl,4-phenyl,1-2-3-6-tetrahydropyridine (MPTP) administration decreases retinal dopamine content in primates. *Life Sci* 1988;43:255-262.

287. Bodis-Wollner I, Tzelepi A. The push-pull action of dopamine on spatial tuning of the monkey retina: the effects of dopaminergic deficiency and selective D1 and D2 receptor ligands on the pattern electroretinogram. *Vision Res* 1998;38:1479-1487.

288. Harnois C, Marcotte G, Bedard PJ. Alteration of monkey retinal oscillatory potentials after MPTP injection. *Doc Ophthalmol* 1987;67:363-369.

289. Tagliati M, Bodis-Wollner I, Yahr MD. The pattern electroretinogram in Parkinson's disease reveals lack of retinal spatial tuning. *Electroencephalogr Clin Neurophysiol* 1996;100:1-11.

290. Nguyen-Legros J. Functional neuroarchitecture of the retina: hypothesis on the dysfunction of retinal dopaminergic circuitry in Parkinson's disease. *Surg Radiol Anat* 1988;10:137-144.

291. Tucker GS, Hamasaki DI, Wong CG. Intranuclear rodlets in the rabbit retina following treatment with MPTP. *Exp Eye Res* 1986;42:569-583.

292. Cuenca N, Herrero MT, Angulo A, et al. Morphological impairments in retinal neurons of the scotopic visual pathway in a monkey model of Parkinson's disease. *J Comp Neurol* 2005;493:261-273.

293. Archibald NK, Clarke MP, Mosimann UP, et al. Retinal thickness in Parkinson's disease. *Parkinsonism & related disorders* 2011;17:431-436.

294. Jaffe MJ, Bruno G, Campbell G, et al. Ganzfeld electroretinographic findings in parkinsonism: untreated patients and the effect of levodopa intravenous infusion. *J Neurol Neurosurg Psychiatry* 1987;50:847-852.

295. Yavas GF, Yilmaz O, Kusbeci T, et al. The effect of levodopa and dopamine agonists on optic nerve head in Parkinson disease. *Eur J Ophthalmol* 2007;17:812-816.

296. Kanthasamy AG, Anantharam V, Zhang D, et al. A novel peptide inhibitor targeted to caspase-3 cleavage site of a proapoptotic kinase protein kinase C delta (PKCdelta) protects against dopaminergic neuronal degeneration in Parkinson's disease models. *Free Radic Biol Med* 2006;41:1578-1589.

297. Kaul S, Kanthasamy A, Kitazawa M, et al. Caspase-3 dependent proteolytic activation of protein kinase C delta mediates and regulates 1-methyl-4-phenylpyridinium (MPP+)-induced apoptotic cell death in dopaminergic cells: relevance to oxidative stress in dopaminergic degeneration. *Eur J Neurosci* 2003;18:1387-1401.

298. Kanthasamy AG, Kitazawa M, Kanthasamy A, et al. Role of proteolytic activation of protein kinase Cdelta in oxidative stress-induced apoptosis. *Antioxid Redox Signal* 2003;5:609-620.

299. Freed S, Hellerstein LF. Visual electrodiagnostic findings in mild traumatic brain injury. *Brain Inj* 1997;11:25-36.

300. Du T, Ciuffreda KJ, Kapoor N. Elevated dark adaptation thresholds in traumatic brain injury. *Brain Inj* 2005;19:1125-1138.

301. Green W, Ciuffreda KJ, Thiagarajan P, et al. Accommodation in mild traumatic brain injury. *J Rehabil Res Dev* 2010;47:183-199.

302. Cockerham GC, Rice TA, Hewes EH, et al. Closed-eye ocular injuries in the Iraq and Afghanistan wars. *The New England journal of medicine* 2011;364:2172-2173.

303. Dougherty AL, MacGregor AJ, Han PP, et al. Visual dysfunction following blast-related traumatic brain injury from the battlefield. *Brain Inj* 2011;25:8-13.

304. Bodis-Wollner I. Retinopathy in Parkinson Disease. *Journal of neural transmission* 2009;116:1493-1501.

305. Kim KH, Puoris'haag M, Maguluri GN, et al. Monitoring mouse retinal degeneration with high-resolution spectral-domain optical coherence tomography. *Journal of vision* 2008;8:17 11-11.

306. Xu J, Molday LL, Molday RS, et al. In vivo imaging of the mouse model of X-linked juvenile retinoschisis with fourier domain optical coherence tomography. *Investigative ophthalmology & visual science* 2009;50:2989-2993.

307. Huber G, Beck SC, Grimm C, et al. Spectral domain optical coherence tomography in mouse models of retinal degeneration. *Investigative ophthalmology & visual science* 2009;50:5888-5895.

308. Wachtmeister L. Oscillatory potentials in the retina: what do they reveal. *Progress in retinal and eye research* 1998;17:485-521.

309. Burguillos MA, Deierborg T, Kavanagh E, et al. Caspase signalling controls microglia activation and neurotoxicity. *Nature* 2011;472:319-324.

310. Schaller BJ. Influence of age on stroke and preconditioning-induced ischemic tolerance in the brain. *Experimental neurology* 2007;205:9-19.

311. Stenzel-Poore MP, Stevens SL, King JS, et al. Preconditioning reprograms the response to ischemic injury and primes the emergence of unique endogenous neuroprotective phenotypes: a speculative synthesis. *Stroke; a journal of cerebral circulation* 2007;38:680-685.

312. Dirnagl U, Becker K, Meisel A. Preconditioning and tolerance against cerebral ischaemia: from experimental strategies to clinical use. *Lancet Neurol* 2009;8:398-412.

ACKNOWLEDGEMENTS

Foremost, I thank my major professor Dr. Sinisa Grozdanic for his mentorship and guidance throughout my PhD program. His continuous encouragement toward independent research and the freedom he afforded in conducting experiments have made me appreciate graduate school life and taught many valuable lessons. I can sincerely state that I would not have reached this milestone in my life without his constant support. I also thank Dr. Matthew Harper, who oversaw and guided most of my dissertation research. He has been a teacher, colleague, ARVO room-mate, and friend through these years. I have been very fortunate to be mentored by two excellent scientists, highly committed to raising the standards of clinical medicine.

I owe great thanks to my POS committee. Dr. Donald Sakaguchi, who cheerfully took part in the drama of my final year and filled many a form for me. I thank him for his enduring support and for being part of my committee. I also thank Dr. Mark Ackermann for being a great teacher and for being part of my committee. I extend thanks to Dr. Vellareddy Anantharam and Dr. Anumantha Kanthasamy for their support through the Iowa Center for Advanced Neurotoxicology and for serving on my committee. I take this opportunity to thank Dr. Randy Kardon, who has provided much encouragement and support in my endeavors. I also thank the various funding agencies, including the National Institute of Health, Veterans Affairs Medical Center, and Iowa Center for Advanced Neurotoxicology.

I thank my lab members, Elena Hernandez-Merino, Helga Kecova, Tanja Lazic, Richard Nzokwe, Laura Dutca, Jack Gallup, and Matthew Yorek, for their help and suggestions, for the good times and lab meetings. I have learnt much from you and have many moments to cherish for life. I also thank the various undergraduate students who have helped with my research, in particular, Whitney Leverich and Deepak Navi. I owe great thanks to Kim Adams, Linda Erickson, MaryAnn Devries, and Dianne Ritz, for stepping in and fixing my financial troubles, ever so often. Also, I owe thanks to Lucas Hicks and David Meyer at the VA Medical Center for their help with various administrative issues.

At this juncture, I thank all my friends in Ames who have shared time in graduate school and have made it a memorable experience for me. In particular, I thank Arunkumar Asaithambi and Rungano Stan Dzikamunhenga, who have helped me through many tough times. I also thank Anamitra Ghosh and Eun-Ah Ye, who have helped me much with my research. I thank the members of the Kanthasamy lab too, who have become great friends over long nights and coffee breaks.

I cannot sufficiently thank my family for all they have done for me. My parents, Mallika and Srinivasan Mohan, for all the love, patience, and support through all these years; my sister, Bharathi, who has been as good a younger sister as one could be; and, not least, Grinu, who has been by my side, one way or another, through good times and bad. I thank you all for being my guides and anchors in life.